DISSERTATION ZUR ERLANGUNG DES DOKTORGRADES
DER FAKULTÄT FÜR CHEMIE UND PHARMAZIE
DER LUDWIG-MAXIMILIANS-UNIVERSITÄT MÜNCHEN

Targeting the tumour microenvironment
– from thyroid hormone signalling to gene therapy

KATHRIN ALEXANDRA SCHMOHL

aus München, Deutschland

2019

Erklärung

Diese Dissertation wurde im Sinne von § 7 der Promotionsordnung vom 28. November 2011 von Frau Prof. Dr. Christine Spitzweg betreut und von Herrn Prof. Dr. Ernst Wagner von der Fakultät für Chemie und Pharmazie vertreten.

Eidesstattliche Versicherung

Diese Dissertation wurde eigenständig und ohne unerlaubte Hilfe erarbeitet.

München, den 06.12.2019

Kathrin Schmohl

Dissertation eingereicht am	11.10.2019
1. Gutachter:	Prof. Dr. Ernst Wagner
2. Gutachterin:	Prof. Dr. Christine Spitzweg
Mündliche Prüfung am	28.11.2019

DEDICATED TO

My parents (obviously), who taught me to think for myself.

And Mike, who lives with the consequences.

"*With magic, you can turn a frog into a prince. With science, you can turn a frog into a Ph.D and you still have the frog you started with.*"

– Terry Pratchett, Ian Stewart, and Jack Cohen in *The Science of Discworld*

TABLE OF CONTENTS

I. INTRODUCTION

This chapter is partially adapted from Schmohl KA, Nelson PJ, Spitzweg C. Tetrac as an anti-angiogenic agent in cancer. *Endocr Relat Cancer* **2019**;26:R287-304 and Schmohl KA, Müller AM, Nelson PJ, Spitzweg C. Thyroid hormone effects on mesenchymal stem cell biology in the tumour microenvironment. *Exp Clin Endocrinol Diabetes* **2019** [Epub ahead of print].

1.1 Cancer – an overview

Cancer is the second leading cause of death, accounting for one in six deaths and an estimated total of 9.6 million deaths worldwide in 2018. In many of the most developed countries, including large parts of Europe and North America, cancer is the leading cause for premature mortality at ages below 70 [1]. Though huge advances in understanding and treating cancer have been made over the past 50 years, many aspects of cancer biology are still poorly understood and, as the numbers above indicate, there is still an urge to develop effective treatment strategies.

Cancer development and progression are highly complex, multi-stage processes that involve multiple genetic and epigenetic changes to transform normal cells into malignant tumour cells. As Peyton Rous said in his Nobel lecture of 1966, "Tumours destroy man in a unique and appalling way, as flesh of his own flesh which has somehow been rendered proliferative, rampant, predatory and ungovernable" [2]. In normal tissues, a homeostasis of cell number and thus tissue composition and function are maintained by the careful control of mitogenic signalling. In cancer cells, this signalling is deregulated, leading to sustained proliferation, circumvention of growth suppressors, and evasion of cell death. To provide the ever-growing cell mass with oxygen and nutrients, new tumour vasculature is established through angiogenesis. Ultimately, tumour cells acquire the ability to escape the primary tumour mass by invading adjacent tissues and disseminating to distant sites to form metastases [3, 4].

1.1.1 The tumour microenvironment

Solid tumours are organ-like structures that develop within a complex microenvironment [5]. Mimicking chronic wounds, tumours hijack the wound healing response to recruit "migratory neighbours and distant invaders" as supporting cells and generate the stroma they need for survival and growth [6-9]. The malignant cancer cells are typically outnumbered by the 'benign' cells of the stromal compartment that is composed of a heterogeneous population of cells, including cancer-associated fibroblasts (CAFs), mesenchymal stem cells (MSCs), pericytes, vascular endothelial cells, and immune cells, besides non-cellular components, i.e. signalling molecules and the extracellular matrix (**Fig. 1**) [10, 11]. The adaptation of cells of the tumour stroma to the harsh conditions a growing tumour faces, such as oxygen and nutrient deprivation, preserves tumour homeostasis by creating a protective niche not only shielding

cancer cells from metabolic stress and immune surveillance, but also fostering resistance to treatment [10, 12].

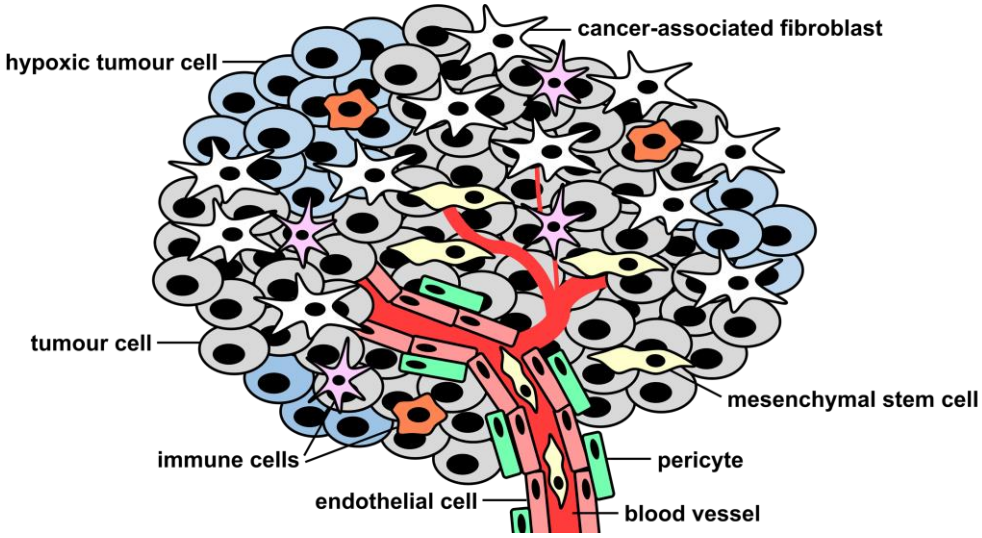

Figure 1. Schematic illustration of the tumour microenvironment. Besides the malignant cancer cells, tumours consist of several different supporting cell types that are recruited to the tumour stroma during tumour growth and progression.

1.1.2 Tumour hypoxia and angiogenesis

As mentioned above, tumour growth and progression require an adequate vascular supply. Rapidly proliferating tumour masses, however, typically outgrow their vasculature, leading to hypoxic areas with low oxygen concentrations. This in turn triggers the hypoxic response, both in tumour and stromal cells, which is initiated by stabilisation of hypoxia-inducible factors (HIFs). HIFs mediate the expression of genes involved in angiogenesis, the formation of new blood vessels from the existing vasculature. Angiogenesis is a highly regulated process, temporally and spatially controlled by a balance between pro- and anti-angiogenic factors [13, 14]. In response to specific stimuli, including hypoxia and inflammation, the angiogenic switch occurs in the quiescent endothelium through the local release of vascular growth factors by tumour cells, endothelial cells, and cells of the tumour stroma, initiating coordinated endothelial cell proliferation, invasion, migration, and, ultimately, tube formation and maturation [14, 15]. Angiogenesis is closely linked to tumour progression, both sustaining tumour growth by providing oxygen and other nutrients, and facilitating metastasis. While physiological angiogenesis in the context of development, tissue growth, and wound-healing is tightly regulated and self-limiting, cancer-associated angiogenesis, though in principle regulated by the same pathways, is usually persistent and abnormal, contributing to the formation of a dysfunctional endothelium that is often leaky and tortuous [16, 17].

1.1.3 Mesenchymal stem cells

MSCs are multipotent non-hematopoietic stromal cells, primarily found in the bone marrow and adipose tissue, that are capable of differentiating into multiple connective tissue lineages, such as osteocytes, chondrocytes, and adipocytes [18]. They contribute to tissue maintenance and regeneration by their recruitment as 'first responders' to sites of tissue injury and inflammation [11]. Hence, MSCs actively home to tumours that are disguised as wounds. The presence and function of MSCs in the tumour microenvironment is still incompletely understood, though our current knowledge suggests that they serve as progenitor cells for CAFs and blood vessel-stabilising pericytes [5, 8, 18-20]. As with fibroblasts associated with wound healing that remodel and regenerate tissues, CAFs are activated fibroblasts that support tumourigenesis by encouraging a pro-angiogenic, immunosuppressive, and pro-inflammatory microenvironment [6, 19, 21]. In addition, they perpetually remodel the extracellular matrix, thus releasing sequestered proteins, besides physically creating space for proliferating and migrating tumour cells [21]. Pericytes, on the other hand, envelop vascular tubes formed by endothelial cells and serve as scaffolding. By their differentiation into pericytes, MSCs support the stabilisation and maturation of newly formed vessels [14]. In addition, numerous pro-angiogenic factors have been identified in the secretome of MSCs that induce endothelial cell proliferation, migration, invasion, and endothelial cell tube formation [14]. Hence, MSCs affect a broad spectrum of angiogenic processes through their interaction and communication with endothelial cells [22, 23]. Ultimately, MSCs and their differentiated progeny support tumour cell survival and growth, angiogenesis, immune evasion, invasion, and metastasis through cell-to-cell interactions and the secretion of tumour-promoting factors [24].

1.2 Thyroid hormones

The thyroid hormones L-thyroxine (T4) and 3,5,3'-triiodo-L-thyronine (T3) are iodinated low molecular mass compounds derived from the amino acid L-tyrosine (**Fig. 2**). Virtually all multicellular animals, including primitive invertebrate species, have the capacity to respond to thyroid hormones [25]. Their diverse functions include the regulation of development, differentiation, growth, and metabolism. Given that they influence such a broad range of processes, it is not surprising that growing clinical and experimental evidence suggests that thyroid hormones are also implicated in cancer development and progression.

In vertebrates, thyroid hormones are produced and released into the circulation by the thyroid gland controlled by feedback mechanisms within the hypothalamic-pituitary-thyroid axis. In response to thyroid-stimulating hormone (TSH; thyrotropin) released by the pituitary, thyroid follicular cells produce T4 and, to a lower extent, T3. Though T4 is quantitatively the major secretory product, T3 is generally considered the metabolically most active thyroid hormone. Relevant T3 production occurs in the periphery by de-iodination of T4. Besides the classical thyroid hormones, several naturally

occurring, biologically active metabolites have been discovered. These include the acetic acid T4 analogue 3,3',5,5'-tetraiodothyroacetic acid (tetrac; **Fig. 2**) that is generated by deamination and decarboxylation at the alanine side chain of the inner tyrosyl ring of T4 and circulates in the blood at low nanomolar concentrations [26-28].

1.2.1 Thyroid hormone signalling

At the cellular level, thyroid hormone activity is mediated through specific receptors in the nucleus, but also the mitochondria, the cytoplasm, and the plasma membrane [29]. Classical or 'genomic' thyroid hormone signalling occurs via the nuclear thyroid hormone receptors TRα and TRβ that act as ligand-dependent transcription factors [30, 31]. In this canonical pathway, T3 is the primary ligand, while T4 functions as pro-hormone [32]. The term non-classical thyroid hormone signalling, in contrast, summarises all those effects where pathway initiation by thyroid hormones is 'non-genomic', i.e. not in the nucleus, though downstream consequences may culminate in effects on gene transcription.

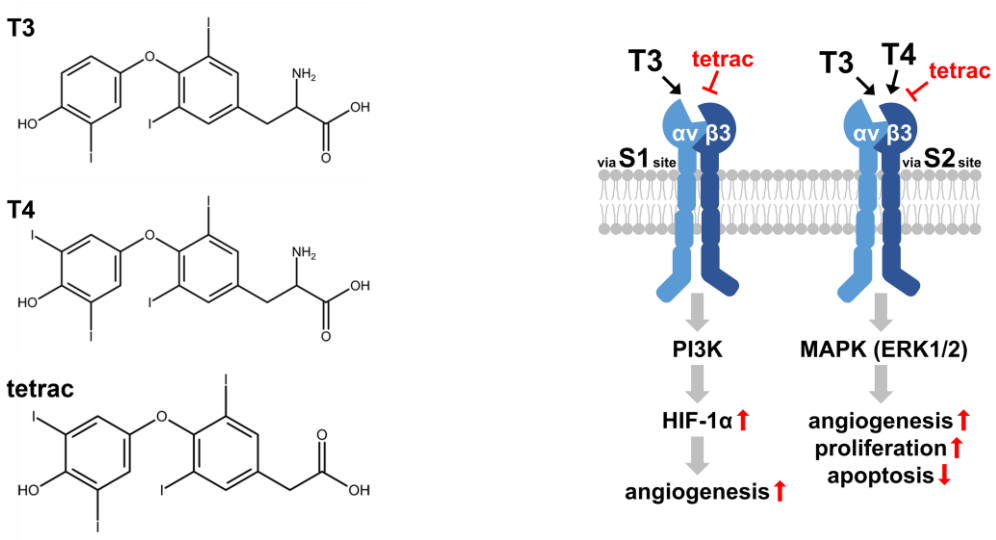

Figure 2. Membrane-initiated thyroid hormone signalling. Left panel: Chemical structures of 3,5,3'-triiodo-L-thyronine (T3), L-thyroxine (T4) and thyroid hormone metabolite 3,3',5,5'-tetraiodoacetic acid (tetrac). Right panel: The thyroid hormone binding site on integrin αvβ3 contains two distinct binding domains, S1 and S2 that activate separate signalling cascades and downstream effects relevant to tumour progression.

Integrin αvβ3

One such non-classical pathway is initiated at integrin αvβ3, a plasma membrane thyroid hormone receptor identified in 2005 by Bergh *et al.* [33]. Integrins are a structurally related family of heterodimeric membrane receptors involved in cell-cell and cell-extracellular matrix protein interactions, and have emerged as major regulators of the activity of various cell-signalling pathways. Though integrins themselves are not oncogenic, their expression by tumour cells and tumour stroma-associated cells critically contributes to tumour progression and metastasis [34]. Ligand binding to the extracellular domain is translated into downstream signalling events via outside-in signalling inside the

cell, usually engaging signal transducing kinase cascades [35]. Integrin signalling is typically transduced into cell motility, adhesion, division, and angiogenesis via direct effects on the cytoskeleton and modulation of gene transcription. Furthermore, crosstalk between integrins and neighbouring growth factor and cytokine receptors, affecting their expression, ligand affinity, and signalling, seems to be required for many of their tumour-promoting effects [34].

Integrin αvβ3 is primarily expressed on cancer cells, dividing endothelial cells, and tumour stroma-associated cells, highlighting its potential importance in oncology [20, 36]. Its prototypic ligand is the extracellular matrix glycoprotein vitronectin that binds to the integrin's extracellular domain via an RGD (arginine-glycine-aspartic acid) sequence [37]. The thyroid hormone binding site on integrin αvβ3 is located near this RGD recognition site and comprises two distinct domains that are related neither structurally nor functionally to nuclear thyroid hormone receptors [38, 39]. The binding site S1 exclusively binds T3 and causes activation of the phosphoinositide 3-kinase (PI3K) cascade, which has been proposed to stimulate HIF-1α expression and thus indirectly affect angiogenesis [39]. The S2 site, in contrast, binds both T3 and T4 and results in MAPK (ERK1/2) pathway activation [39]. From the latter site, thyroid hormones have been reported to stimulate angiogenesis and cell proliferation, and to inhibit apoptosis (**Fig. 2**) [40]. Thus, in contrast to the TR/thyroid hormone axis, both T4 and T3 act as active hormones at the integrin receptor. In fact, as the affinity for T4 is far higher than that for T3, and lies in the physiologic concentration range that is comparable to the T3 affinity for nuclear receptors, T4 may well be the main hormone signalling at the integrin, thus transcending its role of pro-hormone for T3 [41]. Tetrac binds to both thyroid hormone binding sites on the integrin and is a specific inhibitor of integrin-mediated thyroid hormone action [26, 42]. Within the cell, in contrast, tetrac has low-grade thyromimetic activity, both by itself, as well as through its conversion to triiodothyroacetic acid (triac) [43, 44]. Via integrin αvβ3, thyroid hormones have been shown to stimulate proliferation in various tumour cell lines, both *in vitro* and *in vivo*, impede apoptosis, and augment angiogenesis, inflammation, immune escape, and therapy resistance, while tetrac reversed these effects [29, 40, 45, 46].

1.2.2 Thyroid hormones and cancer – the yes, the no, and the maybe

While experimental evidence conclusively demonstrates a link between thyroid hormones and tumour progression, clinical evidence is more ambiguous. Several studies have examined the relationship between cancer and thyroid status. Hyperthyroidism has been associated with an increased risk, mortality, rate of recurrence, and/or progression in many different tumour entities, including gynaecological and gastrointestinal cancers, prostate cancer, glioma, and leukaemia, among others. In hepatocellular carcinoma, in contrast, hyperthyroidism has been shown to be associated with smaller tumours and a decreased mortality. Hypothyroidism is mostly reported to be associated with a decreased cancer risk and a better prognosis, with the exception of uterine and colorectal cancer, and, again, hepatocellular carcinoma. Studies comparing the overall risk and mortality for any type of cancer complicate things further, as for both hyper- and hypothyroidism results range from an increase to a

decrease in cancer risk and/or mortality, with some studies finding no association at all (recently reviewed in [47, 48]). More conclusive evidence of thyroid hormone involvement in cancer progression has derived from the chance observation that cancer patients that develop hypothyroidism as unwanted side effect of treatment often show a more favourable outcome. In addition, in rodent models, hypothyroidism has been reported to reduce tumour growth [31, 49-54]. Based on these findings, hypothyroidism was deliberately induced in cancer patients in a few pioneering studies. Indeed, induction of mild hypothyroidism in glioma patients was associated with tumour regression and prolongation of survival and time-to-progression [55-57]. Interestingly, pharmacologic induction of a euthyroid hypothyroxinaemic state under maintenance of normal circulating T3 levels and euthyroidism with substantial reduction of circulating T4 levels in advanced cancer patients was associated with a significant prolongation of actual *versus* expected survival [58].

1.3 Targeted cancer gene therapy

The simplest definition of gene therapy is the genetic modification of cells to produce a therapeutic effect [59]. As cancer is a genetic disease, high expectations have been placed on cancer gene therapy. Faced with obstacles such as the polygeneity and heterogeneity of tumours, progress, however, has been slow [60]. Trying to correct the many different genes that are abnormal for each individual tumour is not feasible. Instead, the selective modification of tumour cells with therapeutically active genes is a more promising strategy [60].

1.3.1 The sodium iodide symporter NIS

One such therapeutically active gene that has evolved as a highly promising candidate for cancer gene therapy is the sodium iodide symporter (*NIS; SLC5A5*). *NIS* encodes an intrinsic transmembrane glycoprotein that mediates the cellular uptake of iodide from the bloodstream into thyroid follicular cells as the first and rate-limiting step of thyroid hormone synthesis [61]. NIS actively transports one iodide ion (I^-) and two sodium ions (Na^+) across the basolateral membrane of thyroid follicular cells using the sodium gradient generated by the Na^+/K^+-ATPase. Iodide transport is inhibited by the Na^+/K^+-ATPase inhibitor ouabain, and the competitive inhibitors thiocyanate and perchlorate. Thyroidal NIS expression is regulated by pituitary-derived TSH [61]. In addition to its role in thyroid physiology, NIS provides the basis for the diagnostic imaging and therapy of differentiated thyroid cancer and its metastases using radioactive iodine isotopes, and other radionuclides that are also transported by NIS. This has been successfully exploited for the treatment of thyroid cancer patients since 1946, making thyroid cancer one of the most manageable cancers to date [61, 62].

Cloning of the *NIS* gene in 1996 marks the birth of a cytoreductive gene therapy approach based on targeting functional NIS expression to thyroidal and non-thyroidal tumours, thus extending a well-established and highly effective therapeutic strategy beyond the treatment of differentiated thyroid tumours [61, 63, 64]. The feasibility of the *NIS* gene therapy concept in cancer treatment has been

demonstrated in several preclinical studies and as a result, it has entered clinical trials [65]. These trials are based on local or systemic (i.e. by intraperitoneal injection) *NIS* gene delivery by measles virus in various cancer types (NCT01503177, NCT01846091, NCT02364713, and NCT02700230) or by MSCs infected with a NIS-encoding measles virus in recurrent ovarian cancer (NCT02068794).

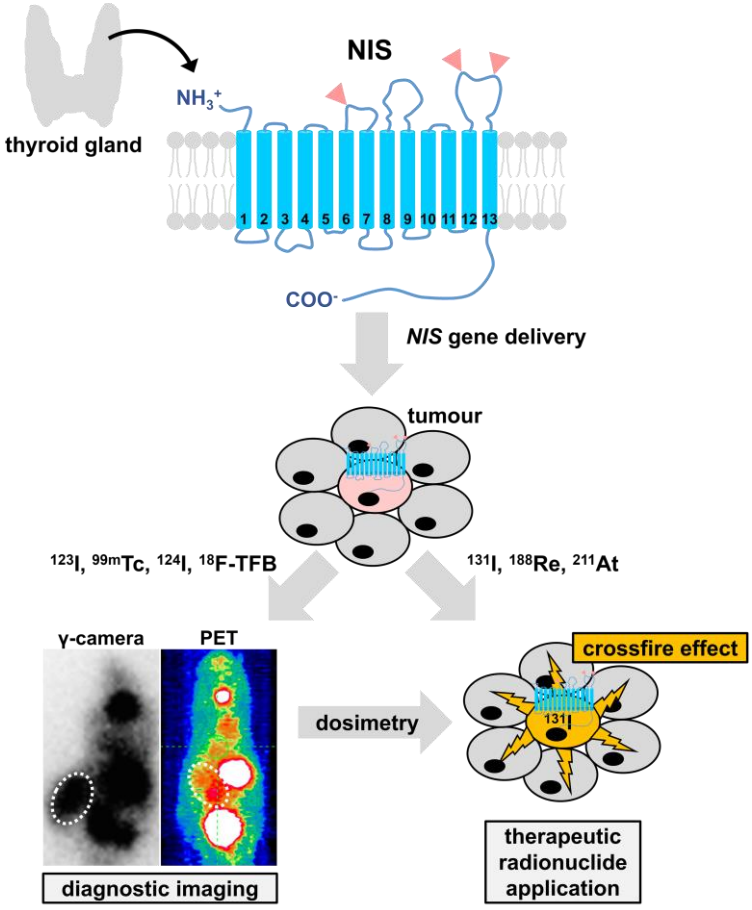

Figure 3. Schematic illustration of the theranostic *NIS* gene therapy concept. Cloning of thyroidal *NIS* has paved the way for *NIS* gene transfer to both thyroidal and extrathyroidal tumours. Application of diagnostic radionuclides allows diagnostic imaging and dosimetric calculations, before the application of therapeutic radionuclides.

The many advantages of *NIS* include its dual function as reporter and therapy gene. This allows the characterisation of vector biodistribution, localisation, level, and duration of transgene expression, as well as dosimetric calculations by standard non-invasive nuclear medicine imaging modalities, including ^{123}I- and ^{99m}Tc-scintigraphy, as well as ^{124}I- and ^{18}F-TFB-positron emission tomography (PET), before the application of a therapeutic dose of therapeutic radionuclides ^{131}I, ^{188}Re, or ^{211}At (**Fig. 3**) [66]. In addition, NIS is non-immunogenic and its biodistribution, expression, and safety profile are well-defined due to the extensive experience gained in differentiated thyroid cancer patients [67, 68]. Notably, NIS-based therapy is associated with a substantial bystander effect on non-transfected cells that are irradiated by the crossfire emanating from adjacent transfected cells (**Fig. 3**). The effective range of the beta emission of the therapeutic radionuclide ^{131}I, for instance, is up to 2.4 mm in tissues. The

significance of this effect is that not only NIS expressing cells are destroyed, but also neighbouring cells, hence compensating incomplete targeting of all tumour cells [68].

1.3.2 Gene transfer concepts

Clinical application of the *NIS* gene therapy concept depends on specific and efficient tumour targeting at low toxicity and requires systemic application for the treatment of disseminated cancer. The biostability and delivery efficiency of naked nucleic acids are very low, limiting their systemic applicability and making the development of gene transfer vehicles indispensable [69]. Prof. Dr. Christine Spitzweg's lab has focussed on the optimisation of selective *NIS* gene transfer into both thyroidal and non-thyroidal tumours in collaboration with Prof. Dr. Ernst Wagner (Pharmaceutical Biotechnology, Department of Pharmacy, Centre for System-Based Drug Research and Centre for Nanoscience, LMU Munich) and Prof. Dr. Peter J Nelson (Clinical Biochemistry Group, Department of Internal Medicine IV, University Hospital of Munich, LMU Munich). To this end, different gene transfer vehicles that allow systemic application are being evaluated, including genetically engineered MSCs, viral vectors, and non-viral synthetic vectors.

MSCs

MSCs, based on their natural tropism for solid tumours and metastases, have been used as Trojan horses to deliver the *NIS* gene deep into the tumour microenvironment. After an initial proof-of-principle study using the constitutively active cytomegalovirus (CMV) promoter to drive NIS expression in MSCs and target hepatocellular carcinoma in a subcutaneous murine xenograft model, tumour specificity was enhanced in subsequent studies using promoters selectively activated in the tumour milieu [66]. These included the chemokine CCL5/RANTES promoter, a hypoxia-inducible promoter, a TGF-β-responsive promoter, and a radiation-inducible promoter [70-75]. These approaches allowed diagnostic imaging of MSC biodistribution and transgene expression followed by successful NIS-based radionuclide therapy in different tumour models, including orthotopic hepatocellular carcinoma xenografts, colon cancer liver metastasis xenografts, and a genetically engineered mouse model of pancreatic ductal adenocarcinoma [71, 72, 76].

Viral vectors

A further method for systemic gene transfer is the use of viral vectors. Since viruses are nucleic acid transfer vehicles optimised by evolution, their transfection efficiency is unrivalled. In a radiovirotherapy approach, a replication-selective oncolytic adenovirus was used to successfully target NIS to hepatocellular carcinoma xenografts, resulting in a significant therapeutic effect [77]. To increase tumour specificity by reduction of off-target effects, viruses were coated with poly(amidoamine) dendrimers, which resulted in successful liver detargeting and effective tumour retargeting of the *NIS* gene transfer vectors [78]. Coupling these dendrimers to GE11, a ligand of the epidermal growth factor

receptor (EGFR), which is highly expressed on many tumour cells, further improved tumour selectivity of the adenoviral *NIS* gene therapy approach [79].

Synthetic vectors

Though widely used and, in principle, highly promising, viral vectors do come with a number of drawbacks, including safety concerns based on their potential immunogenicity and oncogenesis, in addition to limited payload capacity and the difficulty of large-scale production [80]. In an approach to imitate viruses to deliver nucleic acid payloads efficiently without the aforementioned drawbacks, the development of synthetic polymers has gained momentum. In this context, cationic polymers have emerged as the most promising class of non-viral gene delivery vehicles [81]. Polycations stabilise nucleic acids by forming sub-micrometre complexes called polyplexes, thus effectively protecting them from premature degradation and unwanted interactions with extracellular components [81]. Branched polycations based on pseudodendritic oligoamines demonstrated the huge potential of synthetic polymers for tumoural *NIS* gene transfer after systemic application in a syngeneic mouse model of neuroblastoma and a xenograft mouse model of hepatocellular carcinoma [82, 83]. Tumour targeting relied on the high intrinsic tumour affinity of the polyplexes due to the enhanced permeability and retention effect that arises from the dysfunctional and leaky endothelium of tumours and drives the passive accumulation of polyplexes [69, 84, 85]. To enhance tumour-targeting, polyplexes can be equipped with tumour-specific ligands, such as the EGFR-specific peptide GE11 mentioned above. To this end, GE11 was attached to one of the most widely used polycations, linear polyethylenimine (LPEI), via a polyethylene glycol (PEG) linker, thus reducing cytotoxicity by shielding the surface of the polyplex, to target NIS to a high EGFR-expressing xenograft mouse model of hepatocellular carcinoma, resulting in a significant therapeutic effect [81, 86, 87].

1.4 Aims of the thesis

Cancer is a major cause of mortality around the world. Hence, there is a drive to understand the mechanisms contributing to tumour progression with the aim to avoid risk factors and develop more target-oriented, individualised therapy approaches. These two aspects, (1) understanding tumour biology, and (2) development of tumour-targeted treatment strategies, are the two major topics underlying this thesis.

Over the past two decades, there has been increasing evidence linking the thyroid hormones T3 and T4 to critical aspects of tumour growth and progression, including stimulation of tumour cell proliferation, angiogenesis, and inflammation. These effects are thought to be mediated through integrin αvβ3 and are blocked by the T4 derivative tetrac. While thyroid hormone effects on tumour cells and endothelial cells have been described in a variety of integrin αvβ3-positive tumour models *in vitro* and *in vivo*, effects on other critical cells within the tumour microenvironment, including αvβ3-positive MSCs, have not been investigated to date.

Initially, the tools and thyroid hormone treatment strategies required for the analysis of thyroid hormone effects initiated at integrin αvβ3 had to be established *in vitro* and *in vivo*. To eliminate endogenous thyroid hormone synthesis in the mouse, thyroid ablation protocols needed to be devised.

Subsequently, building on the extensive experience with adoptively applied MSCs as tumour-selective gene delivery vehicles in Prof. Dr. Christine Spitzweg's and Prof. Dr. Peter J Nelson's laboratories, the effects of thyroid hormones versus tetrac on the tumour homing capacity of MSCs and their differentiation within the tumour milieu were investigated.

As the analysis of MSC differentiation under thyroid hormone stimulation unearthed a subset of genes relevant to angiogenesis, and MSCs are known to modulate angiogenesis both by paracrine and cell-cell contact effects, the next logical step was to investigate the angiogenic effects of thyroid hormones versus tetrac on MSCs in the tumour milieu in more detail. The unique reporter gene properties of *NIS*, a well-established theranostic gene in the laboratory of Prof. Dr. Christine Spitzweg, provided the basis to examine signalling pathway activation in MSCs in the tumour microenvironment under thyroid hormone stimulation.

Next, a comparison of thyroid hormone versus tetrac effects on tumour growth in an αvβ3-positive tumour cell line and an αvβ3-negative tumour cell line was aimed at to determine the importance of integrin αvβ3 expression on the tumour cells themselves for tumour growth stimulation by thyroid hormones, as opposed to effects on endothelial cells and the tumour stroma.

The second major topic of this thesis is focussed on *NIS* gene transfer for cancer gene therapy using synthetic non-viral polymers as gene delivery vehicles based on previous work in the laboratories of Prof. Dr. Christine Spitzweg and Prof. Dr. Ernst Wagner.

To begin with, the therapeutic efficacy of LPEI-based polymers containing an EGFR-targeting ligand to re-induce NIS expression in undifferentiated thyroid cancer that has lost its endogenous NIS expression, were tested.

In a further step towards clinical application, these polymers were applied in a more advanced tumour model. To this end, a genetically engineered mouse model of pancreatic ductal adenocarcinoma was used that better reflects human disease and is thus highly suitable to predict the clinical effectiveness of a specific therapy approach.

II. CHAPTER 1

Establishment of an effective radioiodide thyroid ablation protocol in mice

Kathrin A Schmohl[1*], Andrea M Müller[1*], Nathalie Schwenk[1], Kerstin Knoop[1], Eddy Rijntjes[2], Josef Köhrle[2], Heike Heuer[3], Peter Bartenstein[4], Burkhard Göke[1], Peter J Nelson[5] and Christine Spitzweg[1]

[1]Department of Internal Medicine II, University Hospital of Munich, LMU Munich, Munich, Germany
[2]Institut für Experimentelle Endokrinologie, Charité-Universitätsmedizin Berlin, Berlin, Germany
[3]Leibniz Institute for Environmental Medicine, Düsseldorf, Germany
[4]Department of Nuclear Medicine, University Hospital of Munich, LMU Munich, Munich, Germany
[5]Department of Internal Medicine IV, University Hospital of Munich, LMU Munich, Munich, Germany
*KAS and AMM contributed equally

This chapter is a pre-copy-edited version of a peer-reviewed article published in the *Eur Thyroid J* **2015**;4:74-80.

Parts of this chapter are included in the doctoral thesis of Andrea M Müller. All the experiments, data collection, and data interpretation were performed by both Kathrin A Schmohl and Andrea M Müller in equal measure. The manuscript was written by Kathrin A Schmohl.

2.1 Abstract

Due to the high variance in available protocols on iodide-131 ablation in rodents, we set out to establish an effective method to generate a thyroid-ablated mouse model that allows the application of the sodium iodide symporter (NIS) as reporter gene without interference with thyroidal NIS. We tested a range of ^{131}I doses with and without pre-stimulation of thyroidal radioiodide uptake by low-iodine diet and TSH application. Efficacy of induction of hypothyroidism was tested by measurement of serum T4 concentrations, pituitary TSHβ and liver deiodinase type 1 (DIO1) mRNA expression, body weight analysis and ^{99m}Tc-pertechnetate scintigraphy.

While 200 µCi (7.4 MBq) ^{131}I alone was not sufficient to abolish thyroidal T4 production, 500 µCi (18.5 MBq) ^{131}I combined with one week of low-iodine diet decreased serum concentrations below the detection limit. However, the high ^{131}I dose resulted in severe side effects. A combination of one week of low-iodine diet, followed by injection of bovine TSH before the application of 150 µCi (5.5 MBq) ^{131}I, decreased serum T4 concentrations below the detection limit and significantly increased pituitary TSHβ concentrations. The systemic effects of induced hypothyroidism were shown by growth arrest and decrease in liver DIO1 expression below the detection limit. ^{99m}Tc-pertechnetate scintigraphy revealed absence of thyroidal ^{99m}Tc-pertechnetate uptake in ablated mice.

In summary, we report a revised protocol for radioiodide ablation of the thyroid gland in the mouse to generate an *in vivo* model that allows the study of thyroid hormone action using NIS as reporter gene.

2.2 Introduction

Mouse models of hypothyroidism increase our understanding of the mechanisms that regulate thyroid hormone action both during normal function and disease. Drug-induced hypothyroidism is a commonly used approach for assessment of thyroid hormone action in rodent models. An alternative approach makes use of the thyroid-lethal properties of the radionuclide iodide-131 to induce hypothyroidism. This is based on the ability of thyroid follicular cells to transport and concentrate radioactive iodide due to their expression of the sodium iodide symporter (NIS). Several non-thyroidal organs physiologically express NIS, such as salivary glands, gastric mucosa and lactating mammary glands and therefore possess the ability to actively transport iodide. They do not, however, organify and store it. These characteristics allow for high thyroid-specific cytotoxicity of ^{131}I with minimal side effects [88].

The first report of selective destruction of thyroid tissue by iodide-131 was published by Hamilton in 1942 [89]. Since then, numerous protocols for radioiodide ablation of the mouse thyroid gland have been published with broad variation of the thyroid-lethal dose of ^{131}I administered to mice ranging from 28 to 1000 µCi (1 to 37 MBq) in the presence or absence of stimulation of thyroidal iodide uptake by treatment with low-iodine diet for one to four weeks or exogenous TSH application prior to the administration of radioiodide [50, 90-98].

We and others have shown the potential of NIS as reporter gene for molecular imaging with a broad range of possible applications [66, 70, 77-79, 82, 83, 87, 99-102]. In our previous work, the role of NIS as a reporter gene allowed non-invasive multimodal imaging of functional NIS expression by ^{99m}Tc or ^{123}I scintigraphy as well as SPECT and ^{124}I PET imaging that correlated well with the results of *ex vivo* gamma counter measurements as well as NIS mRNA and protein analysis. Stem cells have been the object of research in gene and cellular therapies. To date, these studies have lacked detailed information about the exact *in vivo* biodistribution, survival and biological compartment of these cells in tissues. Genetically engineered mesenchymal stem cells that express NIS allow detailed, non-invasive *in vivo* tracking of stem cells from their initial deposition to survival, migration and differentiation by ^{123}I scintigraphy/SPECT and ^{124}I PET, as has been demonstrated in our previous work [66, 70]. Based on these studies, we are now employing this system to study thyroid hormone action on mesenchymal stem cell biology within the tumour microenvironment. In an effort to generate a thyroid-ablated mouse model for the NIS-based evaluation of thyroid hormone action avoiding interference with thyroidal NIS that underlies an exclusive regulation by TSH, in the current study we describe an effective protocol for thyroid radioiodide ablation in mice.

2.3 Materials and Methods

Animals

Male CD1 nu/nu mice from Charles River (Sulzfeld, Germany) were maintained under specific pathogen-free conditions with access to standard nude mouse diet (2.2 mg/kg iodine; ssniff, Soest, Germany) or low-iodine diet (LID; < 15 µg/kg iodine; ssniff) and tap water *ad libitum*. Animals were allowed to acclimatise for one week prior to the start of treatments. At the beginning of the experiments, mice weighed 25-30 g with an average body weight of 26.6 g ± 1.27 g (mean ± standard deviation). After the end of the experiments, animals were sacrificed and tissues and blood were taken for analysis. The experimental protocol was approved by the regional governmental commission for animals (Regierung von Oberbayern, Munich, Germany).

Thyroid radioiodide ablation

Mice were randomly assigned to different treatment groups. For thyroid ablation, animals received a single i.p. injection of 200 µCi (7.4 MBq; according to [96]; n=6), 500 µCi (18.5 MBq; according to [90]; n=6) or 150 µCi (5.5 MBq; according to [97, 98]; n=12) of carrier-free iodide-131 in 250 µl phosphate-buffered saline containing sodium thiosulfate as reducing agent (GE Healthcare, Braunschweig, Germany) or saline for control animals (n=6 for each experiment). Animals that received 500 µCi of ^{131}I were additionally put on LID one week prior to radioiodide application. Before administration of 150 µCi of ^{131}I, mice were fed LID for one week and, on day eight, received an i.p. injection of 10 mIU bovine TSH (Sigma, Munich, Germany) two hours before radioiodide application. A subset of radioiodide-ablated animals (n=6) received daily i.p. injections of 20 ng/g body weight T4 (Sigma) starting the day after the application of ^{131}I.

Serum T4 measurements

T4 concentrations were monitored in pooled serum samples from tail vein blood or in individual serum samples after sacrifice. Serum total T4 concentrations were measured in duplicate by radioimmunoassay using a commercially available kit (RIA-4524; DRG Instruments, Marburg, Germany) according to the manufacturer's instructions. The samples and calibrators were incubated with radiolabelled tracer in antibody-coated tubes. After incubation, the liquid was aspirated and the antibody-bound radiolabelled tracer was counted in a gamma counter (1277 Gammamaster; LKB Wallac, Turku, Finland). The limit of quantification was at 10 nM with an intra-assay coefficient of variation (CV) of 3.6% at 80 nM and 1.1% at 167 nM.

Whole-body planar ^{99m}Tc-pertechnetate scintigraphy

Two hours after i.p. injection of 500 µCi (18.5 MBq) ^{99m}Tc-pertechnetate, a gamma emitter that is also transported by NIS [102], ^{99m}Tc-pertechnetate accumulation was assessed using a gamma camera equipped with a low-energy high-resolution (LEHR) collimator (e.cam, Siemens, Munich, Germany).

Imaging studies were performed under inhalational anesthesia using an isofluorane vaporiser. Regions of interest were quantified and expressed as fraction of the injected dose of applied radionuclide in the cervical region.

RNA extraction and quantitative real-time PCR

After sacrifice, mouse pituitaries and livers were snap frozen on dry ice and stored at -80°C until further processing. Total RNA was prepared using the RNeasy Mini Kit with QIAshredder (Qiagen, Hilden, Germany) according to the manufacturer's instructions. Reverse transcription was performed using SuperScript III First-Strand Synthesis System (Invitrogen Life Technologies, Karlsruhe, Germany). Quantitative real-time PCR was run in duplicate with the QuantiTect SYBR Green PCR Kit (Qiagen) in a Mastercycler ep gradient S PCR cycler (Eppendorf, Hamburg, Germany). Relative expression levels of pituitary TSHβ and liver deiodinase type 1 (DIO1) were calculated from $\Delta\Delta C_t$ values normalised to internal β-actin and 18S rRNA. The following primers were used: *Actb*, forward 5'-AAGAGCTATGAGCTGCCTGA-3', reverse 5'-TACGGATGTCAACGTCACAC-3'; *R18s*, forward 5'-CGCAGCTAGGAATAATGGAA-3', reverse 5'-TCTGATCGTCTTCGAACCTC-3'; *Tshb*, forward 5'-GGGTATTGTATGACACGGGATA-3', reverse 5'-ATTTCCACCGTTCTGTAGATGA-3'; *Dio1*, forward 5'-AAGACAGGGCTGAGTTTGGG-3', reverse 5'-TGAGGAAATCGGCTGTGGAG-3'.

Statistical analysis

Every data point was generated using three to six mice per group. Values are reported as mean ± SEM or mean fold change ± SEM. Statistical significance of T4 and TSHβ concentrations was tested by two-tailed Student's t-test, that of body weight measurements by two-tailed Mann-Whitney U-test (*p<0.05; **p<0.01; ***p<0.001).

2.4 Results

^{131}I ablation and T4 measurements

Three different protocols for radioiodide ablation of the thyroid gland were compared with the aim to establish a thyroid-ablated mouse model of hypothyroidism. Four weeks after administration of a single dose of 200 µCi iodide-131, serum T4 concentrations had dropped by 50% in ablated mice compared to untreated control animals (**Fig. 4A**).

By increasing the ^{131}I dose to 500 µCi with additional treatment with LID for one week prior to ^{131}I application, serum T4 concentrations dropped below the limit of detection (<10 nM) as early as two weeks after radioiodide administration (**Fig. 4A**). However, starting at approximately one week after ablation, mice suffered from drastic weight loss and heavy breathing despite T4 supplementation in a subgroup of mice, and, as a result, had to be sacrificed (**Fig. 4B**).

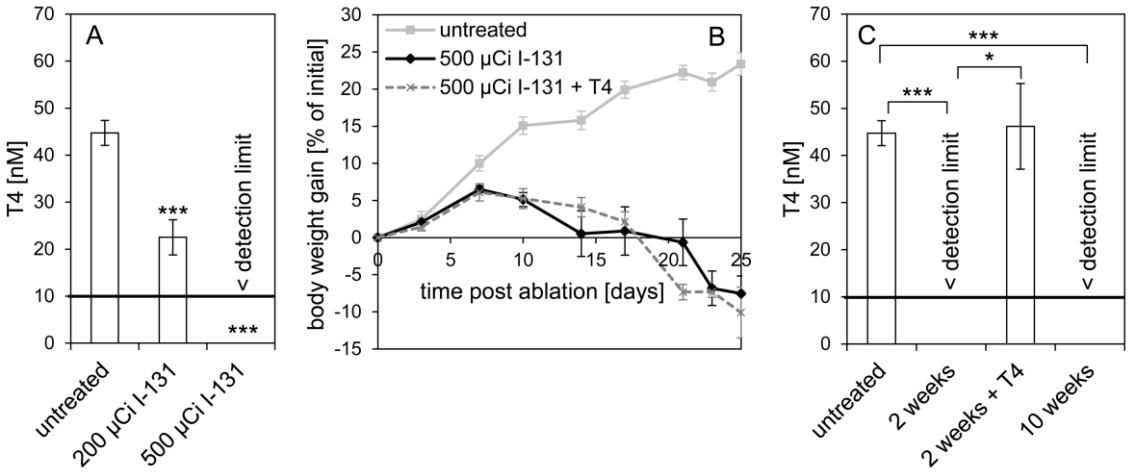

Figure 4. Comparison of radioiodide thyroid ablation protocols. (**A**) Serum T4 concentrations 4 weeks after injection of 200 µCi ^{131}I and 2 weeks after injection of 500 µCi ^{131}I combined with LID compared to untreated controls. The lower ^{131}I dose resulted in a 50 % reduction in serum T4 concentrations only, while the higher dose decreased T4 below the detection limit (<10 nM; ***p<0.001). (**B**) Mice injected with 500 µCi ^{131}I suffered weight loss irrespective of T4 supplementation and had to be sacrificed, while untreated control mice showed continuous growth. Results are expressed as % of initial body weight. (**C**) Serum T4 concentrations 2 and 10 weeks after treatment with LID/TSH/150 µCi ^{131}I compared to untreated controls and mice that additionally received 20 ng/g body weight T4. This treatment led to undetectable serum T4 concentrations as early as two weeks after ^{131}I application that remained undetectable after 10 weeks. T4 supplemented mice showed T4 concentrations in the range of the concentrations measured in untreated and therefore euthyroid control animals (*p<0.05; ***p<0.001).

The combination of one week of low-iodine diet and stimulation with TSH prior to administration of 150 µCi ^{131}I (LID/TSH/150 µCi ^{131}I), resulted in serum T4 concentrations below the detection limit within two weeks after ablation that remained stable until the end of the observation period (ten weeks after ablation; **Fig. 4C**). The ablated mice without T4 supplementation showed only minor side effects such as absence of weight gain (**Fig. 5B**) and slower movement in the cage. Therefore, all further experiments were conducted following this protocol. Serum T4 concentrations in the subgroup of mice that received T4 supplementation by daily i.p. injections of 20 ng T4 per gram body weight were in the same range as in the untreated euthyroid group of mice (**Fig. 4C**).

Monitoring of body weight and analysis of TSHβ and DIO1 mRNA expression

The drop in serum T4 concentrations in ablated mice coincided with a 48- and 45-fold increase, respectively, in pituitary TSHβ concentrations two and ten weeks after thyroid ablation, compared to untreated controls (**Fig. 5A**).

As a drop in serum T4 and elevation of pituitary TSH do not per se prove a systemic state of hypothyroidism, we additionally monitored body weight gain in ablated mice versus untreated control mice. Radioiodide-ablated mice showed an arrest in growth from around one week after ^{131}I injection, while untreated control animals continued to grow throughout the observation period (**Fig. 5B**). We also investigated expression of DIO1 in the liver as a second marker for systemic hypothyroidism. Four

weeks after ^{131}I application, liver DIO1 mRNA concentrations dropped below the detection limit with C_t values >40, whereas for control animals a mean C_t value of 26.11 ± 0.69 was measured with comparable reference gene concentrations between the two treatment groups.

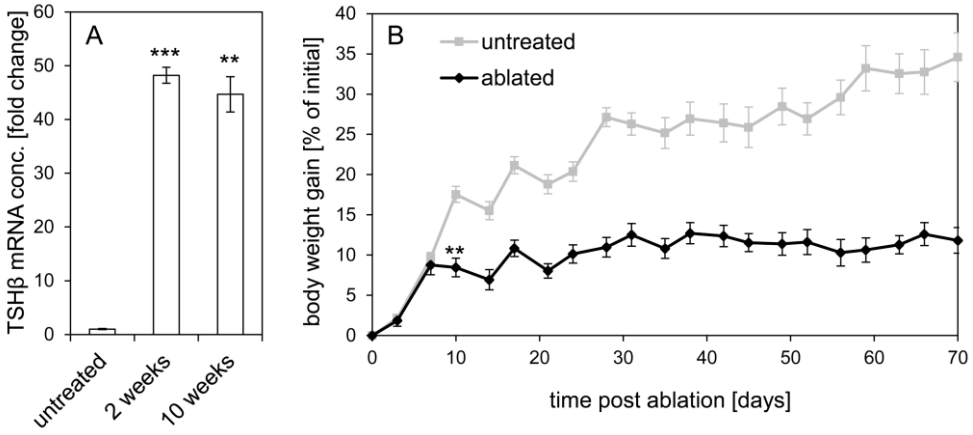

Figure 5. Pituitary TSHβ mRNA expression and body weight analysis. (**A**) 2 and 10 weeks after LID/TSH/150 µCi ^{131}I treatment, pituitary TSHβ mRNA concentrations were increased significantly to 48-fold and 45-fold, respectively, compared to untreated control mice (**p<0.01; ***p<0.001). conc.: concentration. (**B**) While control animals continued to grow throughout the observation period, LID/TSH/150 µCi ^{131}I-treated mice showed a growth arrest starting from around one week after thyroid ablation (day 0). Results are expressed as % of initial body weight (**p<0.01).

^{99m}Tc-pertechnetate whole body imaging

To examine the effects of ^{131}I ablation on thyroidal radioiodide uptake, we monitored ^{99m}Tc-pertechnetate biodistribution by gamma camera imaging. Significant ^{99m}Tc-pertechnetate accumulation was observed in tissues that physiologically express NIS, i.e. thyroid, salivary glands and stomach, as well as the urinary bladder due to renal elimination of the radionuclide (**Fig. 6A, B**).

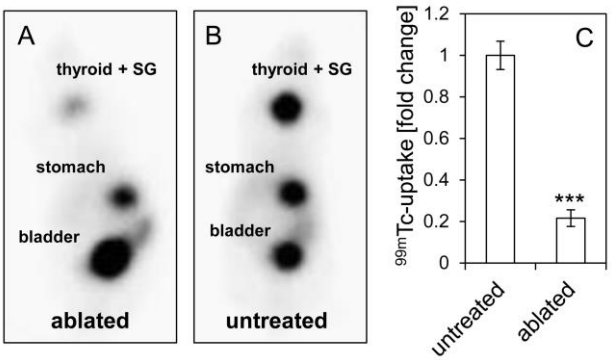

Figure 6. Whole body ^{99m}Tc-pertechnetate scintigraphy. 4 weeks after LID/TSH/150 µCi ^{131}I treatment, ^{99m}Tc-pertechnetate gamma camera imaging showed strongly reduced ^{99m}Tc-pertechnetate uptake in the neck region of ablated animals (approx. 3-5 % (**A**)) compared to untreated control animals (**B**). A representative image for both ablated mice and control mice is shown. SG: salivary glands. (**C**) Quantification of ^{99m}Tc-uptake in the cervical region. Results are expressed as fold change compared to untreated controls (***p<0.001).

Four weeks post ^{131}I injection, ^{99m}Tc-pertechnetate uptake was strongly reduced in the cervical region of ablated mice with a remaining ^{99m}Tc-pertechnetate uptake of approximately 3-5 % which was caused by the salivary glands that in mice are localised in the direct neighbourhood of the thyroid gland and physiologically express NIS (**Fig. 6A, C**) [103]. In comparison, untreated control mice accumulated approx. 35-40% of the injected dose in the cervical region (**Fig. 6B, C**).

2.5 Discussion

The aim of the current study was to generate a mouse model in which endogenous thyroid hormone production is abolished to create an experimental paradigm with a defined baseline for the evaluation of response to thyroid hormone that at the same time allows for the use of NIS as a reporter gene. While treatment of mice with anti-thyroid drugs in drinking water is a widely used approach to render mice hypothyroid, mice have to be treated throughout the experiment, a certain degree of variability remains due to differences in water intake and potential side effects of the drugs have to be taken into consideration [104, 105]. Furthermore, as this approach typically relies on a combination of thionamides (methimazole or propylthiouracil) that have been shown to affect thyroidal NIS expression [106], as well as the NIS-specific inhibitor perchlorate to block thyroid hormone synthesis, the use of NIS as reporter gene to study thyroid hormone action is limited in this setting.

Therefore, a reliable method of thyroid radioiodide ablation was developed in mice that exploits the ability of NIS to transport ^{131}I. This eliminates interference of reporter gene activity from thyroidal NIS that is exclusively regulated by TSH and therefore affected by the thyroid hormone status of the mouse. A literature search revealed a variety of protocols [50, 90-98]. As the "American Thyroid Association Guide to investigating thyroid hormone economy and action in rodent and cell models" [107] had just been published, we initially tested the protocol described there [96]. Here the recommended ^{131}I dose of 200 µCi was not sufficient to completely abolish endogenous thyroid hormone production. This was most likely due to insufficient accumulation of radioiodide in the thyroid, as mice were fed standard chow containing 2.2 mg/kg iodine, which competes with radioiodide for thyroidal uptake. We therefore increased the amount of ^{131}I to 500 µCi, a dose that was reported by Gorbman [90] to destroy thyroid tissue within 24 days after radioiodide application. In addition, we pretreated mice with low-iodine diet for one week prior to ^{131}I application to decrease thyroidal iodine content and increase thyroidal NIS expression to enhance the uptake of radioiodide into thyroid follicular cells. This treatment decreased serum T4 concentrations below the detection limit. However, mice showed severe side effects, i.e. drastic weight loss and breathing difficulties, starting from around one week after iodide injection irrespective of T4 supplementation, and had to be sacrificed prematurely. We assume that the relatively high dose of ^{131}I, while specifically concentrated in the thyroid, caused severe damage to the thyroid surrounding tissues, in particular the radiation-sensitive trachea. Due to the close proximity of these tissues to the thyroid and the thyroid's small size, the β-particles emitted by ^{131}I that have a path length

of up to 2.4 mm in tissue [108], can cause lesions in the trachea, recurrent laryngeal nerve and parathyroid glands, as was observed by Gorbman [91]. Furthermore, transient NIS-mediated transport of high doses of radioiodide across epithelia in the gastrointestinal tract may impair their function and lead to subsequent damage.

To avoid aforementioned problems, we adapted protocols published by Abel *et al.* and Barca-Mayo *et al.* [97, 98], where relatively low doses of ^{131}I were reported to be sufficient for total ablation of the thyroid gland under stimulation of ^{131}I uptake. We decided on a protocol consisting of one week of low-iodine diet, followed by an injection of bovine TSH on day eight, two hours before injection of 150 µCi of ^{131}I. We here show the efficacy of this protocol in inducing hypothyroidism in mice at the level of (1) the first indicators of a disruption of thyroid function, i.e. serum T4 concentrations and pituitary TSHβ content, (2) indicators of systemic hypothyroidism, i.e. growth arrest and decrease in liver DIO1 concentrations and (3) the thyroid itself by ^{99m}Tc-pertechnetate gamma camera imaging.

Two weeks after thyroid ablation serum T4 concentrations had dropped below the detection limit and as expected pituitary TSHβ concentrations reactively increased 48-fold compared to untreated control mice. At the end of the observation period, ten weeks after thyroid ablation, T4 concentrations remained undetectable and TSHβ concentrations remained high. As growth hormone secretion is thyroid hormone-sensitive in rodents [109], ablated mice showed an arrest in growth as a consequence of decreasing serum thyroid hormone concentrations, indicating systemic hypothyroidism. Another marker for systemic thyroid hormone status is the liver type 1 deiodinase that is downregulated in hypothyroidism [110]. Four weeks after thyroid ablation, liver DIO1 mRNA concentrations had dropped below the detection limit. Gamma camera imaging revealed a significant reduction in ^{99m}Tc-pertechnetate uptake in the cervical region four weeks after thyroid ablation, despite maximal TSH stimulation due to thyroid hormone deficiency in ablated animals. The low residual uptake originates from salivary glands that also physiologically express NIS [103, 111]. In mice, the submandibular-sublingual salivary gland complex is relatively large in relation to the thyroid and is located in the ventral cervical region in the direct neighbourhood of the thyroid, therefore causing an overlapping signal on ^{123}I or ^{99m}Tc-pertechnetate scintigraphies [112]. As salivary glands do not possess the ability to organify iodine, retention time of the thyroid-ablative dose of ^{131}I is limited. Thus, salivary glands are preserved, at least in part, as is their ability to accumulate ^{99m}Tc-pertechnetate, while thyroidal uptake is completely eliminated, as was shown by whole body and neck transaxial planar SPECT imaging by Choi *et al.* [113].

In conclusion, our data provide an effective protocol for radioiodide ablation of the thyroid gland that renders mice hypothyroid within the course of two weeks and abolishes thyroidal radioiodide uptake. Based on our findings, we recommend stimulation of NIS-mediated thyroidal iodide uptake by pretreatment with low-iodine diet and TSH application to help deliver a well-tolerated dose of 150 µCi of ^{131}I to mice for successful ablation of the thyroid gland.

2.6 Acknowledgements

We are grateful to E. K. Wirth, Institut für Experimentelle Endokrinologie, Charité-Universitätsmedizin Berlin, Berlin, Germany, for providing TSHβ primer sequences and J. Carlsen and R. Oos, Department of Nuclear Medicine, University Hospital of Munich, Munich, Germany, for their assistance with animal care.

This study was supported by grants from the Deutsche Forschungsgemeinschaft within the Priority Programme SPP1629 to C. Spitzweg and P. J. Nelson (SP 581/6-1), H. Heuer (HE 3418/7-1) and J. Köhrle (KO 922/17-1).

III. CHAPTER 2

Thyroid hormones and tetrac – new regulators of tumour stroma formation via integrin αvβ3

Kathrin A Schmohl[1], Andrea M Müller[1], Alexandra Wechselberger[2], Svenja Rühland[2,3], Nicole Salb[2], Nathalie Schwenk[1], Heike Heuer[4], Janette Carlsen[5], Burkhard Göke[1,6], Peter J Nelson[2] and Christine Spitzweg[1]

[1]Department of Internal Medicine II, University Hospital of Munich, LMU Munich, Munich, Germany
[2]Department of Internal Medicine IV, University Hospital of Munich, LMU Munich, Munich, Germany
[3]Department of Biology II, LMU Munich, Munich, Germany
[4]Leibniz Institute for Environmental Medicine, Düsseldorf, Germany
[5]Department of Nuclear Medicine, University Hospital of Munich, LMU Munich, Munich, Germany
[6]University Medical Center Hamburg-Eppendorf, Hamburg, Germany

This chapter is a pre-copy-edited version of a peer-reviewed article published in *Endocr Relat Cancer* **2015**;22:941-52.

3.1 Abstract

To improve our understanding of non-genomic, integrin αvβ3-mediated thyroid hormone action in tumour stroma formation, we examined the effects of T3, T4 and integrin-specific inhibitor tetrac on differentiation, migration and invasion of mesenchymal stem cells (MSCs) that are an integral part of the tumour's fibrovascular network. Primary human bone marrow-derived MSCs were treated with T3 or T4 in the presence of hepatocellular carcinoma (HCC) cell-conditioned medium, which resulted in stimulation of expression of genes associated with CAF-like differentiation as determined by qPCR and ELISA. In addition, T3 and T4 increased migration of MSCs towards HCC cell-conditioned medium and invasion into the centre of three-dimensional HCC cell spheroids. All these effects were tetrac-dependent and therefore integrin αvβ3-mediated. In a subcutaneous HCC xenograft model, MSCs showed significantly increased recruitment and invasion into tumours of hyperthyroid mice compared to euthyroid and in particular hypothyroid mice, while treatment with tetrac almost completely eliminated MSC recruitment. These studies significantly improve our understanding of the anti-tumour activity of tetrac, as well as the mechanisms that regulate MSC differentiation and recruitment in the context of tumour stroma formation as an important prerequisite for the utilisation of MSCs as gene delivery vehicles.

3.2 Introduction

Tumours are composed of malignant tumour cells and the 'benign' stromal compartment that contains many distinct cell types, including endothelial cells, smooth muscle cells, cells of the immune system, and pericytes/cancer-associated fibroblasts (CAFs) [114, 115]. As the tumour stroma plays a key role in cancer progression with effects on tumour cell proliferation, angiogenesis and metastasis, it has become an attractive target for tumour therapy. Thus, understanding the biology of the tumour microenvironment is becoming as important as knowledge of the neoplastic epithelial cells themselves.

Mesenchymal stem cells (MSCs) are multipotent non-hematopoietic progenitor cells that are characterised by their capacity to self-renew and differentiate into cells of connective tissue lineages such as bone, cartilage, muscle and adipose tissue [18, 116]. In the course of tissue injury or during chronic inflammation, MSCs contribute to tissue remodelling by their mobilisation and subsequent recruitment to the site of injury [18, 116]. Similarities between the wound healing process and tumour stroma formation have led to the suggestion that tumours are "wounds that do not heal" [9]. We and others have shown that MSCs are actively recruited to growing tumour stroma [66, 70, 117-120] mediated by high local concentrations of inflammatory chemokines and growth factors [18, 115, 121, 122]. This tumour tropism constitutes the basis for the 'Trojan horse' approach, in which MSCs are used as shuttle vectors to deliver therapeutic agents into growing tumours [18, 114, 123-126], as we have successfully demonstrated in our previous work using the sodium iodide symporter (NIS) [66, 70, 71] and herpes simplex virus type 1 thymidine kinase (HSV-TK) [118-120] as therapy genes in various tumour models.

Upon homing, MSCs act as important progenitors to subtypes that comprise the tumour stroma, including cells of the tumour vasculature and cancer-associated fibroblast- (CAF-) like cells [24]. A CAF-like phenotype is defined by the following sets of markers: (1) fibroblast surface markers; (2) indicators of tissue remodelling and invasion; (3) markers of angiogenesis; and (4) tumour promoting growth factors [19, 127, 128]. While it is now well established that MCSs play a major role in supporting tumour vasculature and forming the tumour's fibrovascular network, the exact mechanisms behind their migration and differentiation in the tumour microenvironment and their impact on tumour progression are not yet fully understood.

Thyroid hormones 3,3',5-triiodo-L-thyronine (T3) and L-thyroxine (T4) are regulators of differentiation, growth and metabolism in most healthy tissues, but they have also been proposed to play a critical role in tumour stroma formation by stimulation of angiogenesis, proliferation and inflammation [129, 130]. These effects have been shown to be transduced by non-genomic mechanisms via a plasma membrane receptor for thyroid hormone on integrin αvβ3 that was identified in 2005 by P.J. Davis and co-workers [33]. Integrin αvβ3 is predominantly concentrated in the plasma membrane of endothelial cells, vascular smooth muscle cells, osteoclasts and cancer cells, and is an attractive target for attempts

to manipulate tumour cell proliferation and tumour-related neovascularisation [131]. Tetraiodothyroacetic acid (tetrac), a deaminated T4 derivative, is a specific inhibitor of thyroid hormone action at the integrin site [33, 130].

There is growing evidence that iodothyronines act as 'non-classical' pro-angiogenic modulators and induce neovascularisation. Pro-angiogenic actions of T3 and T4 are initiated at the hormone receptor on integrin αvβ3, transduced by the MAPK/ERK pathway, and involve effects on basic fibroblast growth factor (FGF2), vascular endothelial growth factor (VEGF) and epidermal growth factor (EGF) secretion [13, 129]. As an inhibitor of T3/T4 binding to αvβ3, tetrac has been shown to inhibit angiogenic activity of thyroid hormones. In addition, αvβ3-mediated proliferative activity of T3 and T4 has been reported in various cancer cell lines. A recent uncontrolled observational study suggests that lowering of circulating T4 levels is correlated with prolonged survival of terminal stage cancer patients [58]. In contrast, tetrac exerts a tumour growth-inhibitory effect based on the inhibition of T3/T4 effects, but also on agonist-independent direct anti-angiogenic and pro-apoptotic effects [130, 132]. In this context, an array of genes has been identified in human cancer cells that are regulated by tetrac through αvβ3. This regulation includes stimulation of pro-apoptosis genes and downregulation of proto-oncogenes, cyclin genes, the *EGFR* gene, as well as genes in the Wnt/β-catenin pathway, such as *CTNNA1* and *CTNNA2* [133].

MSCs are key players in the tumour microenvironment and thyroid hormones have been shown to play a critical role in the regulation of tumour stoma formation. Therefore, in the current study we sought to investigate the non-genomic effects of T3, T4 and tetrac on important aspects of MSC biology in the tumour milieu, such as differentiation, migration, recruitment and invasion as a critical prerequisite for the application of MSCs as gene delivery vehicles.

3.3 Materials and Methods

Cell lines

Primary human bone marrow-derived CD34-negative MSCs (either prepared in house or provided by apceth, Munich, Germany) were isolated and characterised according to the minimal criteria for MSCs released by the International Society for Cellular Therapy [134]. MSCs were used from passage 2 to 8 for experiments. The integrin αvβ3-negative human hepatocellular carcinoma cell line HuH7 was authenticated and purchased from JCRB Cell Bank (Osaka, Japan) and passaged up to ten times in our laboratories. Both cell lines were grown in DMEM (Sigma-Aldrich, St. Louis, Missouri, USA) containing 10 % (v/v) fetal bovine serum (FBS; FBS Superior, Biochrom/Merck Millipore, Berlin, Germany), 100 U/ml penicillin/100 µg/ml streptomycin (Sigma-Aldrich) and 2 mM L-glutamine (Sigma-Aldrich) and maintained at 37 °C in a humidified 5 % (v/v) CO_2 atmosphere.

Thyroid hormone treatment *in vitro*

T3, T4 and tetrac were dissolved in 0.1 N NaOH at 1 mg/ml. 25 µM (T3 and T4) or 100 µM (tetrac) stock solutions were prepared in sterile culture medium and stored in working aliquots at -20 °C protected from light. For the preparation of conditioned medium (CM), HuH7 were grown for 48 h to 80 % confluence in DMEM containing 10 % (v/v) charcoal-stripped FBS (csFBS; T3: <0.2 pg/ml, T4: 0.2-0.6 ng/dl). Supernatant was removed and centrifuged to eliminate cell debris. Prior to thyroid hormone treatment, MSCs were grown in DMEM/csFBS for 24 hours. Medium was changed to 80 % (v/v) DMEM/csFBS and 20 % (v/v) HuH7 CM for differentiation studies or DMEM/csFBS for migration and invasion studies and supplemented with 1 nM T3 or 1 µM T4 with and without 100 nM tetrac for 24 h. In a pilot study ranges of 1-100 nM T3 as well as 1-1000 nM T4 were tested and optimal concentrations of 1 nM total T3 (~ 30 pM free T3) and 1 µM total T4 (~ 1.5 nM free T4) were used for further experiments.

Flow cytometry

For flow cytometry, MSCs and HuH7 were harvested with EDTA (Sigma-Aldrich) and washed with PBS (Sigma-Aldrich) supplemented with 10 % (v/v) FBS (FACS buffer). Cells were incubated with a mouse monoclonal anti-integrin αvβ3 antibody (2 µg/10^6 cells; Abcam, Cambridge, UK) for 45 min on ice, washed with FACS buffer and then incubated with a Cy3-conjugated polyclonal donkey anti-mouse antibody (2 µg/10^6 cells; Jackson, Baltimore, USA) for 30 min on ice. Cells incubated without the primary antibody served as negative control. Analysis was performed in the FL2 channel of a BD Accuri C6 flow cytometer using Cflow software (BD Biosciences, Franklin Lakes, USA). 10^5 events were recorded for each sample. Cell debris was excluded from analysis by appropriate gating.

Quantitative real-time PCR

Total RNA from MSCs was prepared using the RNeasy Mini Kit with QIAshredder (Qiagen, Hilden, Germany). Reverse transcription and quantitative real-time PCR were performed as described previously [70] and run in a Mastercycler ep gradient S PCR cycler (Eppendorf, Hamburg, Germany). Relative expression levels were calculated from $\Delta\Delta C_t$ values normalised to internal β-actin and 18S rRNA. Primers are listed in table 1.

ELISA

Supernatant from MSCs was removed, centrifuged and stored at -80 °C until assayed for EGF, FGF2, hepatocyte growth factor (HGF), interleukin 6 (IL-6), stromal-derived factor 1 (SDF-1), transforming growth factor β1 (TGF-β1), thrombospondin 1 (TSP1) and VEGF concentrations using the respective DuoSet ELISA kit (R&D Systems, Abingdon, UK). Contributions from medium and HuH7 CM were subtracted.

Migration assay

MSC migration was analysed using the µ-slide Chemotaxis^{3D} system from ibidi (Martinsried, Germany). MSCs were seeded in collagen I (0.3×10^6 cells/ml) and subjected to a gradient between serum-free unconditioned medium and serum-free HuH7 CM. Both media and the collagen gel contained either no thyroid hormone, 1 nM T3 or 1 µM T4 with and without 100 nM tetrac. Chemotaxis was monitored by time-lapse microscopy over a 24 h period on a Leica DM IL microscope (Leica Microsystems, Wetzlar, Germany). Pictures were taken every 15 min with a Jenoptik ProgRes CCD camera (Jenoptik, Jena, Germany) controlled by the open source ImageJ (NIH, Bethesda, Maryland, USA) plug-in µManager [135]. 25 randomly selected cells were manually tracked with the ImageJ plug-in Manual Tracking (Fabrice Cordelières, Orsay, France) and analysed with Chemotaxis and Migration Tool software (ibidi). The migratory behaviour of cells was quantified by forward migration index (FMI), a measure of the efficiency of the migration of cells in relation to the CM gradient and centre of mass (CoM) displacement that is calculated from the averaged point of all cell endpoints.

Table 1. qPCR primer sequences.

gene	forward primer (5' → 3')	reverse primer (5' → 3')
ACTA2 (α-SMA)	ACCCACAATGTCCCCATCTA	GAAGGAATAGCCACGCTCAG
ACTB (β-actin)	AGAAAATCTGGCACCACACC	TAGCACAGCCTGGATAGCAA
CXCL12 (SDF-1)	AGAGCCAACGTCAAGCATCT	CTTTAGCTTCGGGTCAATGC
DES (desmin)	AAGCTGCAGGAGGAGATTCA	GGCAGTGAGGTCTGGCTTAG
EGF	CAGGGAAGATGACCACCACT	CAGTTCCCACCACTTCAGGT
FAP	GGTCTCCCAACAAAGGATGA	CATTGCCTGGAAATCCACTT
FGF2	GGAGAAGAGCGACCCTCAC	AGCCAGGTAACGGTTAGCAC
HGF	CTGGTTCCCCTTCAATAGCA	CTCCAGGGCTGACATTTGAT
IL6	TACCCCCAGGAGAAGATTCC	TTTTCTGCCAGTGCCTCTTT
MMP3 (SL-1)	GCAGTTTGCTCAGCCTATCC	GAGTGTCGGAGTCCAGCTTC
R18s	CAGCCACCCGAGATTGAGCA	TAGTAGCGACGGGCGGTGTG
S100A4 (FSP1)	CCCTGGATGTGATGGTGTCC	CGATGCAGGACAGGAAGACA
TGFB1 (TGF-β1)	CAGCACGTGGAGCTGTACC	AAGATAACCACTCTGGCGAGTC
THBS1 (TSP1)	TTGTCTTTGGAACCACACCA	CTGGACAGCTCATCACAGGA
TNC	TTCACTGGAGCTGACTGTGG	TAGGGCAGCTCATGTCACTG
VEGF	CTACCTCCACCATGCCAAGT	ATGATTCTGCCCTCCTCCTT

Spheroid invasion assay

Invasion assays were performed as described previously [136-139]. In brief, spheroids of 200-300 µm in diameter were grown from HuH7 cells. Single spheroids were rolled in 2.5×104 thyroid hormone-treated, CellTracker Green CMFDA- (5-chloromethylfluorescein diacetate, Life Technologies) labelled MSCs for 2 h, washed and incubated for further 24 h. Spheroids were fixed in 4% formalin, embedded in 1 % (w/v) 2-hydroxyethylagarose (Roth, Karlsruhe, Germany) containing green fluorescent microspheres (F-XC 50 Estapor, Merck, Darmstadt, Germany; 1:50,000 dilution) and aspirated into a

glass capillary. Imaging was performed with a 488 nm laser (2 mW laser power, 120 ms exposure time; Cube, Coherent, Santa Clara, California, USA) and an sCMOS camera (Orca-flash 4.0 V2, Hamamatsu, Hamamatsu City, Japan) from 5 different angles equally spaced over 360°, controlled via the FIJI µManager plug-in [135]. The subsequent registration of beads and fusion of images was performed using SPIM open source software on FIJI [140]. Signals from CMFDA-labelled MSCs and the autofluorescent spheroid were detected and segmented using the FIJI 3D object counter plugin [141]. Invasion depths were quantified by measurement of distances from the centre of each MSC to the border of the spheroid using the FIJI 3D manager plugin [142].

Animals

Male CD1 nu/nu mice from Charles River (Sulzfeld, Germany) were maintained under specific pathogen-free conditions with access to standard nude mouse diet (ssniff, Soest, Germany) and water ad libitum. Animals were allowed to acclimatise for one week prior to the start of treatments. Experiments were conducted with animals between 5-12 weeks of age. Thyroid hormone status was regularly monitored in serum samples as described previously [143]. The experimental protocol was approved by the regional governmental commission for animals (Regierung von Oberbayern, Munich, Germany).

MSC recruitment to tumours *in vivo*

HuH7 xenograft tumours were established by subcutaneous injection of 3.5×10^6 HuH7 cells in 100 µl PBS into the flank region. Three days later, animals received drinking water supplemented with 0.02 % (w/v) 2-mercapto-1-methylimidazole (MMI; Sigma-Aldrich), 1 % (w/v) sodium perchlorate (Sigma-Aldrich) and 0.3 % (w/v) saccharin (Sigma-Aldrich) [144] to induce hypothyroidism to generate the same baseline thyroid hormone levels for all groups. Three weeks later, once small tumours (<3 mm) were visible, mice were randomly assigned to different groups by daily intraperitoneal injections. The hyperthyroid group (n = 8) received 100 ng/g body weight L-T4 (Sigma-Aldrich), the euthyroid group 20 ng/g body weight L-T4 with (n = 8) or without (n = 7) 10 µg/g body weight tetrac (Sigma-Aldrich), hypothyroid animals (n = 8) received saline only. 18 days later (tumour volume approx. 500 mm^3) 5×10^5 MSCs cytoplasmically labelled with 20 µM CMFDA for 30 min were injected via the tail vein in 500 µl PBS. 72 h later, mice were sacrificed and tumours were embedded in Tissue-Tek O.C.T. compound (Sakura Finetek, Alphen aan den Rijn, The Netherlands), snap-frozen on dry ice and stored at -80 °C.

Immunofluorescence microscopy

Tissue sections were fixed in methanol/acetone, counterstained with 5 µg/ml bisbenzimide Hoechst 33258 (Sigma-Aldrich), mounted with Dako Fluorescence Mounting Medium (Dako, Carpinteria, California, USA) and imaged at 10× magnification on an Axiovert 135 TV fluorescence microscope equipped with an AxioCam MRm CCD camera and AxioVision Rel. 4.8 software (Carl Zeiss, Munich, Germany). 4-7 visual fields in perivascular regions were recorded per animal and MSC recruitment was

quantified as percentage of CMFDA positive area using ImageJ software (NIH, Bethesda, Maryland, USA).

Statistics

All *in vitro* experiments were performed at least in triplicate. *In vivo* data were generated in two independent experiments. Values are reported as mean ± SEM or mean fold change ± SEM. Statistical significance was tested by two-tailed Student's t-test or, for invasion assays, by Kruskal-Wallis test. p-values <0.05 were considered significant (*p<0.05; **p<0.01; ***p<0.001).

3.4 Results

Expression of integrin αvβ3 is absent on HuH7 cells and not influenced by thyroid hormones T3 and T4 or tetrac in MSCs

Absence of integrin αvβ3 expression on HuH7, as well as presence of αvβ3 on MSCs was confirmed by flow cytometry (**Fig. 7**). Treatment of MSCs with 1 nM T3 or 1 µM T4 in the presence or absence of tetrac (100 nM) or tetrac alone did not alter expression levels of the integrin (**Fig. 7**).

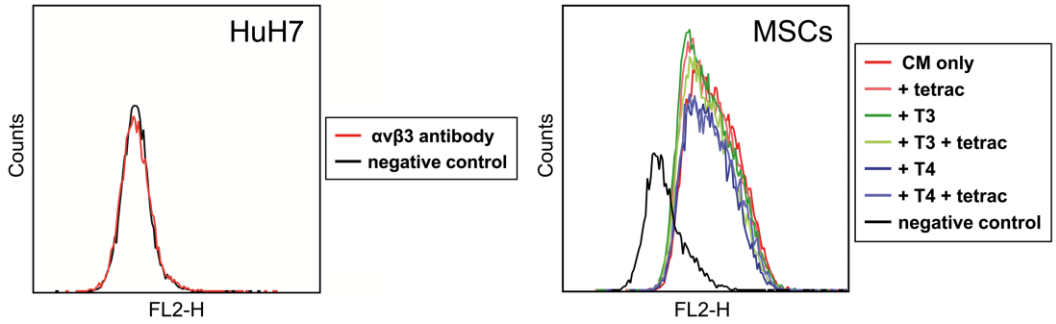

Figure 7. Evaluation of integrin αvβ3 expression on HuH7 and MSCs. MSCs were treated with HuH7 CM alone or in the presence of 1 nM T3 or 1 µM T4 with or without 100 nM tetrac, or in the presence of tetrac alone for 24 h. HuH7 and MSCs were analysed for integrin αvβ3 expression by flow cytometry. A representative image from three experiments is shown.

Thyroid hormones T3 and T4 increase CAF-like differentiation of MSCs *in vitro*

24 h stimulation of MSCs with HuH7 CM in the presence of 1 nM T3 or 1 µM T4 resulted in significantly increased mRNA levels for genes associated with a CAF-like phenotype. Upon T3 treatment, surface marker fibroblast-specific protein 1 (FSP1; S100A4), markers of angiogenesis desmin and VEGF, as well as tumour-promoting growth factors EGF, FGF2, HGF, IL-6, SDF-1 and TGF-β1 were expressed at significantly higher mRNA levels as compared to control cells treated with HuH7 CM alone. Surface marker fibroblast activation protein (FAP), indicators of tissue remodelling and invasion tenascin-C (TN-C) and TSP1 (THBS1), as well as the angiogenesis marker α-smooth muscle actin (α-SMA; ACTA2) showed the same trend that was, however, not significant (**Fig. 8A**). T4 stimulation led to

significant increases in mRNA expression for FAP, TN-C, TSP1, α-SMA and desmin, as well as FGF2, IL-6, SDF-1 and TGF-β1, while the same, albeit not significant trends were seen for FSP1, VEGF, EGF and HGF (**Fig. 8B**). Marker of invasion and remodelling stromelysin-1 (SL-1/MMP3) was not detected for any of the conditions tested (not shown).

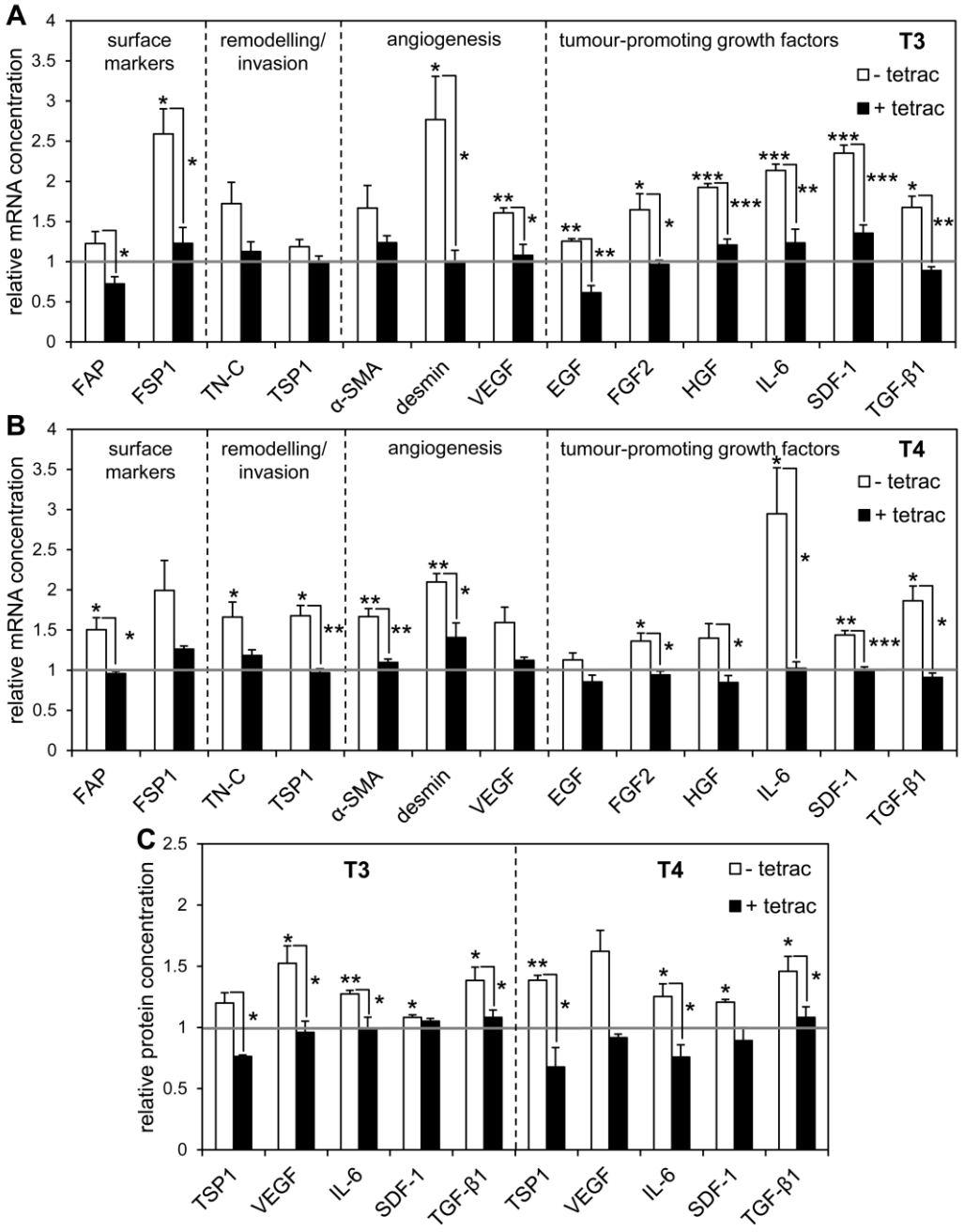

Figure 8. Expression of CAF-like markers in MSCs is stimulated by thyroid hormones T3 and T4 via integrin αvβ3. MSCs were treated with HuH7 CM alone (grey line) or in the presence of 1 nM T3 or 1 µM T4 with or without 100 nM tetrac, or in the presence of tetrac alone for 24 h. Expression of CAF-like markers was assessed at the mRNA level by qPCR ((**A**) T3, (**B**) T4) and at the protein level by ELISA (**C**). Results are expressed as mean fold change compared to control cells treated with HuH7 CM only (n = 4; two-tailed Student's t-test: *p<0.05; **p<0.01; ***p<0.001).

Effects seen at the mRNA level were confirmed at the protein level for TSP1, VEGF, IL-6, SDF-1 and TGF-β1 by ELISA (**Fig. 8C**). Protein levels for EGF, FGF2 and HGF remained below the detection limit of the ELISA kits used for all treatment conditions. The T3- and T4-triggered increases in gene and protein concentrations were found to be tetrac-dependent and therefore αvβ3-mediated. No significant changes were observed when cells were treated with tetrac alone (data not shown).

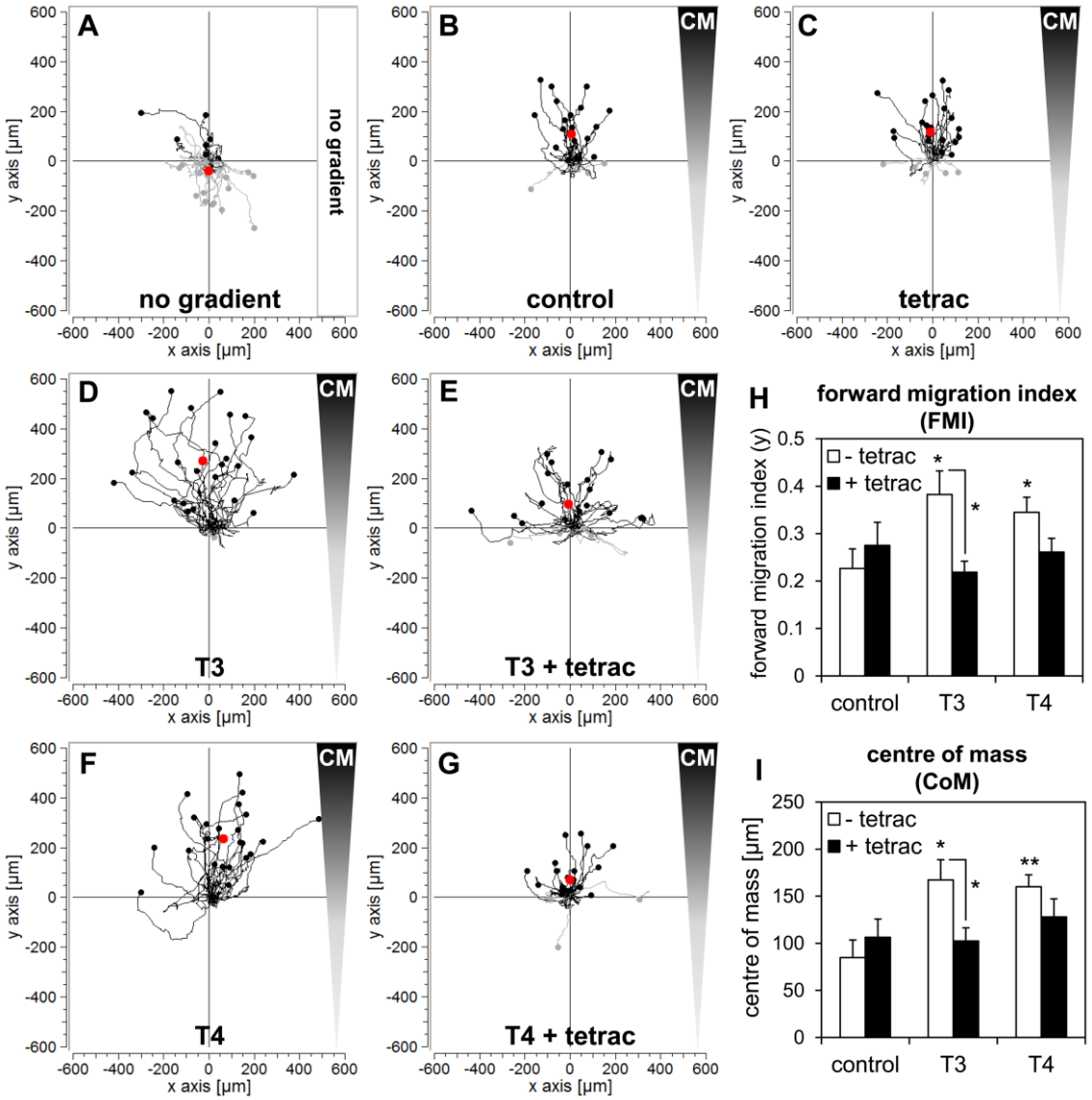

Figure 9. Migration of MSCs towards tumour cell CM is increased upon T3 and T4 treatment mediated by integrin αvβ3. (**A**) Representative trajectories of untreated MSCs without gradient influence. (**B-G**) Representative trajectories of MSCs treated with 1 nM T3 or 1 µM T4 with or without 100 nM tetrac or with tetrac alone for 24 h migrating along a linear gradient of HuH7 CM over 24 h compared to untreated control cells from six independent experiments. Centres of mass are indicated by red dots. (**H, I**) Quantification of chemotaxis parameters FMI and CoM (two-tailed Student's t-test: *p<0.05; **p<0.01).

Thyroid hormones T3 and T4 increase migration of MSCs towards tumour signals

MSCs subjected to a gradient between HuH7 CM and serum-free medium showed directed chemotaxis towards CM with significantly increased FMI and CoM displacement along the gradient of 0.227 ± 0.041 (p<0.001) and 84.7 ± 18.8 µm (p<0.001), respectively (**Fig. 9B, H, I**), compared to untreated cells not subjected to a gradient that showed basal random chemokinesis (FMI -0.060 ± 0.025 and CoM -26.8 ± 11.3 µm; **Fig. 9A**). This set-up was used to analyse the effects of T3, T4 and tetrac on the migratory behaviour of MSCs towards HuH7 CM. MSCs were pretreated with thyroid hormone with or without tetrac for 24 h and kept under the same T3/T4/tetrac concentrations throughout the chemotaxis assay. Migration of MSCs towards CM was significantly increased upon treatment with 1 nM T3 (FMI: 0.383 ± 0.049; p<0.05 and CoM 167.3 ± 21.2 µm; p<0.05; **Fig. 9D, H, I**) or 1 µM T4 (FMI: 0.345 ± 0.032; p<0.05 and CoM 160.0 ± 12.8 µm; p<0.01; **Fig. 9F, H, I**) compared to untreated control cells. Additional treatment with 100 nM tetrac inhibited the effects of T3 and T4, respectively, on MSC migration (T3 + tetrac: FMI: 0.219 ± 0.023; p<0.05 vs. T3 and CoM 102.5 ± 13.8 µm; p<0.05 vs. T3; **Fig. 9E, H, I**; T4 + tetrac: FMI: 0.261 ± 0.029; p=0.055 vs. T4 and CoM 127.9 ± 19.2 µm; p=0.16 vs. T4; **Fig. 9G, H, I**). Cells treated with tetrac alone showed no significant change in migratory behaviour compared to control cells (FMI: 0.275 ± 0.049; p=0.47 and CoM 106.3 ± 19.4 µm; p=0.44; **Fig. 9C**).

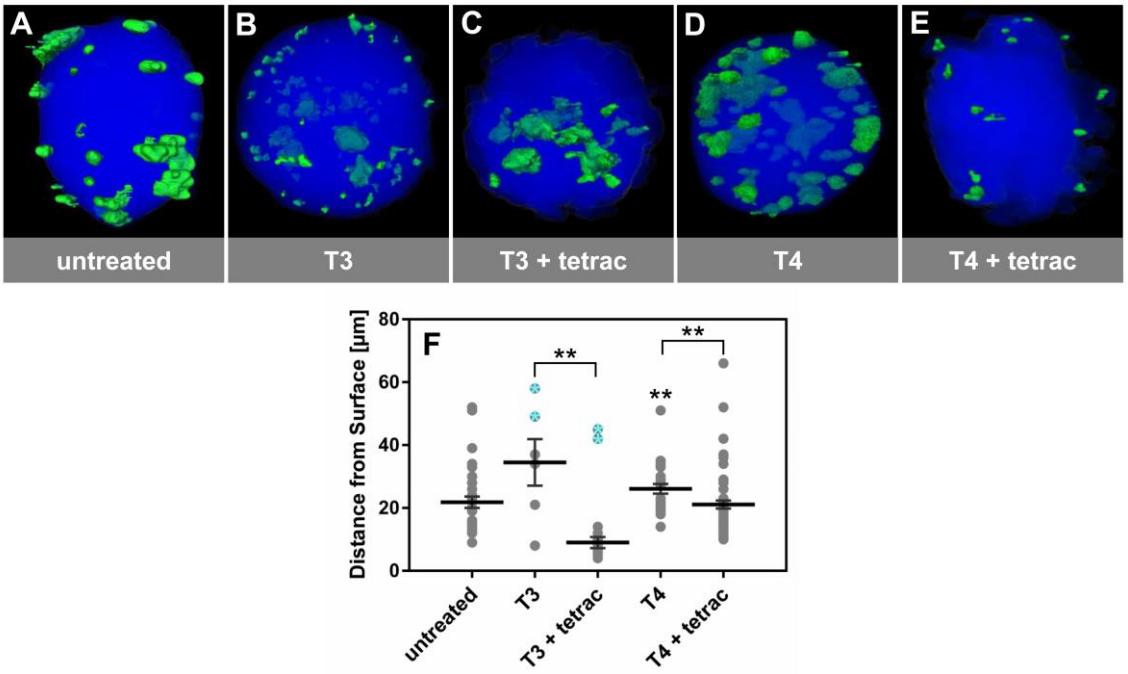

Figure 10. Deeper invasion of MSCs into 3D HuH7 spheroids upon T3 and T4 treatment is reversed upon additional treatment with tetrac. (**A-E**) Representative images of CMFDA-labelled MSCs (green) treated with 1 nM T3 or 1 µM T4 with or without 100 nM tetrac for 24 h invading into HuH7 spheroids (blue). (**F**) Quantification of invasion depths in distance from surface of the spheroid (n = 3; Kruskal-Wallis test: **p<0.01). Cell clusters are indicated by asterisks.

Thyroid hormones T3 and T4 increase invasion of MSCs into tumour cell spheroids

The invasive capacity of MSCs was evaluated in a three-dimensional HuH7 spheroid model. MSCs were pretreated with 1 nM T3 or 1 µM T4 in the presence or absence of 100 nM tetrac before attaching to spheroids. Both after T3 (**Fig. 10B**) and T4 stimulation (**Fig. 10D**), MSCs showed deeper invasion (T3: 34.5 ± 7.42 µm; p=0.15 and T4: 29.00 ± 1.37 µm; $p<0.01$) into the centre of spheroids compared to untreated control cells (21.83 ± 1.79 µm; **Fig. 10A, F**). Cells treated with T3 or T4 in the presence of tetrac (T3 + tetrac: 9.00 ± 1.78 µm; $p<0.05$ vs. T3 and T4 + tetrac: 22.25 ± 1.55 µm; $p<0.01$ vs. T4) showed inhibition of invasion and remained at the surface (**Fig. 10C, E, F**). In some cases, especially after T3 treatment, invaded cells clustered inside the spheroid and could not be resolved to single cells. Clusters (marked by asterisks in Fig. **10F**) were therefore counted as single cells.

T4 increases tumour migration and invasion *in vivo*

To assess the effect of thyroid hormone status and tetrac on MSC recruitment and invasion into tumours *in vivo*, nude mice harbouring HuH7 xenografts were subjected to different thyroid hormone treatments (euthyroid, hyperthyroid, hypothyroid and euthyroid + tetrac; for serum thyroid hormone concentrations see **Fig. 11C**) and, 72 h before sacrifice, were systemically injected with 5×10^5 CMFDA-labelled MSCs. Immunofluorescence microscopy (**Fig. 11A**) revealed significantly increased recruitment of MSCs to perivascular regions in the tumour and invasion into the surrounding tumour tissue in hyperthyroid mice (CMFDA positive area 25.7 ± 2.1%; $p<0.001$; **Fig. 11B**) compared to euthyroid mice (CMFDA positive area 12.2 ± 1.0%; **Fig. 11B**). In hypothyroid mice recruitment and invasion were strikingly reduced (CMFDA positive area 6.7 ± 0.7%; $p<0.001$; **Fig. 11B**). Treatment of euthyroid mice with tetrac resulted in an additional reduction in MSC recruitment revealing only a thin margin of MSCs surrounding blood vessels and no detectable tissue invasion (CMFDA positive area 2.0 ± 0.2%; $p<0.001$; **Fig. 11B**). Neither thyroid hormone status nor tetrac treatment had a significant effect on tumour growth in this model (data not shown).

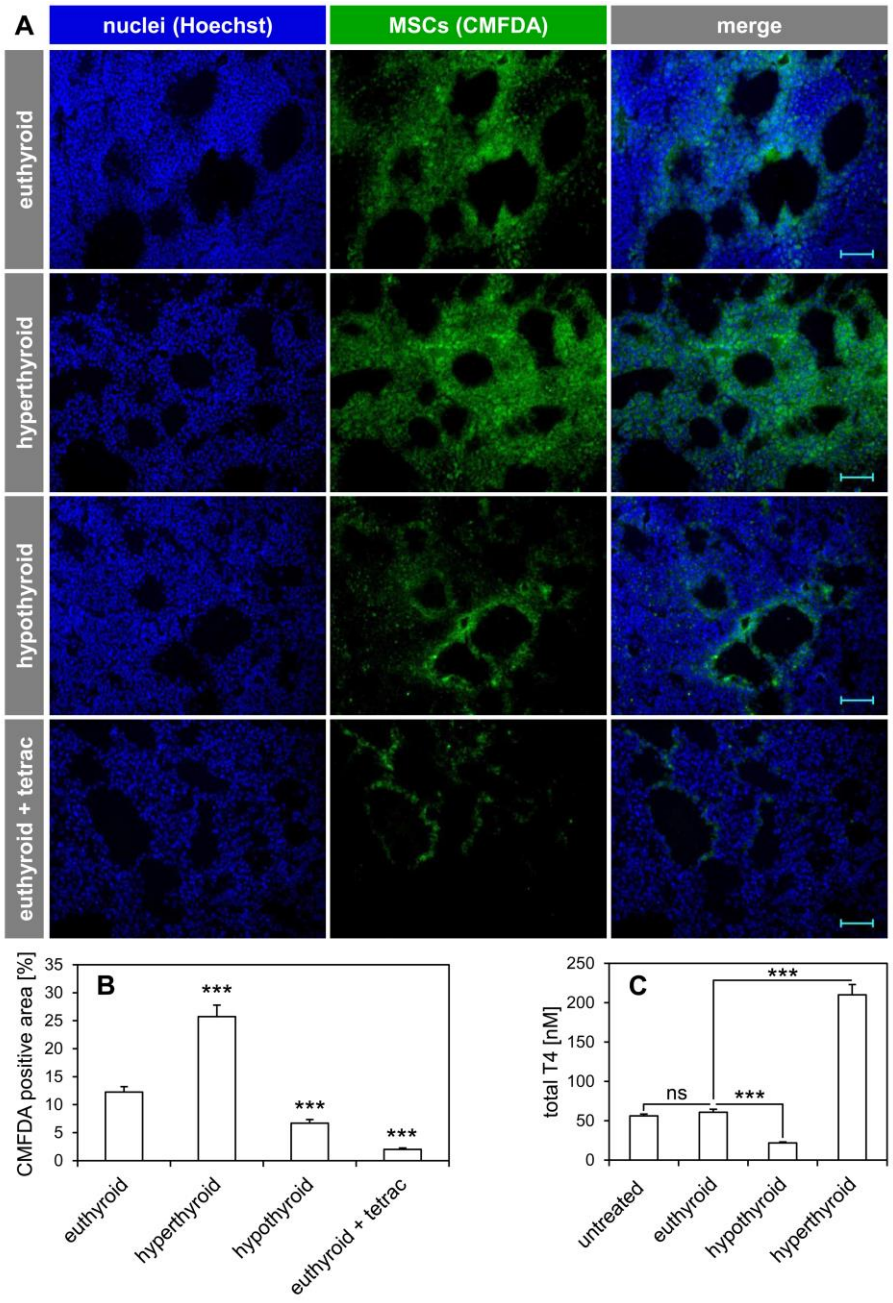

Figure 11. Thyroid hormone status significantly influences MSC recruitment into tumours *in vivo*. In a HuH7 tumour xenograft model, mice were injected daily with 20 ng/g body weight L-T4 (euthyroid; n = 7), 100 ng/g body weight L-T4 (hyperthyroid; n = 8), saline (hypothyroid; n = 8) or 20 ng/g body weight L-T4 + 10 µg/g body weight tetrac (euthyroid + tetrac; n = 8). 72 h before sacrifice, 5×10^5 CMFDA-labelled MSCs were injected i.v. Frozen tumour sections were counterstained with Hoechst dye and imaged by fluorescence microscopy. (**A**) One representative image is shown per group. Magnification: 10×, scale bar = 100 µm. (**B**) Quantification of MSC recruitment to tumours depicted as mean values of CMFDA positive area in % for each group (two-tailed Student's t-test: ***p<0.001). (**C**) Serum total T4 levels of the different treatment groups compared to untreated euthyroid mice (two-tailed Student's t-test: ***p<0.001; ns: not significant).

3.5 Discussion

Based on the fact that both MSCs and thyroid hormones impact crucial steps of tumour stroma formation [24, 130], we investigated the regulation of MSC biology in the tumour microenvironment by non-genomic effects of T3, T4 and tetrac. To distinguish between effects on MSCs/stroma biology as opposed to direct effects on tumour, we selected an αvβ3-negative hepatocellular carcinoma as an experimental model [145].

First we addressed the question as to whether thyroid hormones can enhance the CAF-like phenotype that MSCs acquire when exposed to tumour cell-conditioned medium [19, 24, 127]. Compared to MSCs treated with HuH7 CM alone, upon additional treatment with T3 or T4 we observed an overall enhanced expression of (1) fibroblast surface markers FAP and FSP; (2) indicators of tissue remodelling and invasion TN-C and TSP1; (3) proteins associated with angiogenesis α-SMA, desmin and VEGF; and (4) tumour-promoting growth factors/chemokines EGF, FGF2, HGF, IL-6, SDF-1 and TGF-β1, suggesting a T3/T4-enhanced CAF-like differentiation of MSCs mediated through αvβ3 as shown by inhibition of these effects by tetrac.

In line with our observations, transduction of the thyroid hormone signal via integrin αvβ3 was shown to lead to transcription of angiogenesis relevant genes FGF2 and VEGF in the chorioallantoic membrane (CAM) model, as well as in heart and T-cell lymphoma [129, 146]. A direct effect of thyroid hormones on inflammatory mediators such as IL-6 has been tentatively proposed based on the inhibition of pro-inflammatory cytokines by the iodothyronine antagonist tetrac [147]. Integrin αvβ3 has been shown to engage in crosstalk with tyrosine kinase growth factor receptors such as EGF receptor, FGF receptor, platelet-derived growth factor (PDGF) receptor and VEGF receptor that are all expressed by MSCs [115, 130, 147]. Explanations for the changes in the expression levels of markers of CAF-like differentiation shown here could involve binding of CM-derived growth factors to their respective receptors on MSCs or autocrine stimulation by growth factors secreted by MSCs in response to CM, with potentiation of the signal through integrin αvβ3 crosstalk. A further indirect effect could involve an enhanced expression of hypoxia-inducible factor 1α (HIF-1α) that was shown to be increased upon T3 binding to integrin αvβ3 transduced by the phosphoinositide 3-kinase (PI3K) pathway, which in turn stimulates the secretion of HIF-responsive genes, such as *VEGF*, *FGF2*, *IL6*, *SDF1* and *TGFB1* [130, 147]. However, the exact mechanisms behind the synergistic effects of CM and T3/T4 on MSC differentiation remain to be elucidated.

In addition, we observed enhanced chemotaxis of MSCs towards tumour signals and invasion into three-dimensional HCC cell spheroids under thyroid hormone stimulation, mediated by αvβ3. Balzan et al. [148] reported similar effects on microvascular endothelial cells in a wound healing assay with increased migration after T3 or T4 stimulation that was abolished by treatment with tetrac. Studies on multiple myeloma cells and bone marrow aspirates from multiple myeloma patients by Cohen and co-workers [149] illustrate thyroid hormone-dependent, αvβ3-mediated regulation of cell migration. Furthermore,

there is growing evidence that thyroid hormones increase the motility of αvβ3-expressing immune cells, and, possibly by similar mechanisms, nerve cell migration [150]. An array of growth factors, including PDGF, insulin-like growth factor 1 (IGF-1), HGF, EGF and VEGF, as well as chemokines, such as RANTES/CCL5, CCL22 and, to a lower extent, SDF-1/CXCL12 and their respective receptors have been implicated in MSC migration [115, 121] and many of these have been shown in this and other studies to be regulated by thyroid hormones via differential gene expression and receptor crosstalk [130, 147].

Modulation of recruitment and engraftment efficiency of MSCs is of clinical interest, in settings of tissue regeneration, in the context of general tumour growth and the emerging field of MSC-based gene delivery in cancer therapy [66, 70, 151]. As the tumour stroma plays such a key role in tumour growth, angiogenesis and metastatic potential, it has become an important target for tumour therapy. Due to their natural tropism for solid tumours and metastases, as well as their relative ease of engineering and expansion in vitro, MSCs are excellent gene delivery vehicles to target tumour environments. In a series of previous studies we demonstrated active homing of HSV-TK-transduced MSCs into pancreatic, breast and liver cancer tumour stroma that led to a significant reduction in tumour growth and, depending on the targeting strategy used, reduced incidence of metastases after application of ganciclovir [118-120]. In more recent studies we have shown that MSCs transfected with NIS under control of the CMV promoter or the tumour stroma-specific RANTES/CCL5 promoter are actively recruited to experimental hepatocellular carcinoma as well as disseminated colon cancer liver metastases and induce anti-tumour effects after application of ^{131}I or ^{188}Re based on NIS-mediated radioiodine accumulation [66, 70]. However, full therapeutic potential can only be exploited when MSCs are efficiently recruited to their site of action. Several approaches have been used to increase MSC survival, migration and differentiation, including the application of growth factors and overexpression of stem cell regulatory genes [152]. In agreement with our in vitro data, we observed a significant impact of thyroid hormone status on MSC recruitment and invasion in an αvβ3-negative HCC xenograft mouse model. In hyperthyroid animals both recruitment of MSCs and their subsequent invasion into tumours was markedly enhanced in comparison with euthyroid and in particular hypothyroid mice that showed low levels of MSC recruitment and almost no invasion. These data suggest that MSC conditioning with T3 or T4 and/or T3 or T4 treatment of patients could serve as an effective tool to enhance MSC migration and engraftment in tissue engineering and gene delivery approaches.

At the same time, it should be taken into account that the stimulatory effect of iodothyronines, shown in our study, on the differentiation of MSCs towards CAFs that are known to support a microenvironment that drives tumour progression and metastasis, could enhance tumour growth [153]. However, depending on the approach used, MSC-based cancer gene therapy can include the destruction of exogenously applied engineered MSCs in the context of therapy, which is likely to overcome any endogenous tumour-promoting effects of adoptively applied MSCs. This was demonstrated in our previous work using MSCs as delivery vehicles for tumour-selective NIS gene delivery, showing no

tumour growth-promoting effects in subcutaneous HuH7 or hepatic colon cancer metastasis xenograft mouse models where a significant therapeutic effect of ^{131}I or ^{188}Re was seen [66, 70]. Moreover, we did not observe an effect of thyroid hormone status or tetrac treatment on the growth of the HCC xenograft model used in this study, which we attribute to the absence of integrin αvβ3 on HuH7 cells and also to the short time frame for assessment of tumour stroma-mediated effects on tumour growth in our experimental setting.

Further, we observed a dramatic effect of tetrac treatment in euthyroid mice that led to nearly complete abolishment of MSC recruitment into the tumour. Tetrac also reversed effects of T3 and T4 on CAF marker gene expression, migration and invasion in vitro. While tetrac is known to exert low-grade thyromimetic effects intracellularly [44], it was shown to have anti-tumour effects *in vitro* and *in vivo* in various cancer models via modulation of tumour cell proliferation, apoptosis and angiogenesis by T3/T4 antagonistic action mediated through integrin αvβ3 [130, 154]. Further anti-tumour activity of tetrac includes suppression of invasiveness/metastasis, increased radio- and chemosensitisation and antagonism of inflammation [130, 132, 133, 147]. These effects are thought to be largely mediated by αvβ3 expressed on the tumour cells themselves. Using an αvβ3-negative tumour model, our data suggest a novel mechanism by which tetrac can exert anti-tumoural effects, not by targeting the cancer cells per se, but by targeting the tumour stroma via MSCs as important stomal progenitor cells. Besides presenting an additional aspect of tetrac's anti-tumour action, this effect opens the prospect of using tetrac as therapy agent irrespective of integrin αvβ3 expression on tumour cells.

In conclusion, our data suggest that thyroid hormones T3 and T4 have a profound effect on the biology of MSCs in the tumour microenvironment through stimulation of CAF-like differentiation as well as migration and invasion in vitro. Tetrac-dependency demonstrates that these effects are largely mediated through non-genomic mechanisms via integrin αvβ3. *In vivo*, the thyroid status had a dramatic impact on MSC recruitment and tumour invasion with increased recruitment in the hyperthyroid state that was significantly decreased in the hypothyroid state and almost abolished upon treatment with tetrac. These studies enhance our understanding of the critical role of T3 and T4 in the regulation of MSC differentiation and migration in the context of tumour stroma formation and stroma-targeted cancer therapy, as well as the molecular mechanisms of the anti-tumour activity of tetrac.

3.6 Acknowledgements

We are grateful to Roswitha Beck and Rosel Oos (Department of Nuclear Medicine, University Hospital of Munich, Germany) for their assistance with animal care and Josef Köhrle (Institut für Experimentelle Endokrinologie, Charité-Universitätsmedizin Berlin, Germany) for thyroid hormone measurements in mouse serum within the Priority Programme SPP1629 (Deutsche Forschungsgemeinschaft).

This work was supported by grants from the Deutsche Forschungsgemeinschaft within the Priority Programme SPP1629 to C Spitzweg, PJ Nelson (SP 581/6-1, SP 581/6-2, NE 648/5-2) and H Heuer (HE 3418/7-1), as well as within the Collaborative Research Center SFB 824, project C 08 to C Spitzweg.

IV. CHAPTER 3

Integrin αvβ3-mediated effects of thyroid hormones on mesenchymal stem cells in tumour angiogenesis

Kathrin A Schmohl[1], Andrea M Müller[1], Maike Dohmann[1], Rebekka Spellerberg[1], Sarah Urnauer[1], Nathalie Schwenk[1], Sibylle I Ziegler[2], Peter Bartenstein[2], Peter J Nelson[1] and Christine Spitzweg[1]

[1]Department of Internal Medicine IV, University Hospital of Munich, LMU Munich, Munich, Germany
[2]Department of Nuclear Medicine, University Hospital of Munich, LMU Munich, Munich, Germany

This chapter is a pre-copy-edited version of a peer-reviewed article accepted for publication in *Thyroid* in 10/2019.

4.1 Abstract

Several clinical and experimental studies have implicated thyroid hormones in cancer progression. Cancer-relevant effects, including stimulation of tumour growth and new blood vessel formation by angiogenesis, are thought to be mediated by a non-classical signalling pathway initiated at integrin αvβ3 expressed on cancer cells and proliferating endothelium. In an earlier study, we established mesenchymal stem cells (MSCs), important contributors to the fibrovascular network of tumours, as new thyroid hormone-dependent targets. Here, we evaluated the effects of thyroid hormones T3 and T4 versus tetrac, an integrin-specific inhibitor of thyroid hormone action, on MSCs in tumour angiogenesis. Modulation of the expression and secretion of angiogenesis-relevant factors by thyroid hormones in primary human MSCs and their effect on endothelial cell tube formation was tested *in vitro*. We further engineered MSCs to express the sodium iodide symporter (*NIS*) reporter gene under control of a hypoxia-responsive promoter and the vascular endothelial growth factor (VEGF) promoter to test effects on these pathways *in vitro* and, for VEGF, *in vivo* in an orthotopic hepatocellular carcinoma xenograft mouse model by PET imaging.

T3 and T4 increased the expression of pro-angiogenic genes in MSCs and NIS-mediated radioiodide uptake in both NIS reporter MSC lines in the presence of hepatocellular carcinoma cell-conditioned medium. Supernatant from thyroid hormone-treated MSCs significantly enhanced endothelial cell tube formation. Tetrac and/or inhibitors of signalling pathways downstream of the integrin reversed all of these effects. Tumoural radioiodide uptake *in vivo* demonstrated successful recruitment of MSCs to tumours and VEGF promoter-driven NIS expression. Hyperthyroid mice showed an increased radioiodide uptake compared to euthyroid mice, while tracer uptake was markedly reduced in hypothyroid and tetrac-treated mice.

Our data suggest that thyroid hormones influence angiogenic signalling in MSCs via integrin αvβ3 and further substantiate the anti-angiogenic activity of tetrac in the tumour microenvironment.

4.2 Introduction

Angiogenesis, the formation of new blood vessels from the pre-existing vasculature, is a fundamental process during embryonic development, wound healing and tissue repair. Physiologically, angiogenesis is a highly regulated process controlled by the balance between pro- and anti-angiogenic regulatory molecules [13, 14]. The angiogenic switch occurs when this equilibrium is changed, leading to endothelial cell migration and proliferation from existing vessels, vascular sprouting and three dimensional vessel formation, followed by maturation and stabilisation of newly formed vessels through their coverage by pericytes and smooth muscle cells [13]. Though the endothelium remains mostly quiescent in adulthood, endothelial cells retain their ability to rapidly proliferate in response to specific stimuli such as hypoxia or inflammation - stimuli that are typically found in the tumour microenvironment [155]. As a tumour grows, so does its demand for oxygen and nutrients, requiring an expansion of the vascular network to meet this need. Hypoxia, a common feature of solid tumours, leads to increased activity of hypoxia-inducible transcription factors (HIFs) that in turn initiate the expression of target genes regulating angiogenesis [156]. Thus, pathologically activated angiogenesis contributes to cancer progression.

Numerous angiogenic factors have been discovered in the secretome of mesenchymal stem cells (MSCs). First described by Friedenstein and co-workers in the 1960s, these multipotent non-hematopoietic stromal-like cells migrate to sites of tissue injury and inflammation, where they contribute to recovery of tissue integrity [115, 157, 158]. Governed by highly similar migratory signals, MSCs also home to the growing tumour stroma, where they differentiate into stroma-associated cells, including cancer-associated fibroblast- and pericyte-like cells [19, 20, 24, 127, 128]. In the context of angiogenesis, MSCs influence endothelial cell proliferation, migration and tube formation through their secretion of pro-angiogenic chemokines and growth factors. They are further involved in blood vessel maturation in their function as pericytes that help stabilise newly formed vessels [14]. Further, the secretion of angiogenic factors by MSCs was reported to be upregulated under hypoxic conditions [14].

In an earlier study we observed that the thyroid hormones 3,3',5-triiodo-L-thyronine (T3) and L-thyroxine (T4) stimulate the differentiation of MSCs towards a cancer-associated fibroblast-/pericyte-like phenotype. This included their upregulation of the pro-angiogenic endothelial growth factor genes vascular endothelial growth factor (*VEGF*) and basic fibroblast growth factor (*FGF2*), in addition to the pericyte markers α-smooth muscle actin and desmin, as well as less specific factors that have been reported to be pro-angiogenic, such as hepatocyte growth factor, epidermal growth factor (*EGF*), transforming growth factor β1 and interleukin 6 [20]. The upregulation of these factors by thyroid hormones in MSCs was shown to be initiated at the cell surface at integrin αvβ3 [20].

Discovered as a thyroid hormone receptor in 2005, the integrin αvβ3 is present in the plasma membrane of proliferating endothelial cells and cancer cells, and also MSCs [20, 33, 47, 131, 159]. The role of

integrin αvβ3 in cancer-related angiogenesis has been known since the 1990s [160]. Subsequently, over the last two decades, iodothyronines have emerged as non-classical pro-angiogenic modulators mediated through αvβ3 and have been shown to induce neovascularisation in a variety of settings, such as the heart, ischemic striated muscle and tumour beds [161]. The complex pro-angiogenic actions of T4 and T3 include the stimulation of endothelial cell proliferation, migration and vascular tube formation. This involves the transcription and/or secretion of, among others, FGF2, VEGF and HIF-1α, in addition to the modification of vascular growth factor receptor function via crosstalk between the integrin and co-clustered growth factor receptors [42, 47, 133, 146, 148, 161-163].

The αvβ3 integrin contains two distinct binding sites for thyroid hormones that are localised near the Arg-Gly-Asp (RGD) recognition site that is essential for extracellular matrix binding [164]. Upon binding of T3 to the S1 site, the PI3K/Akt pathway is activated, resulting in downstream effects that may include the transcription of HIF-1α [13, 129, 131]. The second site, S2, binds both T4 and T3 and the hormone signal is transduced via the ERK1/2 (MAPK) pathway that leads to enhanced cell proliferation and the transcription of pro-angiogenic modulators, including FGF2 and VEGF [13, 29]. Of note is that in contrast to classical thyroid hormone signalling via nuclear thyroid hormone receptors (TRs), T4 is not merely a pro-hormone for T3, but actually functions as an active hormone at the integrin. 3,3',5,5' tetraiodothyroacetic acid (tetrac), a deaminated T4 derivative, specifically inhibits thyroid hormone action at both binding sites on the integrin [13, 129, 131].

Based on the observation that MSCs, in their role as progenitor cells of the tumour's fibrovascular network, are sensitive to thyroid hormones and the accumulating evidence for the pro-angiogenic action of thyroid hormones, the aim of the current study was to evaluate the potential effects of T3 and T4 versus tetrac on MSCs in the context of tumour angiogenesis.

4.3 Materials and Methods

Cell culture

Primary human CD34-negative MSCs extracted from bone marrow (apceth GmbH, Munich, Germany) were cultured until passage 8 in DMEM (Sigma-Aldrich, St. Louis, Missouri, USA) containing 10% (v/v) FBS (FBS Superior, Biochrom/Merck Millipore, Berlin, Germany), 100 U/ml penicillin/100 µg/ml streptomycin (Sigma-Aldrich). For reporter gene transfection, the SV40-immortalised human bone marrow-derived MSC line L87 was used [66, 165]. These cells are easily engineered and expandable, show similar differentiation capacity, as well as homing and activation characteristics as primary MSCs [72, 166]. L87 were cultured in RPMI (Sigma-Aldrich) supplemented with 10% (v/v) FBS and 100 U/ml penicillin/100 µg/ml streptomycin. Primary human umbilical vein endothelial cells (HUVECs; provitro AG, Berlin, Germany) were used until passage 8 and cultured in endothelial cell proliferation medium (provitro AG). The human hepatocellular carcinoma (HCC) cell line HuH7 (JCRB Cell Bank, Osaka, Japan) was cultured in DMEM containing 10% (v/v) FBS and 100 U/ml penicillin/100 µg/ml

streptomycin and passaged up to 10 times. All cell lines were maintained at 37 °C in a humidified 5% (v/v) CO_2 atmosphere.

Stable transfection of MSCs

For reporter gene assays, L87 MSCs transfected with the human sodium iodide symporter (*NIS*) gene under control of either a promoter containing hypoxia response elements (HRE-NIS-MSCs; established in [72]) or the VEGF promoter (VEGF-NIS-MSCs) were used. VEGF-NIS-MSCs were established by stable transfection of wildtype L87 MSCs with the expression vector pcDNA6.2ITR_BLASTI_Vegf2.1kb.NIS. The plasmid was generated with the MultiSite Gateway Pro Plus Kit (Thermo Fisher Scientific, Waltham, MA, USA) as described previously [73, 167] and contains the human *NIS* gene driven by the mouse *Vegf* promoter, two Sleeping Beauty transposition sites and a blasticidin resistance gene. Cells were transfected with 2 µg pcDNA6.2ITR_BLASTI_Vegf2.1kb.NIS and 1 µg pCMV(CAT)T7-SB100X (provided by Z Ivics, Max Delbrück Center for Molecular Medicine, Berlin, Germany), which contains the Sleeping Beauty transposase system for transgene insertion into the host cell genome, by electroporation using a single 30 ms pulse at 900 V on the Neon Transfection System (Thermo Fisher Scienific). Blasticidin (InvivoGen, Toulouse, France) was used to select for transfected cells. Single cell clones were isolated and analysed for NIS-mediated iodide uptake activity (see below). The stably transfected clone with the highest iodide uptake was used for all further experiments.

Hormone treatment *in vitro*

The preparation of and treatment with HuH7-conditioned medium and T3 or T4 with or without tetrac was performed as described previously [20]. For *in vitro* experiments, both T3 and T4 were used at physiologic and supraphysiologic concentrations, i.e. 1 nM or 10 nM T3 and 100 nM or 1000 nM T4, respectively. The reference ranges for total hormone concentrations in healthy, euthyroid humans are 64-154 nM for T4 and 1.1-2.9 nM for T3 [168]. Tetrac was applied at an end concentration of 100 nM. As FBS, per se, contains thyroid hormones, charcoal-stripped serum was used for stimulation experiments (T3 concentration <0.2 pg/ml; T4 concentration 0.2-0.6 ng/dl).

Quantitative real-time PCR

RNA extraction, reverse transcription and quantitative real-time PCR (qPCR) were performed as described previously [20]. Primer sequences are listed in table 2. Relative expression levels were calculated from ΔΔCt values normalised to the geometric means of internal β-actin (*ACTB*) and 18S rRNA (*R18S*). Samples were run in duplicate for each of four independent experiments.

ELISA

Supernatant from MSCs after 24 h and 48 h of stimulation was centrifuged and stored at -80 °C until assayed for angiogenin (ANG), angiopoietin 1 (ANGPT1), angiopoietin 2 (ANGPT2), interleukin 8

(CXCL8), insulin-like growth factor 1 (IGF1) and placental growth factor (PGF) using the respective DuoSet ELISA kit (R&D Systems, Abingdon, UK). Where necessary, supernatants were diluted as follows to be within the linear range of the assay: ANG 24 h 1:20, 48 h 1:80; ANGPT1 48 h 1:4; CXCL8 24 h 1:20, 48 h 1:60; IGF1 24 h and 48 h 1:10; PGF 24 h and 48 h 1:2. Samples were analysed in duplicate in four independent experiments.

Table 2. qPCR primer sequences.

gene	forward primer (5' → 3')	reverse primer (5' → 3')
ACTB	AGAAAATCTGGCACCACACC	TAGCACAGCCTGGATAGCAA
ANG	CATCATGAGGAGACGGGG	TCCAAGTGGACAGGTAAGCC
ANGPT1	AACATGAAGTCGGAGATGGC	CAGCAGCTGTATCTCAAGTCG
ANGPT2	GAAGAGCATGGACAGCATAGG	GAGTCATCGTATTCGAGCGG
bsd	CCTCATTGAAAGAGCAACGG	CTGTTCTCATTTCCGATCGC
CCL2	AGCCACCTTCATTCCCCAAG	TTGGGTTTGCTTGTCCAGGT
CCL4	GCTGCTTTTCTTACACCGCG	TACACGTACTCCTGGACCCA
CXCL7	CCTGTAACAGTGCGAGACCA	TCGACTTGGTTGCAATGGGT
CXCL8	TCTGCAGCTCTGTGTGAAGG	TTCTCCACAACCCTCTGCAC
CYR61	TTTGGAATGGAGCCTCGCAT	TTCAGGCTGCTGTACACTGG
HIF1A	GCTTTAACTTTGCTGGCCCC	TTCAGCGGTGGGTAATGGAG
IGF1	GCTGGTGGATGCTCTTCAGT	TTGAGGGGTGCGCAATACAT
NIS	TGCGGGACTTTGCAGTACATT	TGCAGATAATTCCGGTGGACA
PGF	CATCCTGTGTCTCCCTGCTG	GTCTCCTCCTTTCCGGCTTC
R18S	CAGCCACCCGAGATTGAGCA	TAGTAGCGACGGGCGGTGTG
SV40	TTGCTGTGCTTACTGAGGATG	CCAATTATGTCACACCACAGA
TEK	AACTCTGTGTGCAACTGGTCC	AAGTCATCTTCCGAGCTTGG
TIMP1	CTCGTCATCAGGGCCAAGTT	GCAAGAGTCCATCCTGCAGT
TIMP2	GCTGGACGTTGGAGGAAAGA	TGTGACCCAGTCCATCCAGA

Radioiodide uptake *in vitro*

NIS-mediated uptake of ^{125}I (PerkinElmer, Waltham, MA, USA) by HRE-NIS-MSCs, VEGF-NIS-MSCs and wildtype MSCs was measured according to Spitzweg *et al.* [169]. To test inducibility of the hypoxia-responsive and the VEGF promoter, cells were stimulated with 300 µM of the hypoxia-simulating agent cobalt chloride ($CoCl_2$; Sigma-Aldrich) or with 20% FBS, respectively, for 24 h. Thyroid hormone treatment was performed as described above. HRE-NIS-MSCs were additionally stimulated with 300 µM $CoCl_2$ during thyroid hormone treatment. The signalling pathway inhibitors LY 294002 (InSolution LY 294002, Calbiochem/Merck Millipore, Darmstadt, Germany) and RAF265 (Novartis, Basel, Switzerland), both stored as 10 mM stock solutions at -20°C in DMSO, were used at 10 µM and 1 µM end concentrations, respectively, and were added to cells simultaneously with thyroid hormones. For each iodide uptake assay, two to four technical replicates were performed in three independent experiments each. Radioiodide uptake was normalised to cell viability determined by MTS-

assay (Promega, Mannheim, Germany) as described previously [170] using the absorbance at 620 nm relative to control cells.

Tube formation assay

HUVECs were seeded at a density of 7.5×10^3 cells/well in a 96 well µ-Plate Angiogenesis (ibidi, Martinsried, Germany) on growth factor-reduced Matrigel (Becton Dickinson Biosciences, Heidelberg, Germany). Five to six wells were plated for each condition in each of three or four independent experiments. Plates were incubated for 12 h at 37°C before photo microscopy. Images were acquired on a Leica DM IL microscope (Leica Microsystems, Wetzlar, Germany) equipped with a Jenoptik ProgRes CCD camera (Jenoptik, Jena, Germany) at 5× magnification. Tube formation was quantified in an automated fashion with the ImageJ (National Institutes of Health, Bethesda, Maryland, USA) plug-in Angiogenesis Analyzer [171]. Evaluated parameters were the mean number of meshes, junctions and the mean total tube length per well.

Animals

All experiments were conducted with approval from the regional governmental commission for animals (Regierung von Oberbayern, Munich, Germany). Four- to five-week old male CD1 nu/nu mice (Charles River, Sulzfeld, Germany) were allowed to acclimatise for one week under specific pathogen-free conditions with access to standard nude mouse diet (ssniff, Soest, Germany) and water *ad libitum*. HuH7 tumour cells (1×10^6) were implanted into the livers of mice after laparotomy as described previously [72].

Hormone treatment *in vivo*

Starting from one week after tumour cell injection, mice received drinking water supplemented with 0.02% (w/v) 2-mercapto-1-methylimidazole (MMI; Sigma-Aldrich) and 1% (w/v) sodium perchlorate (Sigma-Aldrich) to induce hypothyroidism and generate the same baseline thyroid hormone levels for all groups [20, 144]. 0.3% (w/v) saccharin (Sigma-Aldrich) was added as a sweetener to mask the bitter taste of MMI/perchlorate. Two weeks later, mice were randomly assigned to different treatment groups and received the following intraperitoneal (i.p.) injections daily: The hyperthyroid group (n=6) received 100 ng/g body weight L-T4 (Sigma-Aldrich), the euthyroid group 20 ng/g body weight L-T4 with (n=7) or without (n=6) 10 µg/g body weight tetrac (Sigma-Aldrich), while hypothyroid mice (n=8) received saline only. Three days before imaging (see below), perchlorate was removed from the drinking water and only MMI treatment continued to prevent interference with radioiodide uptake. Thyroid hormone status was regularly monitored in serum samples by ELISA (DRG Diagnostics, Marburg, Germany).

^{124}I positron emission tomography (PET)

Three weeks later, i.e. six weeks after tumour cell inoculation, 5×10^5 VEGF-NIS-MSCs or wildtype MSCs (n=2), were injected systemically in 500 µl phosphate-buffered saline via the tail vein. 72 h later,

10 MBq ^{124}I (PerkinElmer or DSD Pharma, Purkersdorf, Austria) were applied intraperitoneally and radioiodide distribution assessed using an Inveon P120 microPET (Siemens Healthcare, Erlangen, Germany). In three mice the competitive NIS inhibitor sodium perchlorate (2 mg/mouse; Sigma-Aldrich) was injected i.p. 30 min prior to radioiodide administration to verify that tumoural radioiodide accumulation was NIS-mediated. PET images were reconstructed with the software Inveon Acquisition Workplace (Siemens) and analysed with Inveon Research Workplace (Siemens). Three dimensional regions of interest were defined and quantified as mean percent of the injected dose per ml tumour (% ID/ml tumour). After PET imaging, mice were sacrificed and tumours embedded in Tissue-Tek O.C.T. compound (Sakura Finetek, Alphen aan den Rijn, The Netherlands), snap-frozen on dry ice and stored at -80 °C until further processing (see below).

Ex vivo immunofluorescence staining

Immunofluorescence staining for human NIS and mouse CD31 on frozen tissue sections was performed as described previously [72, 170] using the mouse monoclonal anti-NIS antibody clone FP5A (Merck Millipore, Berlin, Germany) or the rat monoclonal anti-mouse CD31 antibody clone MEC 13.3 and a Cy3-conjugated donkey anti-mouse secondary antibody (Jackson ImmunoResearch, Cambridgeshire, UK) or a Cy3-conjugated donkey anti-rat secondary antibody (Jackson ImmunoResearch), respectively. Nuclei were counterstained with 5 µg/ml bisbenzimide Hoechst 33258 (Sigma-Aldrich). Stained sections were mounted with Dako Fluorescence Mounting Medium (Dako, Carpinteria, California, USA) and imaged at 20× (NIS) or 10× (CD31) magnification on a Leica DMI6000 B fluorescence microscope equipped with a Leica DFC365 FX CCD camera, and the software Leica Application Suite X (Leica Microsystems). A minimum of five visual fields was recorded per tumour for three to four mice per treatment group. The number of NIS-positive cells was counted manually, while the CD31 positive area per visual field was quantified using ImageJ, blinded to group assignment.

Ex vivo analysis of NIS mRNA expression

To normalise NIS expression to MSC recruitment, total RNA was isolated from tumours (euthyroid n=5; hyperthyroid n=6; hypothyroid n=5; euthyroid + tetrac n=6) and quantitative real-time PCR was performed as described above using primers specific for *NIS*, *SV40*, which was used for MSC immortalisation, and the blasticidin resistance gene (*bsd*), which is encoded by the *NIS* expression plasmid and constitutively expressed (for primer sequences see table 2). β-actin and 18S rRNA served as internal controls. Results were calculated from ΔΔCt values for *NIS* divided by the mean of the respective ΔΔCt values for *SV40* and *bsd* as a measure of the amount of MSCs present.

Statistics

All data are expressed as mean ± SEM or mean fold change ± SEM. Statistical significance was tested by one-way ANOVA followed by Tukey's post hoc test. *p*-values <0.05 were considered statistically significant (*p<0.05; **p<0.01; ***p<0.001).

4.4 Results

Thyroid hormones increase the expression of angiogenesis modulators in MSCs *in vitro*

Initially, we examined the expression of angiogenesis relevant factors in MSCs. To this end, we treated primary human bone marrow-derived MSCs with physiologic or supraphysiologic concentrations of T3 or T4 and HCC cell-conditioned medium to simulate the tumour environment *in vitro*. mRNA (**Fig. 12A, B**) and protein concentrations (**Fig. 13A, B**) for genes associated with angiogenesis were analysed by qPCR or ELISA, respectively.

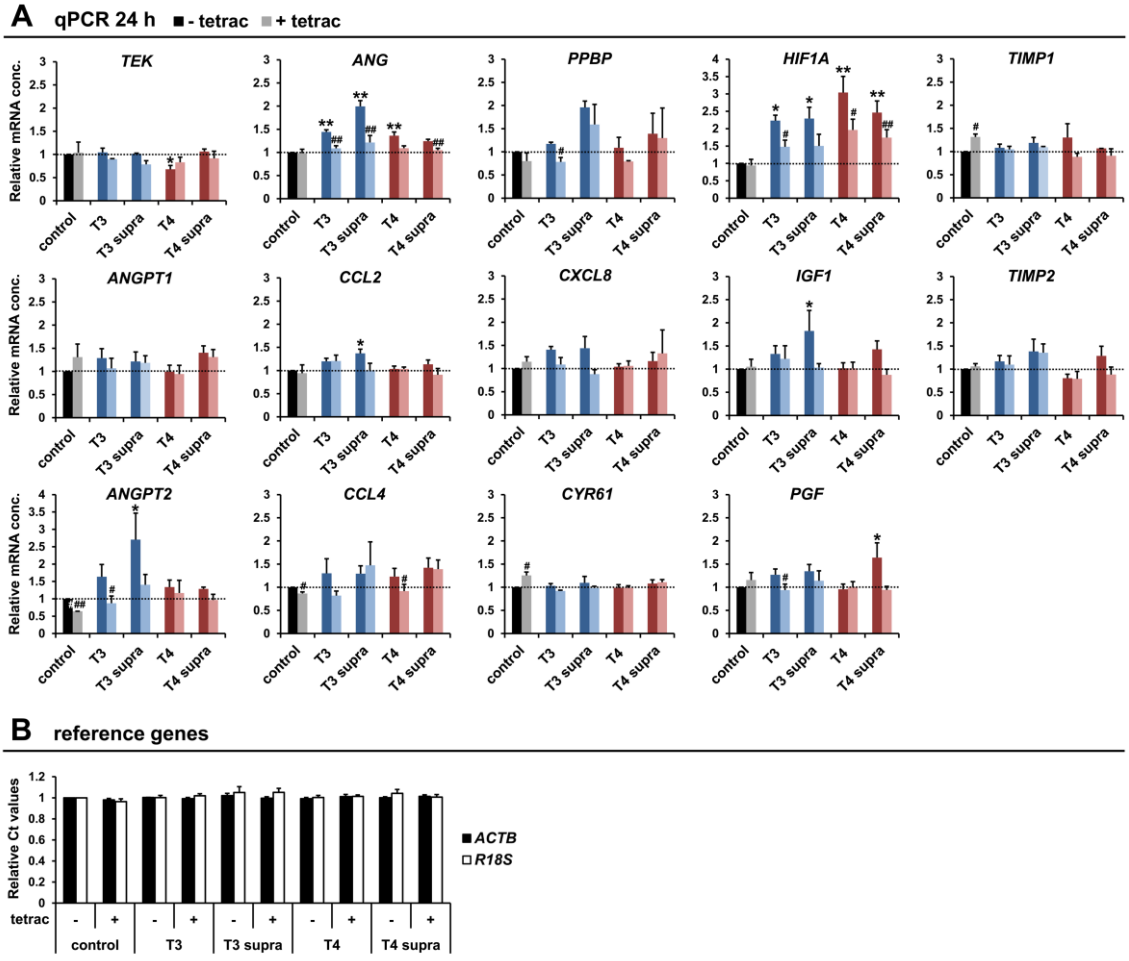

Figure 12: Expression of pro-angiogenic genes. Primary human bone marrow-derived MSCs were treated with hepatocellular carcinoma cell-conditioned medium and either physiological (1 nM, "T3") and supraphysiological (10 nM, "T3 supra") concentrations of T3 or physiological (100 nM "T4") and supraphysiological (1000 nM "T4 supra") concentrations of T4 with and without tetrac (100 nM). (**A**) mRNA concentrations of various genes relevant to angiogenesis were assessed by qPCR after 24 h normalised to (**B**) reference gene expression (mean-fold change ± SEM; n=4). Note that the y-axis for *HIF1A* and *ANGPT2* have a different scale. The dotted lines relate to cells treated with hepatocellular carcinoma cell-conditioned medium only (*p<0.05; **p<0.01 compared to control; #p<0.05; ##p<0.01; ###p<0.001 no tetrac treatment compared to tetrac treatment).

For genes of the angiopoietin/TEK tyrosine kinase (TIE2) axis that control vessel maturation, expression levels of the receptor itself were reduced under stimulation with 100 nM T4, while no significant

changes for its ligand ANGPT1 were detected at the mRNA level. ANGPT1 contributes to the maintenance of the resting endothelial state. In contrast, mRNA concentrations of ANGPT2, the naturally occurring antagonist of ANGPT1 that enhances vascular permeability and destabilises the endothelium, were dose-dependently increased upon T3 stimulation compared to cells treated with tumour cell-conditioned medium alone, an effect that was significant at 10 nM T3 and was blocked by tetrac. Pro-angiogenic ANG and the growth factor IGF1 showed a similar expression pattern. HIF1A mRNA expression was significantly upregulated by both physiological and supraphysiological concentrations of both T3 and T4 and T4 effects were reduced by tetrac. The chemokines CCL4, pro-platelet basic protein (PPBP/CXCL7), and CXCL8 showed only slight, non-significant upregulation under T3 stimulation that was decreased by tetrac, while CCL2 expression was significantly increased under stimulation with 10 nM T3. No T4 effects were observed for these chemokines. PGF showed only weak, non-significant stimulation under T3 treatment, but was significantly increased under stimulation with 1000 nM T4 at the mRNA level. The extracellular matrix-associated angiogenic modulator cysteine-rich 61 (CYR61), as well as tissue inhibitors of metalloproteinases 1 and 2 (TIMP1/2) showed no significant changes in expression levels under thyroid hormone stimulation. CYR61 and TIMP1 mRNAs were upregulated when cells were treated with HCC cell-conditioned medium and tetrac as compared to cells treated with HCC cell-conditioned medium alone (**Fig. 12A**). The reference genes *ACTB* and *R18S* used for normalisation were not impacted by the different treatment conditions (**Fig. 12B**).

For a subset of these genes, the concentrations of secreted proteins in MSC supernatants after 24 h (**Fig. 13A**) and 48 h (**Fig. 13B**) of stimulation were validated by ELISA. Effects seen at the mRNA level were confirmed at the protein level for ANGPT1, ANG, and IGF1 by ELISA (**Fig. 13A, B**). ANGPT2 expression was increased significantly and dose-dependently under T3 stimulation in a tetrac-dependent manner after 48 h, reflecting the effects seen at the mRNA level (**Fig. 13B**). At 24 h, ANGPT2 levels were below the detection limit of the ELISA for all treatment conditions. CXCL8 showed a significant increase in secreted protein at 24 h that was completely absent after 48 h. PGF expression, by contrast, was induced by T4 after 24 h, an effect that was even stronger after 48 h. This effect was blocked by additional treatment with tetrac.

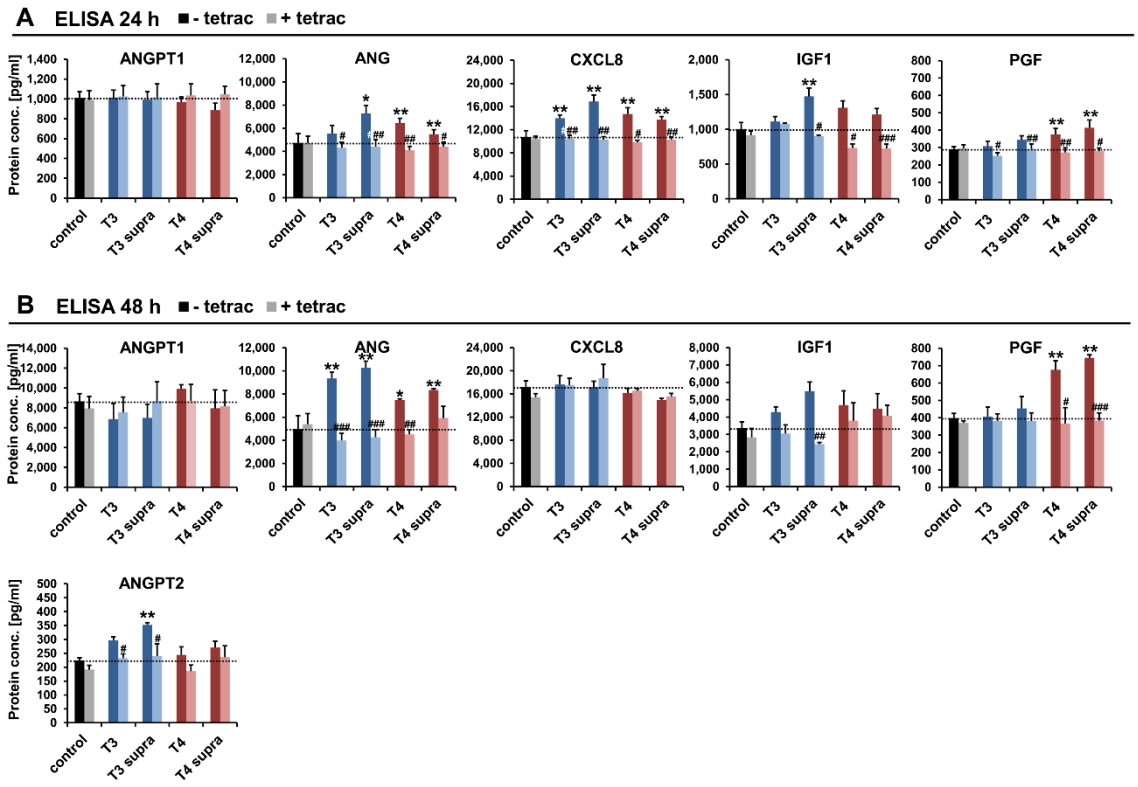

Figure 13: Secretion of pro-angiogenic proteins. Primary human bone marrow-derived MSCs were treated with hepatocellular carcinoma cell-conditioned medium and either physiological (1 nM, "T3") and supraphysiological (10 nM, "T3 supra") concentrations of T3 or physiological (100 nM "T4") and supraphysiological (1000 nM "T4 supra") concentrations of T4 with and without tetrac (100 nM). (**A**) Protein concentrations in supernatants of stimulated MSCs were measured by ELISA after 24 h or (**B**) 48 h (mean ± SEM; n=4). Note that compared to the 24 h diagrams, the y-axis at 48 h is 10× and 4× larger for ANGPT1 and IGF1, respectively. The dotted lines relate to cells treated with hepatocellular carcinoma cell-conditioned medium only (*p<0.05; **p<0.01; compared to control; #p<0.05; ##p<0.01; ###p<0.001 no tetrac treatment compared to tetrac treatment).

Supernatant from thyroid hormone-treated MSCs stimulates endothelial cell tube formation

To examine the paracrine effects of angiogenic factors secreted by MSCs on endothelial cells, HUVECs were seeded on growth factor-reduced Matrigel and subjected to conditioned medium from stimulated MSCs. Tube formation was analysed and quantified in an automated manner on microscopy images after 12 h (**Fig. 14A**). Compared to untreated HUVECs, supernatant from MSCs enhanced tube formation, as evidenced by more intricate tubular networks with a larger number of meshes and junctions as well as a higher total tube length after 12 h (**Fig. 14B, C**). This effect was further enhanced when MSCs had been additionally treated with thyroid hormones (**Fig. 14B, C**). While tetrac had no effect on basal HUVEC tube formation, or MSC supernatant-stimulated tube formation, supernatant from MSCs stimulated with tetrac in addition to thyroid hormone reduced tube formation to, or even below, basal levels (**Fig. 14B, C**). To estimate potential effects of residual thyroid hormones in the MSC supernatant on HUVEC tube formation, HUVECs were treated with thyroid hormones alone in a further tube

formation experiment. No significant effects were observed at the thyroid hormone concentrations used, though the data do imply a slight inhibiting effect of tetrac on HUVEC tube formation under parallel T3 stimulation (**Fig. 14D**).

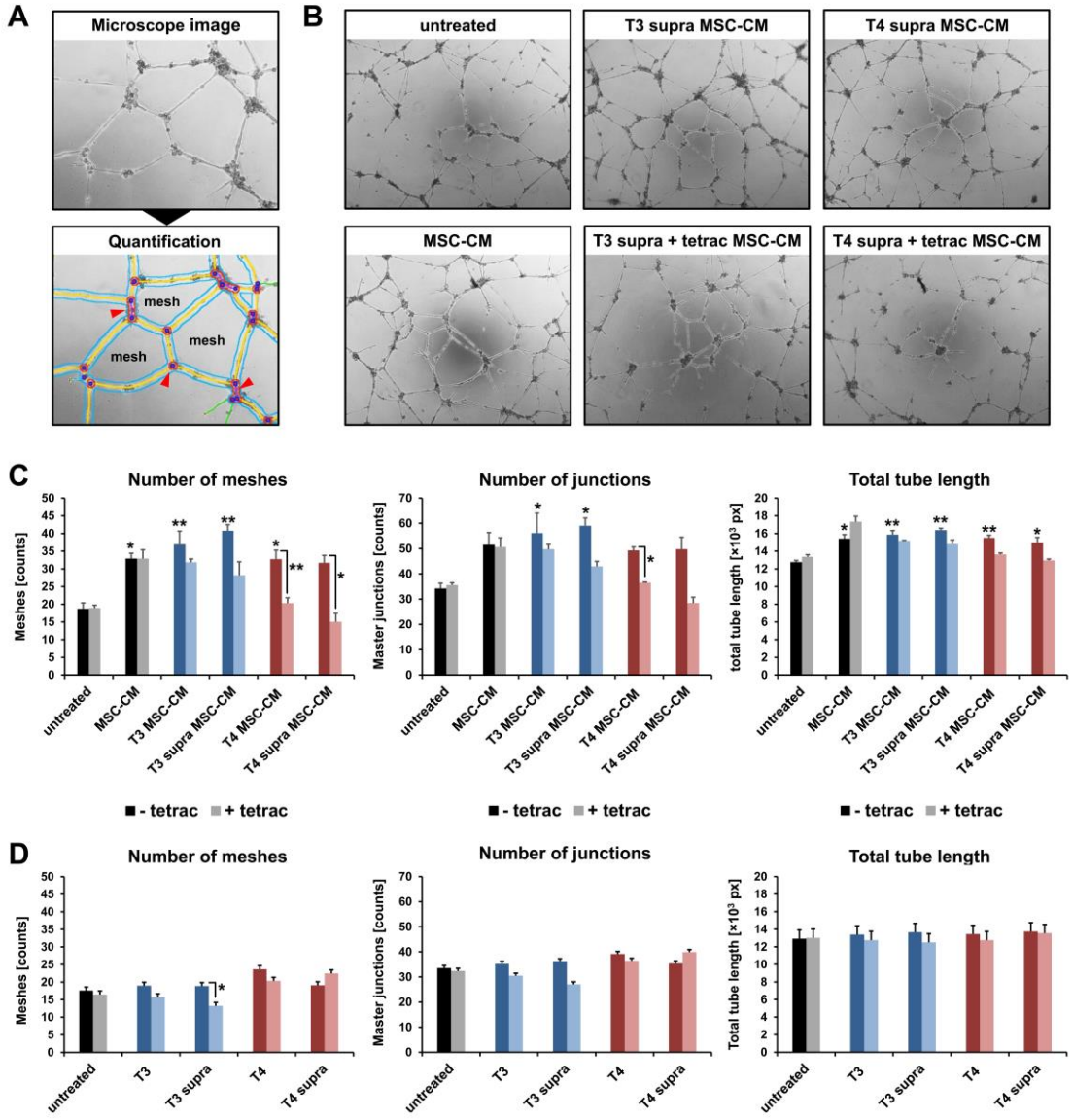

Figure 14: Tube formation assay. (**A**) HUVEC tube formation on growth factor-reduced Matrigel was quantified on microscope images after 12 h in an automated fashion by analysing the number of meshes and junctions (red arrows) and the total tube length. (**B**) HUVECs were subjected to supernatant from MSCs stimulated with hepatocellular carcinoma cell-conditioned medium and T3 (1 or 10 nM) or T4 (100 or 1000 nM) with and without tetrac (100 nM). Representative images from supraphysiological hormone treatment are shown. Magnification: 5×. (**C**) Quantification of effects on tube formation (mean ± SEM; n=3; *p<0.05; **p<0.01 compared to untreated). (**D**) HUVECs were treated with T3 (1 or 10 nM) or T4 (100 or 1000 nM) with and without tetrac (100 nM) and effects on tube formation were quantified (mean ± SEM; n=4; *p<0.05). MSC-CM: MSC-conditioned medium. px: pixel.

Thyroid hormone affects VEGF signalling in MSCs *in vitro*

As the hypoxia response/VEGF axis critically mediates angiogenesis, we established two reporter gene systems to monitor the involvement of HIF-1 and VEGF signalling in thyroid hormone-mediated angiogenic effects of MSCs in more detail. We engineered MSCs to express the reporter gene NIS under the control of the hypoxia-responsive promoter (HRE-NIS-MSCs) or the VEGF promoter (VEGF-NIS-MSCs). We could then use radioiodide uptake by NIS in transfected cells as readout of active hypoxia or VEGF signalling. To induce promoter activity, HRE-NIS-MSCs were stimulated with the hypoxia-simulating agent $CoCl_2$ and VEGF-NIS-MSCs with FBS. In a functional assay, both HRE-NIS-MSCs and VEGF-NIS-MSCs showed inducible radioiodide uptake activity that was blocked upon treatment with the competitive NIS inhibitor perchlorate (**Fig. 15A**). While untreated HRE-NIS-MSCs and wildtype MSCs showed no ^{125}I uptake above background levels, unstimulated VEGF-NIS-MSCs showed some basal activity (**Fig. 15A**).

We then stimulated HRE-NIS-MSCs with HCC cell-conditioned medium and thyroid hormones with or without tetrac in the presence of $CoCl_2$ to simulate hypoxia and thus stabilise newly expressed HIF-1α. Compared to HRE-NIS-MSCs treated with HCC cell-conditioned medium only, additional stimulation with T3 or T4 led to a slight, non-significant increase in iodide uptake activity (**Fig. 15B**, left panel). VEGF-NIS-MSCs showed a stronger, more robust response to thyroid hormone stimulation, as evidenced by a significant tetrac-dependent increase of 1.50- and 1.53-fold for 1 nM and 10 nM T3 and 1.57- and 1.73-fold for 100 nM and 1000 nM T4, respectively (**Fig. 15B**, right panel). Tetrac reduced ^{125}I uptake induced by thyroid hormones in both cell lines, though only reaching statistical significance for VEGF-NIS-MSCs.

To further verify integrin αvβ3 involvement, we applied inhibitors of signalling pathways downstream of the integrin in addition to the integrin-specific inhibitor tetrac. The PI3K inhibitor LY 294002 was used to probe for T3 signalling via the S1 binding site in the thyroid hormone binding domain of integrin αvβ3 and the ERK1/2 (MAPK) pathway inhibitor RAF265 for T3 and T4 signalling via the S2 binding site (**Fig. 15C**). In both HRE-NIS-MSCs and VEGF-NIS-MSCs the T3 effects were blocked upon tetrac, LY 294002 and RAF265 treatment, while T4 effects were only blocked by tetrac and RAF265 and not by LY 294002 (**Fig. 15D**). Note that in this set of experiments T3 and T4 effects did reach statistical significance in HRE-NIS-MSCs.

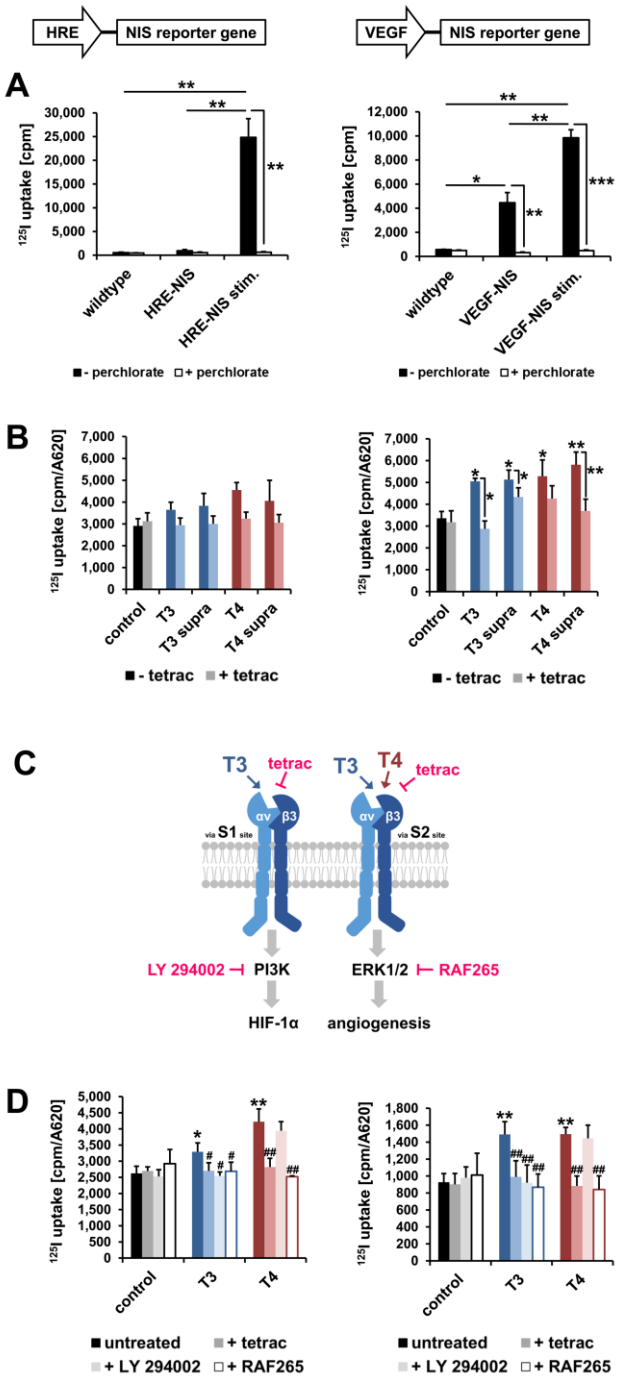

Figure 15: Hypoxia and VEGF signalling *in vitro*. Two different reporter constructs were established by placing the NIS gene under control of a hypoxia-responsive promoter (HRE-NIS, left panel) or the VEGF promoter (VEGF-NIS, right panel). (**A**) L87 MSCs transfected with these constructs showed inducible ^{125}I uptake activity compared to wildtype MSCs. Sensitivity to perchlorate indicates NIS specificity. Stim.: stimulated (mean ± SEM.; n=3; **p*<0.05; ***p*<0.01; ****p*<0.001). (**B**) HRE-NIS-MSCs (left panel) or VEGF-NIS-MSCs (right panel) were treated with hepatocellular carcinoma cell-conditioned medium only (control) or additionally with T3 (1 or 10 nM) or T4 (100 or 1000 nM) with and without 100 nM tetrac (mean ± SEM; n=3; **p*<0.05; ***p*<0.01). (**C**) Schematic representation of thyroid hormone signalling versus inhibition via integrin αvβ3. (**D**) Control cells and cells treated with 1 nM T3 or 100 nM T4 were additionally treated with 100 nM tetrac, 10 µM LY 294002 or 1 µM RAF265 and 125I uptake activity assessed (mean ± SEM; n=3; **p*<0.05; ***p*<0.01 compared to control; #*p*<0.05; ##*p*<0.01 with versus without inhibitors). The thyroid hormones and the inhibitors were added to the cells simultaneously.

Thyroid hormone stimulates VEGF signalling in MSCs in liver tumours *in vivo*

Based on the stronger thyroid hormone-dependent effects seen *in vitro* using the VEGF-NIS-MSCs, compared to the HRE-NIS-MSCs, the former were further evaluated *in vivo* by ^{124}I PET in an orthotopic HCC xenograft nude mouse model (**Fig. 16A**). Mice were subjected to different thyroid hormone treatments (euthyroid, hyperthyroid, hypothyroid and euthyroid + tetrac; **Fig. 16B**). 72 h after systemic injection of VEGF-NIS-MSCs, tumoural ^{124}I accumulation and thus functional NIS expression was assessed by three-dimensional high-resolution small animal PET (**Fig. 16B**).

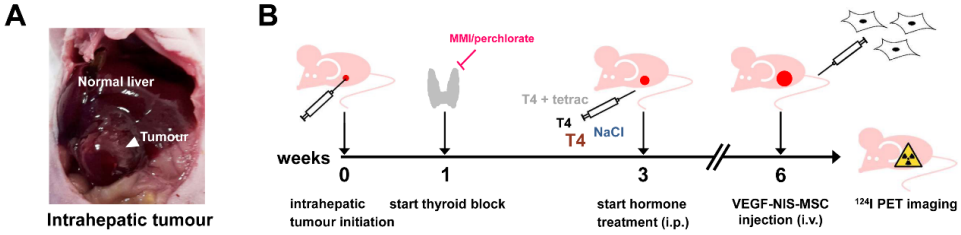

Figure 16: Experimental set-up *in vivo*. (**A**) Orthotopic tumours were established by injection of the human hepatocellular carcinoma cell line HuH7 into the livers of nude mice. (**B**) One week after tumour cell inoculation, endogenous thyroid hormone production was blocked by MMI/perchlorate via the drinking water. Two weeks later, mice were assigned to different thyroid hormone groups that received either 20 ng/g body weight T4 (euthyroid), 100 ng/g body weight T4 (hyperthyroid), saline (hypothyroid) or 20 ng/g body weight T4 alongside 10 µg/g body weight tetrac (euthyroid + tetrac) i.p. daily. Finally, mice received a single tail vein injection of VEGF-NIS-MSCs and radioiodide uptake in the tumour region was assessed by ^{124}I PET 72 h later.

Radioiodide signals in the liver region demonstrated successful tumoural recruitment of VEGF-NIS-MSCs after systemic application followed by VEGF promoter-driven NIS expression in tumours (**Fig. 17A**). Compared to euthyroid mice, the tumours of hyperthyroid mice accumulated markedly more radioiodide one hour after ^{124}I injection, while hypothyroid and tetrac-treated mice accumulated less radioioide in their liver tumours (**Fig. 17A, B**). Tracer uptake was also observed in mouse tissues that endogenously express NIS (thyroid, stomach, nasal mucosa and salivary glands) as well as in the urinary bladder, due to renal radioiodide elimination (**Fig. 17A**). The competitive NIS inhibitor perchlorate inhibited both tumoural NIS expression as well as endogenous expression, thus verifying that tracer uptake in tumours was indeed NIS-mediated (**Fig. 17A**). No ^{124}I uptake above background was observed in tumours of mice injected with wildtype MSCs (**Fig. 17A**).

Immunofluorescence staining for human NIS in tumours reflected PET imaging results with a significantly higher number of NIS positive cells in hyperthyroid mice and significantly less in hypothyroid and tetrac-treated animals compared to euthyroid mice (**Fig. 17C, D**). Normalisation to MSC recruitment confirmed the observed effects on NIS expression levels (**Fig. 17E**).

Tumour growth was not affected by thyroid hormone status or tetrac treatment in this model (data not shown). Thyroid hormone concentrations in serum at sacrifice reflected the different thyroid states of the treatment groups (**Fig. 17F**). The ELISA used could not differentiate between T4 and tetrac, leading

to false high serum T4 values in tetrac-treated mice (data not shown). Tetrac-treated animals received the same body weight-adjusted dose of T4 as the euthyroid group, which leads to highly reproducible serum T4 levels in the range of untreated naturally euthyroid mice.

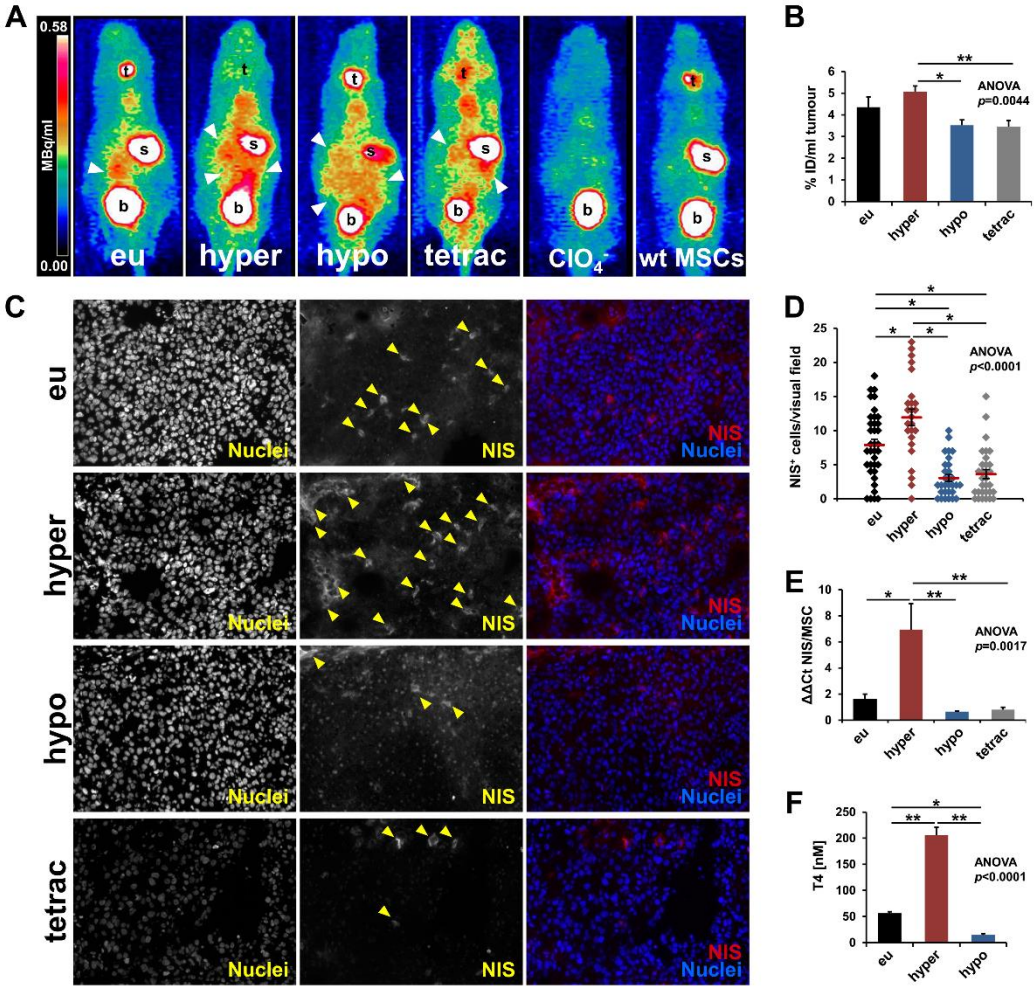

Figure 17: VEGF signalling *in vivo*. (**A**) ^{124}I PET imaging of mice bearing intrahepatic HuH7 tumours demonstrated tumoural radioiode accumulation (indicated by arrows) in animals that were injected with VEGF-NIS-MSCs, while no signal was detected in the tumours of wildtype MSC-treated mice (wt MSCs). Endogenous NIS expression led to tracer uptake in the thyroids (t) and stomachs (s) of mice. Signals in the bladder (b) are due to renal excretion of the PET tracer. Treatment with the NIS-specific inhibitor perchlorate (ClO_4^-) extinguished tracer uptake both in the tumour and in organs with endogenous NIS expression. (**B**) Tumoural radioiodide uptake was quantified 1 h after radioiodide injection by placing three-dimensional regions of interest over the tumours (mean % of the injected dose/ml tumour ± SEM; euthyroid: n=6, hyperthyroid: n=6, hypothyroid: n=8, euthyroid + tetrac: n=7; *p<0.05; **p<0.01). (**C**) Tumoural NIS expression was further confirmed by NIS-specific immunofluorescence staining. Magnification: 20×. (**D**) Quantification of NIS staining on tumour sections (diamonds represent counts in a single visual field, red lines represent mean ± SEM; n=4/treatment group; *p<0.05). (**E**) NIS expression relative to MSC recruitment was assessed by qPCR (mean ± SEM of ΔΔCt for *NIS*/mean of ΔΔCts for *SV40* and *bsd*; n=5 for euthyroid and hypothyroid mice, n=6 for hyperthyroid and tetrac-treated mice; *p<0.05; **p<0.01). (**F**) Thyroid hormone concentrations in serum samples from the individual treatment groups at sacrifice (mean ± SEM; n=4/treatment group; *p<0.05; **p<0.01).

To further assess effects on angiogenesis, *ex vivo* CD31 straining on tumour sections was performed. The blood vessel densities of the different treatment groups showed a trend reflecting the effects on angiogenesis seen *in vitro* and *in vivo* with a significantly decreased tumour vascularisation in hypothyroid mice compared to euthyroid mice, and a significantly increased vascularisation in hyperthyroid mice as compared to hypothyroid and tetrac-treated mice (**Fig. 18A, B**).

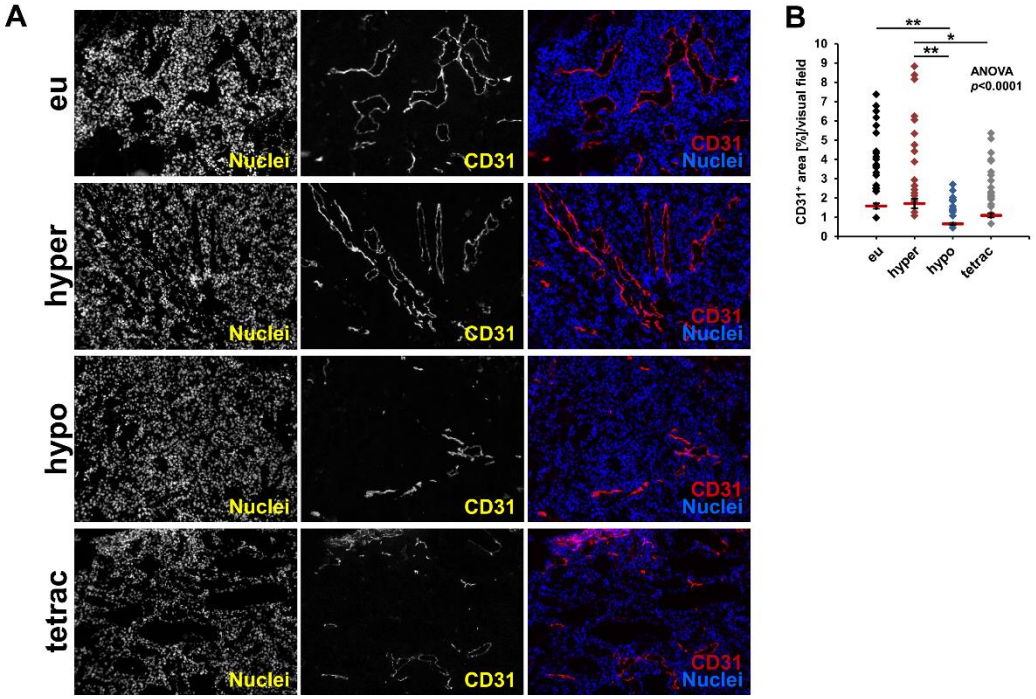

Figure 18: *Ex vivo* CD31 staining. (**A**) Immunofluorescence staining for CD31 was performed on tumour sections to visualise vascularisation. Magnification: 10×. (**B**) Quantification of CD31 staining (diamonds represent the % CD31 positive area in a single visual field, red lines represent mean ± SEM; n=3-4/treatment group; **p*<0.05; ***p*<0.01).

4.5 Discussion

Angiogenesis is pivotal to tumour growth and progression. Therefore, understanding the molecular regulation of cellular events involved in angiogenesis has immense clinical implications. MSCs have been shown to secrete pro-angiogenic factors in the tumour microenvironment upon their homing to the tumour stroma and their differentiation into cancer-associated fibroblast-like and pericyte-like cells [19, 20]. It is assumed that the angiogenic effect of MSCs is predominantly caused by their secretion of pro-angiogenic factors [14]. In a previous study, we observed that the thyroid hormones T3 and T4 stimulate the differentiation of MSCs towards a tumour-promoting, pro-angiogenic phenotype via a cell surface receptor on integrin αvβ3 [20]. The thyroid hormone metabolite tetrac, a specific inhibitor of thyroid hormone action at the integrin site, reversed the effects of agonist thyroid hormone. Indeed, thyroid hormone has been shown to be pro-angiogenic via integrin αvβ3 expressed on tumour cells and endothelial cells in numerous studies [47, 146, 162]. Our data suggested another layer to the story, in that non-hematopoietic cells of the tumour stroma, namely MSCs, can be driven towards a more pro-

angiogenic phenotype by thyroid hormones via their signalling through the αvβ3 integrin. Hence, we decided to take a closer look at thyroid hormone regulation of angiogenic effects of MSCs in the current study.

Analysing the response of a broader range of angiogenic factors found in the MSC secretome to thyroid hormone versus tetrac treatment, we here show that thyroid hormones, especially T3, stimulate pro-angiogenic gene expression and protein secretion in MSCs at physiologically relevant hormone concentrations. Interestingly, HIF-1α expression was significantly induced by both T3 and T4. The transcription factor HIF-1 is a key modulator of a cell's adaptation to hypoxia and an important angiogenesis mediator. It is a heterodimer composed of the constitutively expressed HIF-1β and the oxygen-sensitive HIF-1α subunit that is tightly regulated and degraded under normoxia [172]. Under hypoxia, HIF-1α accumulates leading to transcriptional activation of genes containing hypoxia response elements, such as *VEGF* [156]. The HIF-1α-related pro-angiogenic activity of thyroid hormones is especially interesting in the context of solid tumours that are typically associated with local hypoxia [161]. T3 has been reported to induce HIF-1α expression by a PI3K-dependent mechanism in human skin fibroblasts, an effect that has been proposed to be mediated by cytoplasmically located TRβ [173, 174]. Further, T3, and not T4, has been shown to induce HIF-1α expression in human glioma cells, again via PI3K [39]. Whether PI3K-dependent induction of HIF-1α expression is initiated at the cell surface at integrin αvβ3 or at a cytoplasmically located TR, or both, has, however, not yet been conclusively shown [39, 47, 129, 174]. T4, on the other hand, has been shown to induce internalisation of integrin αvβ3 in human non-small cell lung cancer and ovarian carcinoma cells, resulting in a complex formed between the αv monomer and ERK1/2 (MAPK), leading to nuclear import [175]. Tetrac inhibited internalisation of integrin αvβ3. In the nucleus, αv acts as a transcriptional co-activator that helps drive the transcription of HIF-1α. [45, 161, 176]. The pro-angiogenic effect of thyroid hormones on MSCs was further confirmed in an *in vitro* endothelial tube formation assay demonstrating significantly enhanced tube formation under treatment with supernatant from T3-stimulated MSCs. The increased expression and secretion of pro-angiogenic factors by MSCs under thyroid hormone stimulation detected by qPCR and ELISA directly stimulated HUVEC tube formation. The tube formation data also reflect the observation that T3 generally seems to have stronger effects in our system. Many of the effects on gene expression could be directly blocked by additional treatment with tetrac. The inhibitory effects of tetrac on angiogenesis were strikingly apparent in the tube formation assay. Thus, we conclude that the observed effects are largely initiated at integrin αvβ3. Interestingly, we observed no tetrac effects on basal tube formation, or on the increased tube formation triggered by MSC-conditioned medium. A possible explanation for the strong tetrac effects only under parallel treatment with thyroid hormone may lie in integrin activation and/or clustering in the cell membrane of MSCs as a result of agonist thyroid hormone stimulation. Tetrac would then be able to exert its inhibitory effects only once this activation has occurred. In this context, tetrac was shown to prevent radiation-induced activation of the β3 monomer *in vitro*, while it did not affect the basal, non-irradiated activation state [177]. Furthermore,

integrin cluster formation and resulting activation is not only known to be essential for extracellular matrix adhesion, but has also been proposed to influence integrin-related signalling [178]. Indeed, when the binding site for RGD, which provokes integrin clustering, is blocked, thyroid hormone action at the integrin is inhibited [133]. Whether thyroid hormone influences integrin cluster formation has not been thoroughly investigated to date, though T4 was reported to regulate integrin clustering in astrocytes [179, 180]. The observation that co-clustering and resulting crosstalk between integrin αvβ3 and angiogenesis-relevant growth factor receptors for VEGF, FGF2, EGF, platelet-derived growth factor and IGF1 occurs, adds a further dimension to the complex regulation of angiogenesis by thyroid hormones [161, 181]. Tetrac has been proposed to interfere with this crosstalk on the surface of endothelial cells and similar effects in MSCs are conceivable [161].

HIF-1α and VEGF are two master regulators of angiogenesis with central importance in angiogenic signalling, whose expression by MSCs has been shown to be regulated by thyroid hormones and tetrac in the current study (HIF-1α), and in a previous study (VEGF; [20]). We therefore established hypoxia-responsive and VEGF-promoter reporter constructs. As reporter gene we used the transmembrane protein NIS that transports iodide into thyroid follicular cells and thus provides the molecular basis for the diagnostic and therapeutic application of radioiodide in thyroid cancer patients [88]. In our previous work, we have gathered extensive experience in targeting NIS to non-thyroidal tumours using genetically engineered MSCs as gene transfer vehicles based on their inherent tumour homing capacity [66, 70-73, 75, 76]. One of the many advantages of NIS is that it allows detailed, non-invasive *in vivo* tracking of MSCs, as well as quantifiable functional NIS expression, by ^{123}I scintigraphy and ^{124}I PET. Based on these studies, we employed this system to study thyroid hormone action on MSC biology within the tumour microenvironment. *In vitro* we observed a thyroid hormone-dependent up-regulation of hypoxia-responsive and VEGF promoter activity that was already evident at physiological hormone concentrations and could be blocked by tetrac, as well as inhibitors of signalling pathways downstream of the hormone binding site at the integrin. These observations further support the involvement of integrin αvβ3.

Based on the more promising *in vitro* results using the VEGF-NIS reporter construct and the central role of VEGF in regulating practically all relevant aspects of tumour angiogenesis, we applied VEGF-NIS-MSCs *in vivo* in an orthotopic HCC xenograft mouse model. We then measured ^{124}I uptake by PET in mice with different thyroid hormone states. Tumoural radioiodide uptake demonstrated successful recruitment of VEGF-NIS-MSCs after systemic application followed by VEGF promoter-driven NIS expression. In hyperthyroid animals, a strongly enhanced radioiodide signal was detected compared to euthyroid mice, while hypothroidism or treatment with tetrac markedly reduced the signal seen. *Ex vivo* analysis of NIS-specific immunoreactivity and NIS mRNA expression normalised to MSC recruitment, reflected the PET imaging results. These data confirm the *in vitro* data suggesting thyroid hormone-mediated stimulation of VEGF that is inhibited by tetrac. In addition, tumour vascularisation reflects the

pro-angiogenic effects of thyroid hormones seen *in vitro* and *in vivo* as evidenced by a lower blood vessel density in hypothyroid and tetrac-treated mice as compared to euthyroid and hyperthyroid mice. Our data imply that T3 and T4 influence angiogenic signalling via integrin αvβ3 in the tumour microenvironment not only in tumour cells and endothelial cells, but also in MSCs, further establishing MSCs as thyroid hormone-dependent targets via integrin αvβ3. Stimulation of cancer-related angiogenesis is obviously undesirable in cancer patients and thyroid hormones have been proposed to limit anti-angiogenic therapy [162, 182]. Growing experimental evidence, supported by clinical data and population-based studies, suggests that thyroid hormones are involved in cancer development, progression and metastasis, with established effects on cancer cell proliferation and cancer cell defence pathways, in addition to angiogenesis [45, 47, 183]. Against this background, understanding the complex mechanisms underlying pro-angiogenic effects of thyroid hormones is of paramount importance, not least due to the promising anti-angiogenic activity of tetrac.

4.6 Acknowledgements

We are grateful to Dr. Barbara von Ungern-Sternberg and Rosel Oos (Department of Nuclear Medicine, LMU Munich, Munich, Germany) for their assistance with animal care and PET imaging studies.

This work was supported by grants from the Deutsche Forschungsgemeinschaft within the Priority Programme SPP1629 to CS and PJN (SP 581/6-1, SP 581/6-2, NE 648/5-2), and within the Collaborative Research Center SFB 824 to CS (project C8) as well as a grant from the Wilhelm-Sander-Stiftung to CS (2014.129.1).

V. CHAPTER 4

Thyroid status affects tumour growth in integrin αvβ3-positive tumours only

Kathrin A Schmohl[1], Yang Han[1], Mariella Tutter[1], Nathalie Schwenk[1], Sibylle I Ziegler[2], Peter Bartenstein[2], Peter J Nelson[1] and Christine Spitzweg[1]

[1]Department of Internal Medicine IV, University Hospital of Munich, LMU Munich, Munich, Germany
[2]Department of Nuclear Medicine, University Hospital of Munich, LMU Munich, Munich, Germany

5.1 Abstract

Thyroid hormones are emerging as critical regulators of tumour growth and progression via a non-classical signalling pathway initiated at integrin αvβ3 expressed on many tumour cells, proliferating endothelial cells, and tumour stroma-associated cells. To assess the contribution of thyroid hormone signalling via integrin αvβ3 to tumour growth, we compared the effects of thyroid hormones versus tetrac, a specific inhibitor of thyroid hormone action at integrin αvβ3, in two murine xenograft tumour models with and without integrin αvβ3 expression.

Integrin αvβ3-positive human anaplastic thyroid cancer cells SW1736 and integrin αvβ3-negative human hepatocellular carcinoma cells HuH7 were injected into the flanks of nude mice. Tumour growth was monitored in euthyroid, hyperthyroid, hypothyroid, and euthyroid tetrac-treated mice in both models. In SW1736 xenograft mice, hyperthyroidism led to a significantly increased tumour growth resulting in a decreased survival compared to euthyroid mice. In hypothyroid and tetrac-treated mice, in contrast, tumour growth was significantly reduced and, hence, survival prolonged compared to euthyroid and hyperthyroid animals. Both proliferation and vascularisation, as determined by Ki67 and CD31 immunofluorescence staining, respectively, were significantly increased in tumours from hyperthyroid mice as compared to hypothyroid and tetrac-treated mice. No differences in tumour growth, survival, or Ki67 staining were observed between the different thyroid hormone states in mice bearing integrin αvβ3-negative HuH7 xenografts. The blood vessel density, however, was significantly decreased in hypothyroid and tetrac-treated mice compared to both euthyroid and hyperthyroid mice. Apoptosis was not affected in either tumour model, nor was cell proliferation *in vitro*.

Both the reduced tumour growth rate in tetrac-treated mice bearing integrin αvβ3-positive tumours and the unaffected growth of integrin αvβ3-negative tumours imply integrin αvβ3-dependency. The regulation of tumour growth by thyroid hormones in αvβ3-positive tumours has important implications for cancer patients, especially for those with cancer treatment-related or unrelated thyroid dysfunction or thyroid cancer patients treated with thyroid-stimulating hormone- (TSH-) suppressive L-thyroxine doses.

5.2 Introduction

The thyroid hormones 3,5,3'-triiodo-L-thyronine (T3) and L-thyroxine (T4) have a broad spectrum of biological activity relating to embryonic development, differentiation, growth, and metabolism in the healthy organism. Several decades of both clinical and experimental evidence suggest that they are also critical regulators of tumour progression [47, 184]. Indeed, thyroid hormones have been shown to stimulate tumour cell proliferation and inhibit apoptosis, besides modulating angiogenesis, inflammation, and tumour stroma formation [29, 47, 147, 161, 184-186]. These effects are thought to be mediated mainly by non-classical thyroid hormone signalling initiated at integrin αvβ3. This heterodimeric transmembrane adhesion receptor links the extracellular matrix to the intracellular cytoskeleton and is expressed at high levels on many tumour cells, dividing endothelial cells, and stromal cells [20, 187, 188]. Discovered in 2005 by Bergh *et al.*, the thyroid hormone binding site on integrin αvβ3 is located on the extracellular domain and shows neither structural nor functional homology to the classical nuclear thyroid hormone receptors (TRs) [33, 38, 39]. The binding site is subspecialised into two distinct sites: one binds T3 and stimulates the PI3K pathway, while the other binds both T3 and T4 and activates MAPK (ERK1/2) signalling [39]. The latter has been shown to enhance cell proliferation and decrease apoptosis in tumour cells upon thyroid hormone binding [29, 39], while angiogenesis may be modulated from both binding sites [39]. The naturally occurring thyroid hormone metabolite 3,3',5,5'-tetraiodothyroacetic acid (tetrac) blocks thyroid hormone binding and thus signalling at both binding sites on the integrin [39].

Physiological concentrations of T4 and supraphysiological concentrations of T3 have been reported to enhance the proliferation of tumour cell lines *in vitro*, including breast and ovarian cancer, follicular and papillary thyroid carcinoma, small cell and non-small cell lung carcinoma, glioma, T-cell lymphoma, and multiple myeloma [39, 146, 189-199]. In addition, T3 and T4 have been shown to drive angiogenesis via stimulation of endothelial cell proliferation, migration, and vascular tube formation. This can occur either directly by stimulation of the endothelial cells themselves, or indirectly by stimulation of the secretion of pro-angiogenic modulators by tumour cells and tumour-educated mesenchymal stem cells that in turn act on endothelial cells [20, 42, 47, 148, 162, 163, 185]. In all cases, the observed effects on proliferation and angiogenesis were attributed to integrin αvβ3-mediated thyroid hormone signalling, as shown by inhibitors that selectively block αvβ3, including tetrac. *In vivo* data support these observations: In rodents bearing syngeneic and xenograft tumours, induction of hypothyroidism, by pharmaceutical inhibition of thyroid hormone synthesis, radioiodine ablation, or surgical thyroidectomy, led to reduced tumour growth in models of breast, prostate, and lung carcinoma, as well as sarcoma, fibrosarcoma, and hepatoma [31, 49-54]. Further, T4 has been shown to increase tumour growth in syngeneic mouse models of sarcoma and fibrosarcoma [50]. In a murine Lewis lung carcinoma model, T4, but not T3, treatment increased tumour growth, an effect that was inhibited by tetrac [200]. In addition, tetrac

reduced tumour mass and haemoglobin content in breast, renal, follicular thyroid, medullary thyroid, lung, and pancreas carcinoma xenografts in mice via stimulation of apoptosis and inhibition of angiogenesis [132, 154, 190, 196, 201-203].

Thus, the impact of thyroid hormone signalling via integrin αvβ3 on tumour growth can be attributed to a direct response of the cancer cells themselves through increased proliferation and/or inhibition of apoptosis, and to indirect effects on the stromal compartment, particularly on angiogenesis, via stimulation of integrin αvβ3-positive endothelial cells and stromal cells. In order to better understand the contributions of these separate effects on tumour growth and to confirm the central role of tumoural integrin αvβ3 expression, we used an integrin αvβ3-positive and an integrin αvβ3-negative tumour cell line to compare thyroid hormone versus tetrac effects on tumour growth in murine xenografts in the current study.

5.3 Materials and Methods

Cell culture

The human anaplastic thyroid carcinoma cell line SW1736 and the human hepatocellular carcinoma cell line HuH7 were cultured in RPMI (Sigma-Aldrich, St. Louis, MO, USA) and DMEM low-glucose (Sigma-Aldrich), respectively, supplemented with 10% (v/v) FBS (FBS Superior, Biochrom/Merck Millipore, Berlin, Germany) and 100 U/ml penicillin/100 µg/ml streptomycin (Sigma-Aldrich). Both cell lines were maintained at 37 °C in a humidified 5% (v/v) CO_2 atmosphere.

Quantitative real-time PCR

mRNA expression of the two integrin αvβ3 subunit genes *ITGAV* and *ITGB3* was determined by quantitative real-time PCR (qRT-PCR) as described previously [20] on a LightCycler 96 (Roche Diagnostics, Mannheim, Germany) using the following primers: *ACTB*, fwd 5'-AGAAAATCTGGCACCACACC-3', rev 5'-TAGCACAGCCTGGATAGCAA-3'; *R18S*, fwd 5'-CAGCCACCCGAGATTGAGCA-3', rev 5'-TAGTAGCGACGGGCGGTGTG-3'; *ITGAV*, fwd 5'-CACCAGCAGTCAGAGATGGA-3', rev 5'-GGCAACCGTGTCATTCTTTT-3'; *ITGB3*, fwd 5'-AAGGATAACTGTGCCCCAGA-3', rev 5'-CACAGGCTTGTCCACAAATG-3'. Relative expression levels are expressed as $\Delta\Delta C_t$ values normalised to internal *ACTB* (β-actin) and *R18S* (18S rRNA). Samples were run in duplicate for each of four independent replicates.

Flow cytometry

Cell surface expression of integrin αvβ3 was assessed by flow cytometry as described previously [204]. Per sample, 10^6 cells were incubated with 0.5 µg of a mouse monoclonal IgG1 antibody against integrin αvβ3 (clone 27.1 (VNR-1); Abcam, Cambridge, UK). As secondary antibody an Alexa Fluor 488-conjugated goat anti-mouse antibody (Abcam) was used.

Thyroid hormone treatment *in vitro*

SW1736 and HuH7 were serum-starved overnight prior to treatment with physiological or supraphysiological total concentrations of thyroid hormones (all from Sigma-Aldrich), i.e. 1 nM or 10 nM T3 and 100 nM or 1000 nM T4, with and without 100 nM tetrac in medium containing charcoal-stripped serum (<0.2 pg/ml T3, 0.2-0.6 ng/dl T4). Cell proliferation was assessed by MTT assay (Promega, Mannheim, Germany) as described previously [170] after 24, 48, 72, and 96 h of thyroid hormone treatment.

Animals

All animal experiments were performed in accordance with German animal welfare laws and the approval of the regional governmental commission for animals (Regierung von Oberbayern, Munich, Germany). Male immunodeficient CD1 nu/nu mice (Charles River, Sulzfeld, Germany) were allowed to acclimatise for one week and kept under specific pathogen-free conditions with access to standard nude mouse diet (ssniff, Soest, Germany) and water *ad libitum*. To establish xenograft tumours, five- to six-week old mice were implanted with either 15×10^6 SW1736 or 5×10^6 HuH7 in 100 µl PBS subcutaneously into the right hind flank. Tumour growth was monitored by calliper measurement of three dimensions at least every second day and the volume calculated as $4/3 \times \pi \times \text{length}/2 \times \text{width}/2 \times \text{height}/2$.

Thyroid hormone treatment *in vivo*

Once tumours were visible, mice received drinking water supplemented with 0.02% (w/v) 2-mercapto-1-methylimidazole (MMI; Sigma-Aldrich) and 1% (w/v) sodium perchlorate (Sigma-Aldrich) to induce hypothyroidism and generate the same baseline treatment for all groups [20, 144]. Saccharin (Sigma-Aldrich) was added at a concentration of 0.3% (w/v) to mask the bitter taste of the anti-thyroid drugs. Thyroid hormone treatment was started when tumours reached a size of >100 mm^3. Mice were randomly assigned to different treatment groups that received daily intraperitoneal injections of 100 ng/g body weight L-T4 (Sigma-Aldrich) to induce hyperthyroidism (SW1736 n=6; HuH7 n=7), 20 ng/g body weight L-T4 to render mice euthyroid, with (SW1736 n=5; HuH7 n=8) or without (SW1736 n=6; HuH7 n=8) 10 µg/g body weight tetrac (Sigma-Aldrich), or saline for the hypothyroid group (SW1736 n=5; HuH7 n=7). The thyroid hormone status was monitored in final serum samples by ELISA (DRG Diagnostics, Marburg, Germany). Mice were sacrificed and dissected when tumours reached a size >1500 mm^3, or, as was the case for one tetrac-treated mouse bearing an SW1736 tumour, the tumour started to exulcerate.

Ex vivo analysis

Immunofluorescence staining of frozen tissue sections was performed as described previously [205]. For Ki67 (proliferating cells) and CD31 (blood vessels) co-staining, a rabbit polyclonal antibody against human Ki67 (Abcam; dilution 1:200) and a rat monoclonal antibody against mouse CD31 (BD

Pharmingen, Heidelberg, Germany; dilution 1:100) followed by an Alexa Fluor 488-conjugated anti-rabbit secondary antibody (Jackson ImmunoResearch, West Grove, PA, USA) and a Cy3-conjugated anti-rat secondary antibody (Jackson ImmunoResearch), respectively, were used. To stain for apoptotic cells, a terminal deoxynucleotidyl transferase dUTP nick end labelling (TUNEL) assay was performed (Click-iT TUNEL Alexa Fluor 488, Thermo Fisher Scientific, Waltham, MA, USA) according to the manufacturer's instructions. Nuclei were counterstained with 5 µg/ml bisbenzimide Hoechst 33258 (Sigma-Aldrich). Stained sections were mounted with Dako Fluorescence Mounting Medium (Dako, Carpinteria, CA, USA) and imaged at 10× (Ki67/CD31 staining) or 20× (TUNEL) magnification on a Leica DMI6000 B fluorescence microscope equipped with a Leica DFC365 FX CCD camera, and the software Leica Application Suite X (Leica Microsystems, Wetzlar, Germany). A minimum of five visual fields was recorded per tumour. The percentage of Ki67-positive and apoptotic nuclei, or the percent CD31-positve area per visual field were determined using ImageJ (National Institutes of Health, Bethesda, MD, USA).

Statistics

All data are expressed as mean ± SEM, mean fold change ± SEM, or, for survival plots, percent. Statistical significance was tested by one-way ANOVA followed by Tukey's Honestly Significant Difference post hoc test, except for the qRT-PCR data and mouse survival, where Student's *t*-test and log-rank test were performed, respectively. *p*-values <0.05 were considered statistically significant (**p*<0.05; ***p*<0.01; ****p*<0.001; n/s not significant).

5.4 Results

Integrin αvβ3 is expressed on SW1736, but not on HuH7 cells

Integrin αvβ3 expression in human anaplastic thyroid cancer cells SW1736 and human hepatocellular carcinoma cells HuH7 was analysed by qRT-PCR and flow cytometry. In SW1736, mRNA for both integrin subunits was detected, while HuH7 only express *ITGAV*, the gene for the αv subunit, and no mRNA for the gene coding for the β3 subunit (*ITGB3*) was detected (**Fig. 19A**). Accordingly, cell surface expression of integrin αvβ3 was only detected in SW1736 by flow cytometry (**Fig. 19B**).

Thyroid hormone stimulation *in vitro*

Thyroid hormone (1 and 10 nM T3 or 100 and 1000 nM T4) and/or tetrac (100 nM) treatment had no effect on tumour cell proliferation *in vitro*, neither in integrin αvβ3-positive SW1736, nor in integrin αvβ3-negative HuH7 cells after 24, 48, 72, or 96 h of stimulation (data not shown).

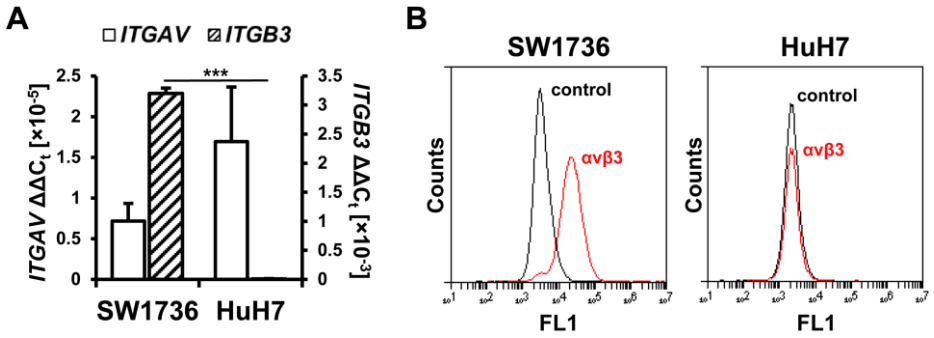

Figure 19: Integrin αvβ3 expression on SW1736 and HuH7 cells. (**A**) Average mRNA expression of integrin subunits αv (*ITGAV*) and β3 (*ITGB3*) in human anaplastic thyroid carcinoma cells SW1736 and hepatocellular carcinoma cells HuH7 (n=4, mean ± SEM; ***p<0.001) was determined by qRT-PCR. (**B**) Cell surface expression of integrin αvβ3 was analysed by flow cytometry using an integrin αvβ3-specific primary antibody followed by an Alexa Fluor 488-labelled secondary antibody. Controls were incubated with the secondary antibody only.

Thyroid hormone stimulates tumour growth via integrin αvβ3

Mice bearing either integrin αvβ3-positive anaplastic thyroid carcinoma SW1736 xenograft tumours or integrin αvβ3-negative hepatocellular carcinoma HuH7 xenograft tumours were assigned to different thyroid hormone treatment groups and tumour growth was observed until a tumour size of 1500 mm^3 was reached (**Fig. 20A**). One mouse bearing an SW1736 tumour treated with tetrac had to be sacrificed prematurely due to ulceration of the tumour. The respective thyroid hormone status was confirmed by T4 measurement in serum after sacrifice (**Fig. 20B**). As the ELISA could not distinguish tetrac from T4, serum values for euthyroid tetrac-treated mice are not shown. However, the same body weight-adjusted dose of T4 was used for the tetrac-treated group as for the euthyroid group, leading to highly reproducible serum T4 levels in the range of untreated naturally euthyroid mice (control in **Fig. 20B**).

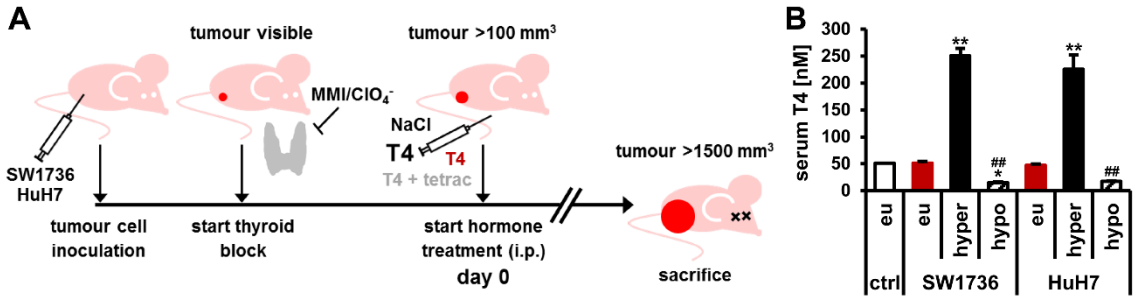

Figure 20: Experimental set-up *in vivo*. (**A**) SW1736 or HuH7 tumour cells were injected subcutaneously into nude mice and endogenous thyroid hormone production was blocked by MMI/perchlorate in the drinking water. Mice were assigned to different thyroid hormone treatment groups by daily injections once tumours reached a size >100 mm^3 and tumour growth was monitored until the tumour size exceeded 1500 mm^3. (**B**) The thyroid hormone status of the different groups was verified by serum T4 measurement and compared to untreated euthyroid control mice (ctrl).

Tumour growth of integrin αvβ3-positive anaplastic thyroid carcinoma SW1736 xenograft tumours was significantly increased in hyperthyroid compared to euthyroid mice, while tumour growth was

significantly reduced both in hypothyroid and tetrac-treated euthyroid animals (**Fig. 21A**). This led to a significantly increased survival, defined by a maximum tumour size of 1500 mm^3, in the hypothyroid (median survival 25 days) and the tetrac-treated group (median survival 23 days), and a significantly reduced survival in the hyperthyroid group (median survival 11 days) as compared to euthyroid animals (median survival 16 days; **Fig. 21A**). In the integrin αvβ3-negative HuH7 tumour model, in contrast, no significant differences in tumour growth or survival were detected between the different treatment groups (**Fig. 21B**).

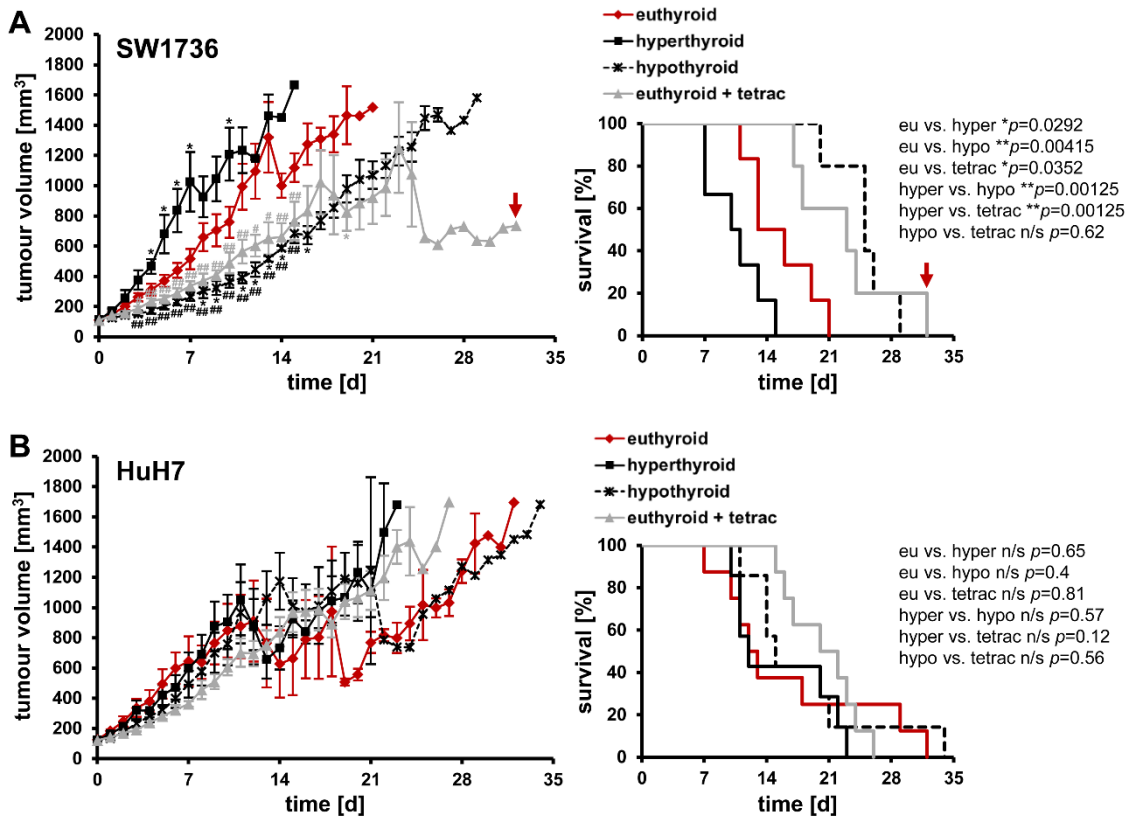

Figure 21: Thyroid hormone status influences tumour growth in murine xenografts via tumoural integrin αvβ3 expression. For both (**A**) integrin αvβ3-positive SW1736 xenografts (euthyroid: n=6, hyperthyroid: n=6, hypothyroid: n=5, euthyroid + tetrac: n=5) and (**B**) integrin αvβ3-negative HuH7 xenografts (euthyroid: n=8, hyperthyroid: n=7, hypothyroid: n=7, euthyroid + tetrac: n=8), the average tumour growth (left panels; mean ± SEM; $*p<0.05$ versus euthyroid; $^{\#}p<0.05$, $^{\#\#}p<0.01$ versus hyperthyroid) and survival (right panels; percent; $*p<0.05$, $**p<0.01$, n/s not significant) of the different treatment groups were compared. One SW1736 tumour-bearing mouse had to be sacrificed prematurely due to tumour ulceration (red arrows in (A)).

Effects on tumour growth arise from increased proliferation and angiogenesis

Ex vivo analysis of frozen tumour sections revealed an increase in proliferating cells and vascularisation in the tumours of hyperthyroid mice compared to both hypothyroid and tetrac-treated mice in SW1736 tumours as evidenced by the results of Ki67 and CD31 staining, respectively (**Fig. 22A**).

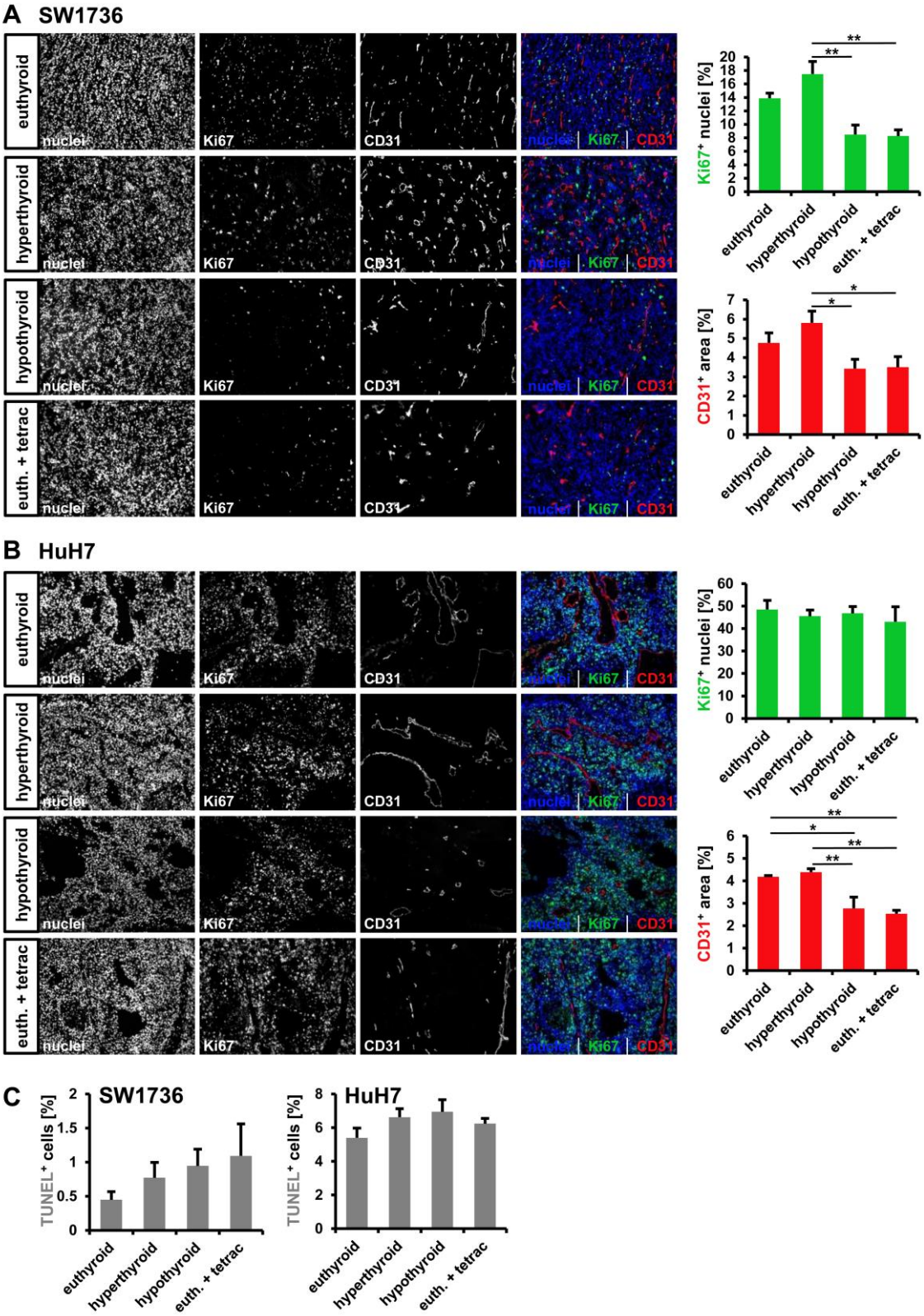

Figure 22: ***Ex vivo*** **analysis of tumoural cell proliferation, vascularisation, and apoptosis.** Tumour cell proliferation was assessed by Ki67 immunofluorescence staining and blood vessel density by CD31 staining on frozen SW1736 (**A**) and HuH7 (**B**) tumour sections. A minimum of five visual fields was quantified per tumour (mean ± SEM; **p*<0.05, ***p*<0.01). Magnification: 10×. (**C**) Apoptosis was analysed by TUNEL assay on a minimum of seven visual fields per frozen tumour section at 20× magnification (mean ± SEM).

In HuH7 tumours, the blood vessel density was significantly decreased in hypothyroid and tetrac-treated animals compared to both euthyroid and hyperthyroid animals (**Fig. 22B**). Tumour cell proliferation, in contrast, was not affected by any of the treatment regimens (**Fig. 22B**). No significant differences in the number of apoptotic cells were detected between the different treatment groups in either of the tumour models (**Fig. 22C**).

5.5 Discussion

Growing clinical and experimental evidence suggests that thyroid hormones are implicated in cancer development and progression, affecting tumour cell proliferation, survival, and angiogenesis [29, 147, 161, 185]. Besides canonical thyroid hormone signalling via nuclear receptors, thyroid hormone action can also be exerted via the plasma membrane receptor integrin αvβ3. The integrin is highly expressed on many cancer cells, proliferating endothelial cells, and stromal cells in the tumour milieu [20, 187, 188]. Hence, it stands to reason that signalling via integrin αvβ3 is linked to cancer-relevant thyroid hormone effects. Indeed, previous studies in tumour models expressing integrin αvβ3 have conclusively demonstrated that thyroid hormones and tetrac, a T4 derivative that functions as a specific inhibitor of thyroid hormone action at integrin αvβ3, modulate tumour growth and angiogenesis. To our knowledge, thyroid hormone effects specifically on integrin αvβ3-negative tumours, however, have not been examined to date. To evaluate the contribution of integrin αvβ3 expression on tumour cells to thyroid hormone effects on tumour growth *in vivo*, we employed an integrin αvβ3-positive and an integrin αvβ3-negative murine xenograft tumour model in the current study.

We here show that only for the integrin-positive tumour cell line SW1736 tumour growth was influenced by thyroid hormone status and tetrac. While hyperthyroid mice showed a significantly faster tumour growth, both hypothyroid and tetrac-treated euthyroid mice showed a significantly reduced tumour growth as compared to euthyroid mice. Accordingly, the study endpoint of tumour sizes exceeding 1500 mm^3 was reached significantly later in hypothyroid and tetrac-treated euthyroid mice, and significantly earlier in hyperthyroid mice as compared to euthyroid animals. These results confirm observations made in a number of different tumour models *in vitro* and *in vivo* [31, 39, 49-54, 132, 146, 154, 189-203] that were attributed to effects on tumour cell proliferation [39, 54, 146, 189-199, 201], apoptosis [132, 203], and angiogenesis [132, 154, 190, 196, 200, 202, 203]. To assess the mechanisms contributing to the differences observed in the current study, we evaluated these same parameters, i.e. tumour cell proliferation, apoptosis, and angiogenesis, *ex vivo* on tumour sections.

Tumour cell proliferation was influenced by thyroid hormone status only in the integrin-positive SW1736 tumours with a significantly decreased number of proliferating cells in tumours of hypothyroid and tetrac-treated mice as compared to hyperthyroid mice. Surprisingly, considering this *in vivo* observation, we did not detect effects on tumour cell proliferation *in vitro*. This may stem from the oversimplification of the system under observation in 2D cell culture, where crucial components such

as extracellular matrix and stromal cell interactions, as well as concentration gradients of oxygen, nutrients, and effector molecules are virtually non-existent [206]. Apoptosis was not significantly influenced in either of the models, though in SW1736 tumours a trend with lowest apoptosis rates in euthyroid animals and highest in tetrac-treated animals was observed that may have additionally slightly contributed to the differences in tumour growth rates.

Vascularisation, in contrast, was decreased in tumours of the hypothyroid and tetrac-treated groups in both the integrin-positive SW1736 and the integrin-negative HuH7 tumour model. This is not surprising, as proliferating endothelial cells are known to express high levels of integrin αvβ3 and, indeed, endothelial cell proliferation, migration, and vascular tube formation have been shown to be modulated by thyroid hormones via integrin αvβ3 [42, 148, 162, 163]. However, though tumour vascularisation was influenced in integrin αvβ3-negative HuH7 tumours, this effect was not sufficient to significantly influence tumour growth. This observation is in accordance with a previous study, where, analysing thyroid hormone effects on tumour angiogenesis in an orthotopic HuH7 mouse model, we found that differences in angiogenesis did not affect tumour growth [185]. Taking a closer look at tumour growth and survival in the HuH7 model, the hypothyroid and especially the tetrac-treated group seem to initially (for the first 10-13 days) slightly lag behind the euthyroid and hyperthyroid groups, though differences were not statistically significant. In tetrac-treated animals, where this effect is more pronounced, median survival amounted to 22 days, compared to 13, 12, and 15 days in the eu-, hyper-, and hypothyroid groups, respectively. Following this initial lag, however, tetrac-treated mice caught up with the other groups and no significant differences in overall survival were observed. Yalcin *et al.* made the interesting observation that mouse xenografts of human medullary thyroid cancer show an acute reaction to tetrac treatment within the first few days that the authors' attribute to the anti-angiogenic activity of tetrac [203]. This acute phase is followed by a long-term progressive, albeit weaker, inhibiting effect on tumour growth thought to be caused by the pro-apoptotic activity of tetrac on the tumour cells themselves [203]. As we do see effects on angiogenesis in the HuH7 model, the initial slight delay in tumour growth may stem from this acute response.

The differences in tumour growth and, as a consequence, survival between the integrin αvβ3-positive and -negative tumour models along with the fact that in the integrin-positive tumour cell line tetrac inhibited tumour cell proliferation in euthyroid mice to the same extent as the induction of hypothyroidism, are further compelling evidence for pathway initiation at integrin αvβ3. Obviously, stimulation of tumour growth, be it by endogenous or exogenously applied thyroid hormones, is undesirable in cancer patients. In this context, a myriad of population-based and clinical studies have examined the potential link between thyroid state and the risk of developing cancer and cancer progression and survival. Overall, data remain inconclusive, ranging from no detectable effects to both higher and lower cancer risk and better and worse prognosis in existing cancers for both hyper- and hypothyroidism [47]. Compelling clinical evidence for a tumour-promoting effect of thyroid hormones, however, stems from the observation that cancer patients that develop hypothyroidism as an unwanted

side effect of tyrosine kinase inhibitor, interleukin-2 or radiation treatment, often show a more favourable outcome [47]. Against this background, T4 supplementation as standard hormone replacement therapy for hypothyroidism and the application of thyrotropin (TSH)-suppressive doses of T4 in differentiated thyroid cancer patients may have to be reconsidered – at least in those patients with tumoural integrin αvβ3 expression [47, 184]. The affinity for T4 is far higher than for T3 at integrin αvβ3 [41]. Indeed, several experimental studies have observed that T3 in the physiological concentration range does not elicit effects on tumour growth, suggesting that T3 supplementation may have an advantage over T4 supplementation, at least in a subset of patients [29, 41, 58, 184, 200]. In addition, as integrin αvβ3 is rarely expressed at high levels on normal cells and allows targeting of multiple cancer-relevant mechanisms from a single receptor site, blocking integrin αvβ3 function without affecting physiologic thyroid hormone signalling at nuclear thyroid hormone receptors is a feasible alternative.

The comparison of the effects on tumours derived from αvβ3-positive and αvβ3-negative tumour cells demonstrates that integrin expression on the tumour cells themselves is more critical than effects on angiogenesis via the endothelium itself. These observations highlight the importance of tumoural receptor status and identify a possible explanation for the discrepancies in clinical studies examining thyroid hormone effects on cancer.

5.6 Acknowledgements

We are grateful to Dr. Barbara von Ungern-Sternberg and Rosel Oos (Department of Nuclear Medicine, LMU Munich, Munich, Germany) for their assistance with animal care and to Dr. Sarah Urnauer (Department of Internal Medicine IV, LMU Munich, Munich, Germany) for performing flow cytometry experiments.

VI. CHAPTER 5

Reintroducing the sodium iodide symporter (NIS) to anaplastic thyroid carcinoma

Kathrin A Schmohl[1*], Patrick Dolp[1*], Christina Schug[1], Kerstin Knoop[1], Kathrin Klutz[1], Nathalie Schwenk[1], Peter Bartenstein[2], Peter J Nelson[1], Manfred Ogris[3], Ernst Wagner[4] and Christine Spitzweg[1]

[1]Department of Internal Medicine IV, University Hospital of Munich, LMU Munich, Munich, Germany
[2]Department of Nuclear Medicine, University Hospital of Munich, Munich, Germany
[3]Department of Pharmaceutical Chemistry, University of Vienna, Vienna, Austria
[4]Department of Pharmacy, LMU Munich, Munich, Germany
*KAS and PD contributed equally

This chapter is a pre-copy-edited version of a peer-reviewed article published in *Thyroid* **2017**;27:1534-43.

Parts of this chapter are included in the doctoral thesis of Patrick Dolp. Kathrin A Schmohl performed NIS stainings and the therapy study. Patrick Dolp performed *in vitro* iodide uptake studies, *in vivo* scintigraphies and the therapy study. The manuscript was written by Kathrin A Schmohl.

6.1 Abstract

Anaplastic thyroid carcinoma (ATC), the most aggressive form of thyroid cancer, is unresponsive to radioiodide therapy. In the current study, we aimed to extend the diagnostic and therapeutic application of radioiodide beyond the treatment of differentiated thyroid cancer by targeting the functional sodium iodide symporter (NIS) to ATC.

We employed nanoparticle vectors (polyplexes) based on linear polyethylenimine (LPEI), shielded by polyethylene glycol (PEG) and coupled to the synthetic peptide GE11 as an epidermal growth factor receptor (EGFR)-specific ligand in order to target a *NIS*-expressing plasmid (LPEI-PEG-GE11/NIS) to EGFR overexpressing human thyroid carcinoma cell lines. Using ATC xenograft mouse models, we evaluated transfection efficiency by ^{123}I scintigraphy and potential for systemic radioiodide therapy after systemic polyplex application.

In vitro iodide uptake studies in SW1736 and Hth74 ATC cells, and, for comparison, in more differentiated follicular (FTC-133) and papillary (BCPAP) thyroid carcinoma cells demonstrated high transfection efficiency and EGFR-specificity of LPEI-PEG-GE11/NIS that correlated well with EGFR expression levels. After systemic polyplex injection, *in vivo* ^{123}I gamma camera imaging revealed significant tumour-specific accumulation of radioiodide in an SW1736 and an Hth74 xenograft mouse model. Radioiodide accumulation was found to be higher in SW1736 tumours, reflecting *in vitro* results, EGFR expression levels and results from *ex vivo* analysis of NIS staining. Administration of ^{131}I in LPEI-PEG-GE11/NIS-treated SW1736 xenograft mice resulted in significantly reduced tumour growth associated with prolonged survival compared to control animals.

Our data open the exciting prospect of NIS-mediated radionuclide imaging and therapy of ATC after non-viral reintroduction of the *NIS* gene. The high tumour-specificity after systemic application makes our strategy an attractive alternative for the treatment of highly metastatic ATC.

6.2 Introduction

The sodium iodide symporter (NIS) is an intrinsic transmembrane protein that actively transports iodide from the blood into thyroid follicular cells as the first step in thyroid hormone synthesis [88]. Functional NIS expression provides the molecular basis for the diagnostic and therapeutic application of radioiodide, which has successfully been in use since 1946 to treat thyroid cancer patients [62]. This approach still represents the most effective form of anticancer radiotherapy in clinical use to date and makes differentiated thyroid carcinoma one of the most manageable cancers [61, 65]. Anaplastic (undifferentiated) thyroid carcinoma (ATC) cells, in contrast, have lost the ability to concentrate iodide and are subsequently unresponsive to radioiodide therapy [207]. ATC is the most lethal form of thyroid cancer and one of the most aggressive solid tumours in humans, characterised by rapid progression, early dissemination and a high propensity for distant metastasis [207]. Typically, ATC is treated with a multimodal therapeutic approach, consisting of surgery, chemotherapy and loco-regional radiotherapy, though with limited success [208, 209], clearly demonstrating the need for new therapeutic strategies.

Cloning of *NIS* in 1996 was the first step in the development of a novel cytoreductive gene therapy strategy based on targeting functional NIS to both thyroidal and extrathyroidal malignancies, thus extending an established and highly effective anti-cancer strategy beyond the treatment of differentiated thyroid cancer [63, 64, 68]. We and others have shown that selective *NIS* gene transfer into tumour cells allows systemic application of radionuclides resulting in tumour-specific radionuclide concentration that can be used both for non-invasive imaging as well as therapy [66, 67, 70-72, 77-79, 82, 83, 87, 99, 205, 210]. Clinical development of the *NIS* gene therapy concept is dependent on highly specific and efficient tumour targeting at low toxicity and requires systemic application of the therapeutic gene, especially for the treatment of disseminated cancer. However, the biostability and delivery efficiency of ‘naked’ nucleic acids are very low, limiting their systemic applicability [69]. Cationic polymers, such as linear polyethylenimine (LPEI), are a class of non-viral gene delivery vehicles that form sub-micrometre complexes with nucleic acids called polyplexes and thus stabilize the DNA by eliminating unwanted interactions with blood components and other non-target sites [69]. After intravenous application, nanoparticle concentration builds up in the plasma with a long half-life, as nanoparticles escape both renal clearance and penetration of normal endothelium due to their size [85]. LPEI-based polyplexes are internalised with high efficiency and exhibit intrinsic endosomolytic activity allowing efficient release into the cytoplasm followed by nuclear import of the therapeutic gene. Tumour targeting is based on the so-called enhanced permeability and retention (EPR) effect that drives passive accumulation of polyplexes due to the leaky vasculature prevalent in tumours in conjunction with a tumour’s slow venous return and poor lymphatic clearance [69, 84, 85]. Due to inter- and intratumoural heterogeneity, nanoparticle-based drugs that rely on the EPR effect alone for efficient delivery have their limitations in the clinical setting and efficiency will vary from patient to patient [211]. However, tumour specificity

and delivery efficacy can be further increased using ligands that bind to receptors overexpressed on tumour cells. To this end, we attached the epidermal growth factor receptor- (EGFR-) specific ligand GE11 to LPEI *via* a polyethylene glycol (PEG) link that facilitates surface shielding of polyplexes and thus reduces cytotoxicity [86]. GE11 polyplexes undergo efficient clathrin-mediated endocytosis and are quickly transported to the nucleus [212]. In our previous work, LPEI-PEG-GE11 polymers were shown to be highly efficient *NIS* gene delivery vehicles in a high EGFR expressing liver cancer xenograft mouse model, as well as an advanced genetically engineered mouse model of pancreatic ductal adenocarcinoma, as evidenced by tumour-specific radioiodide accumulation and therapeutic efficacy of ^{131}I [87, 210].

As EGFR is typically overexpressed on ATC cells [213], we used the LPEI-PEG-GE11 nanoparticle vectors for *NIS* gene transfer to ATC in the present study to capitalise on the dual diagnostic and therapeutic function of NIS.

6.3 Materials and Methods

EGFR and NIS immunohistochemistry of human anaplastic tumour tissue

In total, nine different tumours stored in the database of the Institute of Pathology from anaplastic thyroid carcinoma patients, which had been operated on between 2003 and 2012, were examined. Immunohistochemical staining of EGFR was performed on a BenchMark XT slide staining system (Ventana Medical Systems, Tucson (AZ), USA) using a monoclonal (IgG1) mouse-antibody (clone: 3C6; Ventana Medical Systems). Evaluation of the staining pattern was performed by visual scoring. No staining resulted in a score of 0; little, non-circumferential staining in more than 10% of the tumour cells was scored as 1+; weak, but thin circumferential staining in more than 10% of the tumour cells was rated with the score 2+; a score of 3+ signifies an intense, thick circumferential staining in more than 10% of the tumour cells. Scores of 0 were rated as negative, while scores of 1+, 2+ and 3+ indicated a weak, moderate and strong positive expression of EGFR, respectively [214]. NIS staining was performed as described previously using a mouse monoclonal antibody (Millipore, Damrstadt, Germany) diluted 1:500 [215].

Cell lines

Anaplastic thyroid carcinoma cell lines SW1736 and Hth74, follicular thyroid carcinoma cell line FTC-133 and papillary thyroid carcinoma cell line BCPAP were grown in RPMI (Thermo Fisher Scientific, Waltham (MA), USA) supplemented with 10% (v/v) fetal bovine serum (FBS; PAA, Colbe, Germany) and 100 U/mL penicillin/100 µg/mL streptomycin (Thermo Fisher Scientific, Waltham (MA), USA). Cells were maintained at 37°C and 5% (v/v) CO_2 in an incubator with 95% humidity. Cell culture medium was replaced every second day and cells were passaged at 70% confluence.

Flow cytometry

For analysis of cell surface EGFR expression by flow cytometry, cells were trypsinised, re-suspended in FACS buffer (phosphate-buffered saline supplemented with 10% (v/v) FBS) and diluted to a density of 6×10^5 cells/100 µL. Cells were incubated with a mouse monoclonal anti-human EGFR antibody (Dako, Hamburg, Germany) or control antibody (mouse IgG; Dako) for 1.5 hours at 4°C. Cells were washed with FACS buffer and incubated with an Alexa488 conjugated polyclonal goat anti-mouse antibody (1:400; Dianova, Hamburg, Germany) for 1 hour at 4°C. To discriminate live and dead cells, propidium iodide (Sigma-Aldrich, Taufkirchen, Germany) was added before acquisition. Analysis was performed on a BD FACSCanto II flow cytometer (BD, Heidelberg, Germany). Cell aggregates and debris were excluded from analysis by appropriate gating.

Polyplex formation

LPEI-based polymers were condensed with plasmid DNA at specific conjugate to plasmid ratios (c/p) in HEPES-buffered glucose as described previously [216] and incubated on ice for 20 minutes before use. Final DNA concentrations were 2 µg/mL for *in vitro* studies and 200 µg/mL for *in vivo* studies.

Transient transfection

For *in vitro* transfection experiments, cells were grown to 70-80% confluency, washed and incubated with LPEI-PEG-GE11/NIS polyplexes at c/p 0.8 in the absence of serum and antibiotics for 4 h. As controls, cells were transfected with LPEI-PEG-Cys/NIS, a polyplex without the active EGFR-targeting ligand or non-coding LPEI-PEG-GE11/antisenseNIS (*NIS* sequence back to front). LPEI-PEG-GE11/NIS-transfected cells treated with the NIS-specific inhibitor perchlorate (1 mM potassium perchlorate; Merck, Darmstadt, Germany) served as additional control. After further incubation in full growth medium for 24 h, transfection efficiency was measured by iodide uptake activity.

^{125}I uptake assay

Iodide uptake was analysed as described previously [169, 170].

Establishment of SW1736 and Hth74 xenografts

Female CD1 nu/nu mice (Charles River, Sulzfeld, Germany) were maintained under pathogen-free conditions with free access to standard nude mouse diet containing 2.2 mg/kg iodine (ssniff, Soest, Germany) and water *ad libitum*. Tumours were established by subcutaneous injection of 5×10^6 tumour cells in 100 µL phosphate-buffered saline into the flank region. Tumours were measured twice a week and tumour volumes were calculated using the equation: tumour volume = length × width × height × 0.52. To reduce thyroidal iodide uptake and thus enhance tumoural uptake, animals were orally pre-treated with 5 mg/L L-thyroxine (Sigma-Aldrich) for 10 days prior to radioiodide (^{123}I, ^{131}I) application as described previously [78, 82, 99]. The experimental protocol was approved by the regional governmental commission for animals (Regierung von Oberbayern, Munich, Germany).

Radioiodide uptake *in vivo*

Once subcutaneous tumours reached a diameter of 8-10 mm (approx. 10-12 weeks after tumour cell injection), two rounds of LPEI-PEG-GE11/NIS (n=3 per tumour model) were injected intravenously (i.v.) via the tail vein 48 h and 24 h prior to intraperitoneal (i.p.) injection of 18.5 MBq (0.5 mCi) ^{123}I (GE Healthcare, Braunschweig, Germany). As a control, a subset of mice (n=1 per tumour model) received 2 mg/mouse of the competitive NIS inhibitor sodium perchlorate (Sigma-Aldrich) 30 minutes before ^{123}I injection. Radioiodide biodistribution was assessed using a gamma camera equipped with a UXHR collimator (e.cam; Siemens, Erlangen, Germany). Regions of interest were quantified by measuring the percentage of the total injected radioiodide dose per gram (% ID/g) tumour. The retention time of radioiodide in the tumour was determined by serial scanning. Dosimetric calculations for ^{131}I were done according to the Medical Internal Radiation Dose (MIRD) technique with a RADAR dose factor (http://www.doseinfo-radar.com).

Indirect immunofluorescence assay

Immunofluorescence staining of frozen tissue sections from LPEI-PEG-GE11/NIS-treated mice was performed as described previously [170] using a rabbit polyclonal NIS-specific primary antibody (Acris Antibodies, Herford, Germany; 1:1,000) and a Alexa488-conjugated secondary antibody (Jackson ImmunoResearch, Suffolk, UK; 1:400). Sections were imaged at 40× magnification on an Axiovert 135 TV fluorescence microscope equipped with an AxioCam MRm CCD camera and AxioVision Rel. 4.8 software (Carl Zeiss, Munich, Germany).

In vivo ^{131}I therapy study

Therapy trials were initiated in SW1736 xenografts eight weeks after tumour cell injection at tumour diameters of approx. 5-10 mm. A cycle consisting of polyplex administration on two consecutive days and a single radioiodide application 24 h later was repeated for a total of three times: polyplexes LPEI-PEG-GE11/NIS or, as controls, LPEI-PEG-GE11/antisenseNIS or NaCl, were administered systemically via the tail vein on days 0/1, 3/4 and 7/8 followed by i.p. application of 55.5 MBq (1.5 mCi) ^{131}I (GE Healthcare), or, as control, saline, on days 2, 5 and 9 (LPEI-PEG-GE11/NIS + ^{131}I, n=10; LPEI-PEG-GE11/antisenseNIS + ^{131}I, n=10; LPEI-PEG-GE11/NIS + NaCl, n=15; NaCl + NaCl, n=11). Mice were sacrificed when at least one endpoint criterion was reached, i.e. when a tumour volume >1500 mm^3 was reached or when tumours started to exulcerate.

Statistics

All *in vitro* experiments were performed in triplicate. Results are expressed as mean ± S.E.M., mean-fold change ± S.E.M or, for visual EGFR scoring of human ATC samples and survival plots, percent. Statistical significance was tested by two-tailed Student's t-test, or, for tumour volumes, one-way ANOVA, followed by Tukey's Honestly Significant Difference test. Statistical significance of Kaplan-

Meier plots was analysed by log-rank test. *p*-values <0.05 were considered statistically significant (**p*<0.05; ***p*<0.01; ****p*<0.001).

6.4 Results

EGFR and NIS immunoreactivity of human ATC tissue

In total, nine anaplastic thyroid tumours from different patients were examined and ranked according to their EGFR expression. Seven (78%) of the nine examined tumours were categorised as 3+ (**Fig. 23A, C**), while one tumour (11%) was classified as 2+ and one (11%) showed no EGFR-specific immunoreactivity (**Fig. 23B, C**). Immunohistochemical staining for NIS revealed no differences in NIS staining between EGFR positive (score 3+) and EGFR negative (score 0) ATC tissue (**Fig. 23D, E**). Graves' tissue served as positive control for NIS staining (**Fig. 23F**).

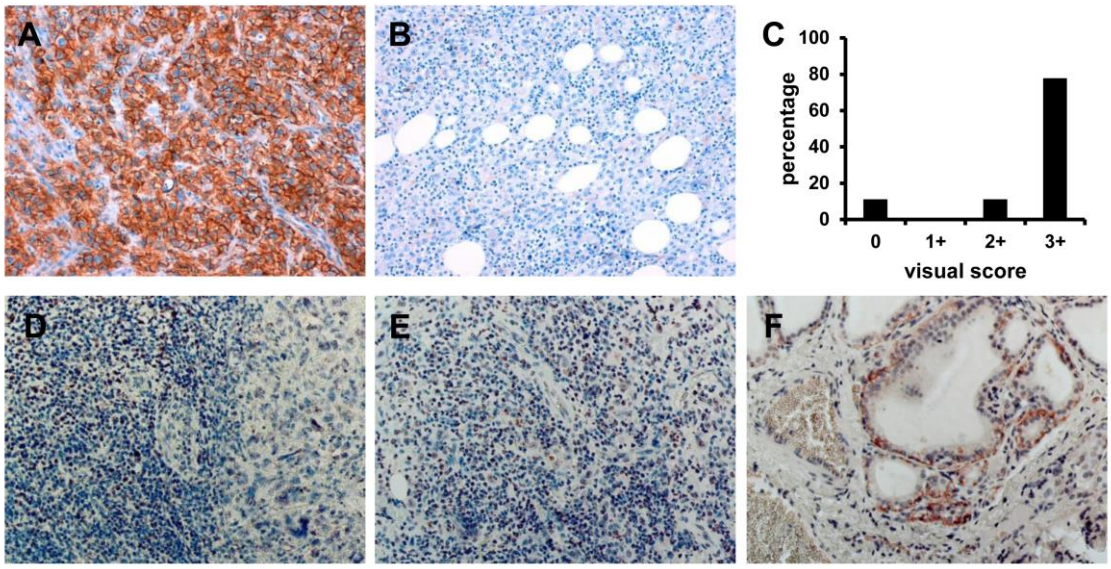

Figure 23. EGFR and NIS expression in human ATC. Human ATC samples (n=9) were ranked according to their EGFR expression. Highly EGFR-positive sections were classified as 3+ (**A**), while a score of 0 indicated no EGFR-specific staining (**B**). (**C**) Quantification of visual scores. NIS staining of human ATC sections revealed no NIS-specific immunoreactivity without differences between highly EGFR positive (**D**) and EGFR negative (**E**) samples. Graves' tissue served as positive control for NIS staining (**F**).

EGFR-targeted NIS gene transfer *in vitro*

Two different human anaplastic thyroid cancer cell lines and, for comparison, more differentiated follicular and papillary thyroid carcinoma cell lines were examined for their EGFR expression levels by flow cytometry. SW1736 cells showed high EGFR expression, while intermediate EGFR levels were measured on Hth74, FTC-133 and BCPAP cells (**Fig. 24A**).

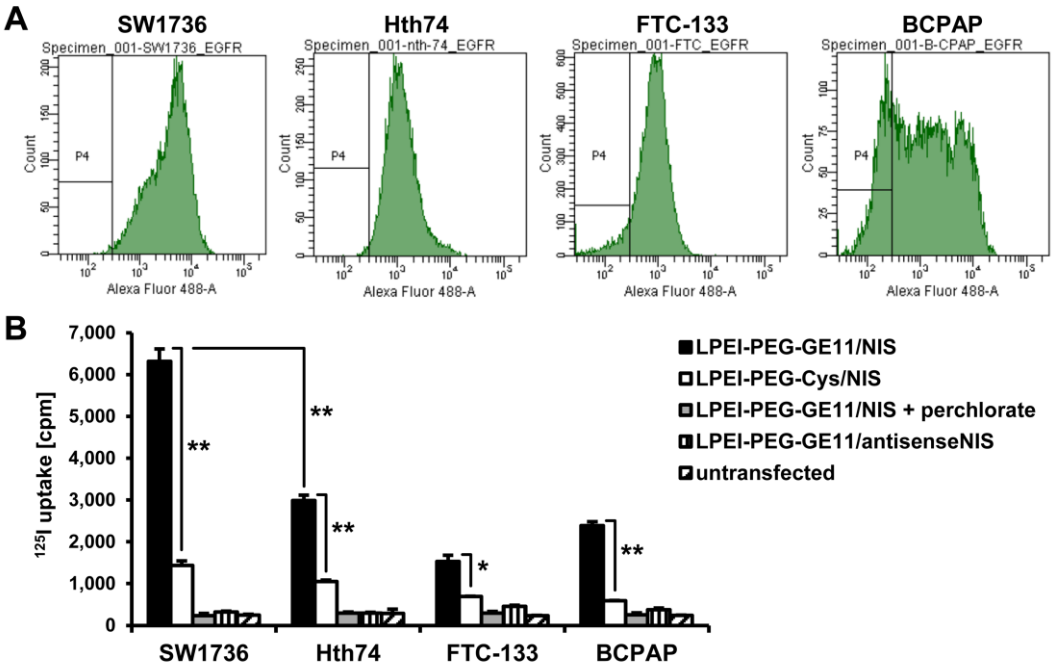

Figure 24. EGFR-targeted NIS gene transfer *in vitro*. (**A**) Human ATC cell lines SW1736 and Hth74, follicular thyroid carcinoma cell line FTC-133 and papillary thyroid carcinoma cell line BCPAP showed high (SW1736) to intermediate (Hth74, FTC-133, BCPAP) EGFR expression levels as determined by flow cytometry. (**B**) *In vitro* transfection with LPEI-PEG-GE11/NIS showed a significant increase in perchlorate-sensitive ^{125}I accumulation compared to transfection with untargeted LPEI-PEG-Cys/NIS (mean ± S.E.M.; n=3; *p<0.05, **p<0.01). No iodide uptake above the background levels observed for untransfected cells was detected after transfection with non-coding LPEI-PEG-GE11/antisenseNIS.

Twenty-four hours after transient transfection with LPEI-PEG-GE11/NIS, NIS-specific iodide uptake was detected in all four cell lines. SW1736 cells showed a 25-fold, Hth74 and BCPAP cells a 10-fold increase and FTC-133 cells a 7-fold increase in ^{125}I uptake compared to background levels measured in untransfected cells. The NIS-specific inhibitor perchlorate completely blocked iodide uptake in all cell lines. After transfection with unspecific LPEI-PEG-Cys/NIS, iodide uptake was significantly reduced compared to EGFR-targeted polyplexes LPEI-PEG-GE11/NIS. Cells transfected with LPEI-PEG-GE11/antisenseNIS showed no gain in uptake compared to untransfected cells (**Fig. 24B**). The amount of iodide uptake correlated well with EGFR levels measured by flow cytometry. Comparing the two ATC cell lines to each other, SW1736 cells showed a significantly higher iodide uptake than Hth74 cells (**Fig. 24B**).

EGFR- targeted NIS gene transfer *in vivo*

24 hours after two rounds of systemic NIS gene transfer *via* i.v. application of LPEI-PEG-GE11/NIS, ^{123}I uptake was evaluated on a gamma camera. Serial scanning revealed maximum tumoural iodide accumulation one hour post ^{123}I injection based on NIS-mediated iodide influx from the blood circulation. Over time, iodide content in the circulation decreased due to renal clearance. In the tumour, the radioiodide recirculated to a certain extent, as iodide lost by one tumour cell was taken up by

neighbouring NIS-transduced cells. Due to lack of iodide organification, however, tumoural iodide content slowly decreased over time, as ^{123}I was completely cleared from the circulation (**Fig. 25A-C**).

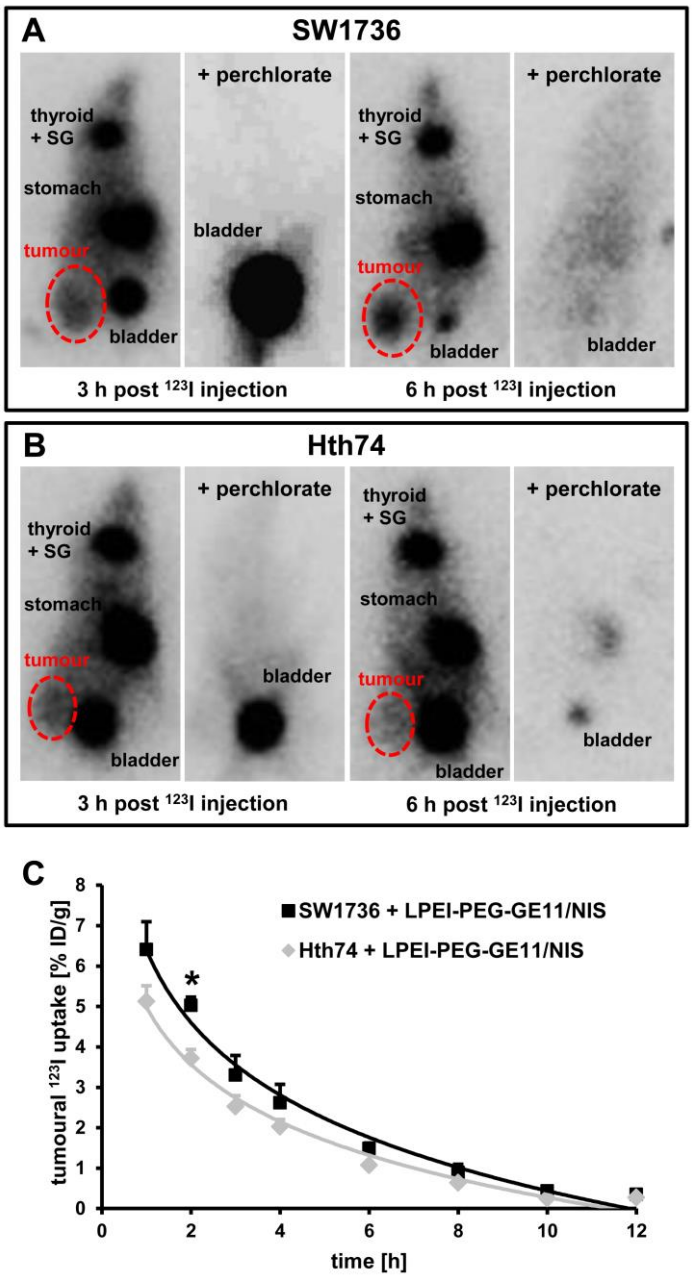

Figure 25. ***In vivo*** **imaging of NIS-mediated iodide uptake.** ^{123}I scintigraphy revealed tumour-specific radioiodide uptake in SW1736 (**A**) and Hth74 (**B**) xenografts after injection of LPEI-PEG-GE11/NIS that was perchlorate sensitive. SG: salivary glands. (**C**) Radionuclide retention time in tumours was determined by serial scanning over 12 h (mean ± S.E.M.; n=3 each; **p*<0.05).

A maximum ^{123}I uptake of 5.6-7.8% ID/g was observed for SW1736 tumours, whereas Hth74 tumours accumulated 4.5-5.8% ID/g (**Fig. 25A-C**). For ^{131}I, this translates to a tumour-absorbed dose of 35.1 mGy/MBq/g tumour with an effective half-life of 3.1 h in the SW1736 model and 25.0 mGy/MBq/g tumour with an effective half-life of 2.7 h in the Hth74 model. Pre-treatment of LPEI-PEG-GE11/NIS transfected xenografts with perchlorate inhibited tumoural accumulation of radioiodide in both models

(**Fig. 25A, B**). Physiological iodide uptake in the thyroid, salivary glands and stomach was also blocked upon perchlorate treatment. Radioiodide accumulation in the bladder is due to renal elimination of radioiodide (**Fig. 25A, B**).

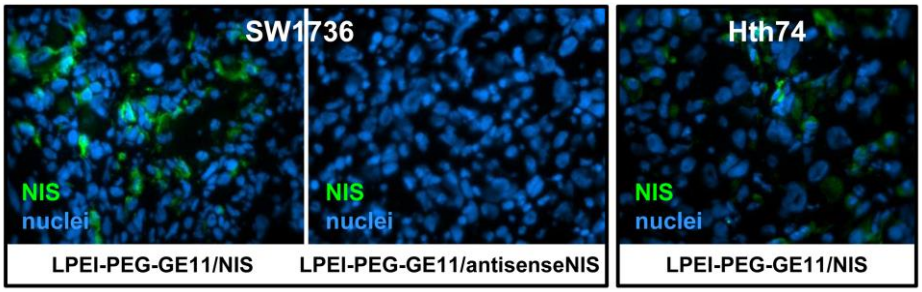

Figure 26. ***Ex vivo*** **NIS staining.** Immunofluorescence staining verified more robust NIS gene transfer to SW1736 tumours as compared to Hth74 tumours. No NIS-specific staining was detected after transfection of non-coding antisenseNIS. 40× magnification.

After gamma camera imaging, mice were sacrificed and dissected. In both SW1736 and Hth74 tumours from LPEI-PEG-GE11-treated mice, immunofluorescence staining revealed areas of NIS-specific staining, and the amount of NIS-positive cells in SW1736-derived tumours seemed higher than in Hth74 tumours (**Fig. 26**). SW1736 tumours transfected with LPEI-PEG-GE11/antisenseNIS, in contrast, showed no NIS-specific immunoreactivity (**Fig. 26**).

^{131}I therapy after *in vivo* NIS gene transfer

Mice harbouring SW1736 xenograft tumours were treated with three cycles of LPEI-PEG-GE11/NIS followed by ^{131}I 24 h later (**Fig. 27A**). Mice injected with LPEI-PEG-GE11/NIS and saline, LPEI-PEG-GE11/antisense-NIS and ^{131}I or saline only served as controls and exhibited a continuous, exponential tumour growth (**Fig. 27B**). Mice injected with LPEI-PEG-GE11/NIS and ^{131}I, in contrast, showed a significant delay in tumour growth which resulted in prolonged survival (**Fig. 27B, C**). Thirty-five days after therapy start the last control mouse was sacrificed, while 60% of mice injected with LPEI-PEG-GE11/NIS and ^{131}I were still alive (**Fig. 27C**). Median survival times were 42 days for the therapy group, 28 days for both LPEI-PEG-GE11/antisenseNIS + ^{131}I- and NaCl + NaCl-treated animals, and 18 days for the LPEI-PEG-GE11/NIS + NaCl group.

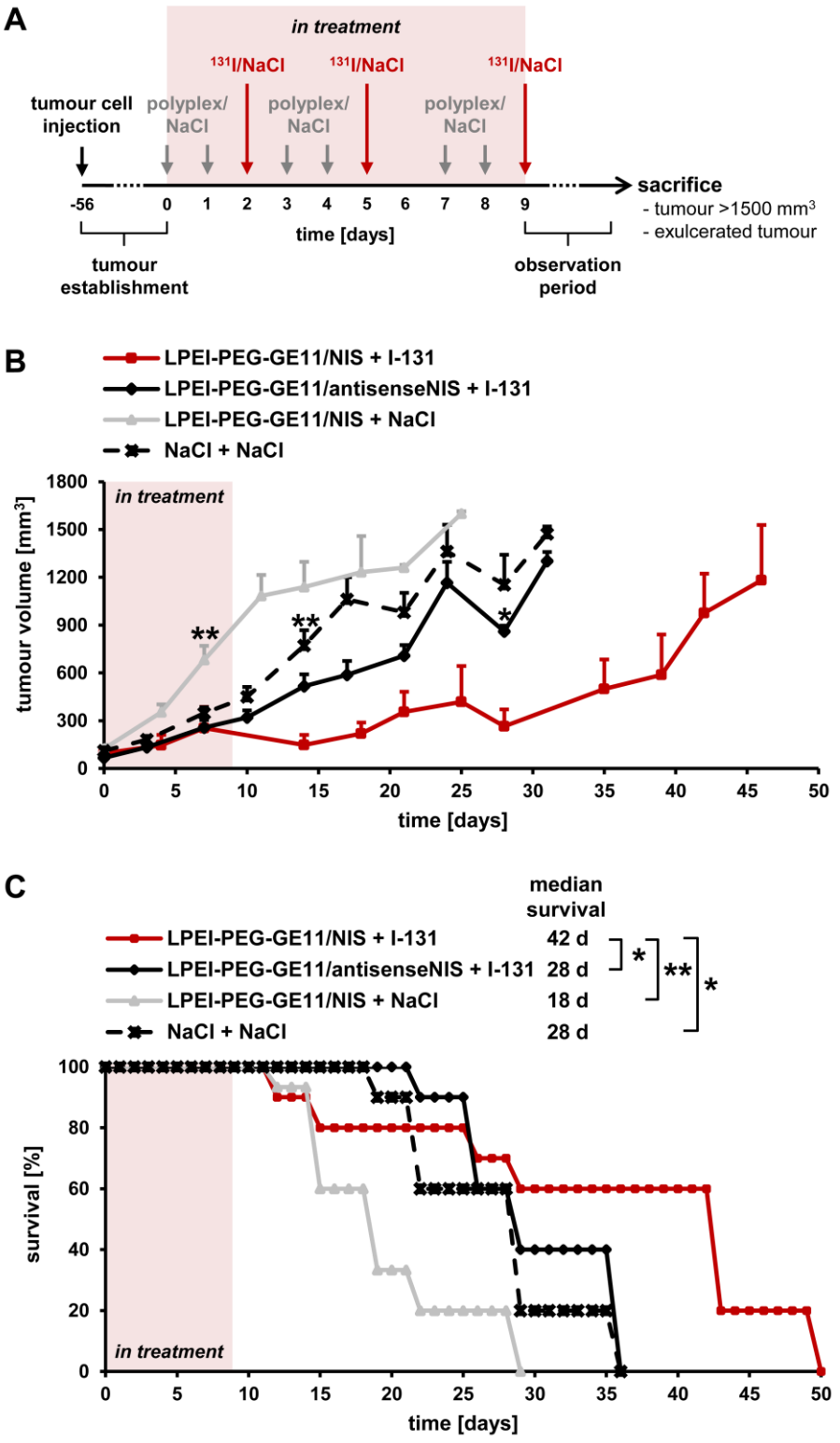

Figure 27. Therapeutic application of ^{131}I after NIS gene transfer *in vivo*. Mice harbouring SW1736 xenograft tumours were treated with three cycles of dual i.v. injections of polyplexes followed by i.p. injection of 55.5 MBq ^{131}I (**A**). (**B**) Mice treated with LPEI-PEG-GE11/NIS + ^{131}I (mean ± S.E.M; n=10) showed a stabilisation in tumour volumes compared to control groups LPEI-PEG-GE11/antisenseNIS + ^{131}I (mean ± S.E.M; n=10; **p*<0.05), LPEI-PEG-GE11/NIS + NaCl (n=15; mean ± S.E.M.; ***p*<0.01) and NaCl + NaCl (n=11; mean ± S.E.M.; ***p*<0.01). (**C**) This led to an increased overall and median survival in the therapy group compared to control groups LPEI-PEG-GE11/antisenseNIS + ^{131}I (**p*<0.05), LPEI-PEG-GE11/NIS + NaCl (***p*<0.01) and NaCl + NaCl (**p*<0.05).

6.5 Discussion

Besides its key role in healthy thyroid physiology, NIS-mediated iodide uptake provides the molecular basis for diagnostic imaging and targeted radionuclide therapy for the treatment of differentiated thyroid carcinomas. This concept, however, has proven ineffective in poorly differentiated and undifferentiated forms of thyroid cancer that lose the ability to accumulate iodide due to reduced or absent expression of functional NIS [217]. A very elegant and obvious therapy approach is to reinstate NIS expression and thus make it susceptible to radioiodide therapy either by redifferentiation aimed at recovery of endogenous NIS expression or by transfection with exogenous NIS.

Substances for the induction of redifferentiation in dedifferentiated thyroid cancer that have been tested to date include retinoids, thiazolidinediones, such as rosiglitazone, and regulators of epigenetic modifications, i.e. histone deacetylase (HDAC) inhibitors and DNA methyltransferase inhibitors [218-223]. Clinical success rates, however, have remained unexpectedly low for all of these compounds [222, 224]. More recently, the MAPK kinase inhibitor selumetinib and the selective BRAF inhibitor dabrafenib were shown to induce clinically relevant levels of radioiodide uptake in patients with radioiodine-refractory differentiated thyroid cancer [225, 226].

The alternative strategy of exogenously introducing NIS was made available by the cloning of the *NIS* gene in 1996 [63, 64]. Early work in tumourigenic Fisher rat thyroid follicular cells transfected stably with rat NIS demonstrated iodide uptake capacity *in vitro* and *in vivo* [227]. Similarly, after transfection of human ATC cells with NIS and subsequent injection into nude mice, tumours could be imaged by scintigraphy and were susceptible to radionuclide therapy [228-230]. Intratumoural injection of NIS using adenoviral vectors in a medullary thyroid carcinoma xenograft mouse model and measles virus vectors in an ATC xenograft mouse model restored radioiodide uptake as shown by gamma camera or SPECT imaging, respectively, and therapeutic efficacy of ^{131}I [215, 231]. For the development of this concept towards clinical application, especially in metastatic disease, however, systemic application of NIS followed by safe, efficient and tumour-specific delivery are essential.

Our previous work has focused on systemic delivery of the *NIS* gene to extrathyroidal tumours using viral vectors, mesenchymal stem cells and synthetic polymers as gene transfer vehicles [66, 70-72, 77-79, 82, 83, 87, 99, 205, 210]. Based on the high efficiency of EGFR-targeted LPEI-PEG-GE11 polymers for tumour-specific delivery of functional NIS to a liver cancer xenograft mouse model, as well as an advanced genetically engineered mouse model of pancreatic ductal adenocarcinoma in our earlier studies and the high expression levels of EGFR in human ATC tissue samples, we chose these synthetic polymers as delivery vehicles for the *NIS* gene to ATC. High EGFR expression on ATC was confirmed by FACS analysis of human ATC cell lines SW1736 and Hth74. Both cell lines express wild type EGFR protein, though Hth74 harbour a heterozygous silent polymorphism in the EGFR gene [232, 233]. Transient *in vitro* transfection of these cells with LPEI-PEG-GE11/NIS led to significant perchlorate-sensitive and therefore NIS-mediated radioiodide uptake. In comparison, iodide uptake was significantly

lower after transfection with non-targeted LPEI-PEG-Cys/NIS, demonstrating improved transfection efficiency using the peptide ligand GE11. NIS-dependency was further confirmed by the absence of iodide uptake activity using non-coding antisenseNIS DNA. The higher EGFR levels detected on SW1736 cells by FACS were reflected in higher iodide uptake activity as compared to Hth74 cells. Similar results were obtained in more differentiated follicular and papillary thyroid carcinoma cell lines, demonstrating the feasibility of this strategy for NIS gene transfer in EGFR-positive radioiodine refractory thyroid carcinoma in general.

Transferring these results to systemic vector application *in vivo*, intravenous administration of LPEI-PEG-GE11/NIS resulted in significant perchlorate-sensitive, tumour-specific iodide uptake in xenograft mouse models derived from both ATC cell lines, although, again, SW1736 showed higher ^{123}I uptake, as determined by gamma camera imaging and confirmed by immunofluorescence staining. The biological half-life measured in ATC tumours was similar to what we have observed in previous studies in other tumour models, which is clearly long enough for a significant therapy effect [71, 72, 205, 210]. The radiation dose that reaches the tumour depends on the rate of iodide uptake, its retention time in the tumour cell, i.e. iodide efflux, iodide recirculation within the tumour and iodide organification [234]. Due to loss of thyroid peroxidase (TPO) and thyroglobulin expression in ATC as a result of dedifferentiation, we did not see any iodide organification in neither of the ATC xenografts. However, the iodide retention time is longer than one would expect without organification, as the iodide is recirculated within the tumour. A possible approach to enhance iodide retention time and the delivered dose in non-organifying tissues, is co-transfection of NIS and TPO [234]. In this context, co-expression of both genes decreased iodide efflux in non-small cell lung cancer cell lines and enhanced tumour cell apoptosis as compared to single transfection with NIS [235]. In contrast, after co-infection of human cervix carcinoma cells with two adenoviral vectors encoding NIS and TPO, no increase in iodide retention time was detected, though active TPO was produced and a significant increase in organification was observed [236]. To date, there is no clear evidence that TPO-mediated organification does indeed enhance the efficacy of NIS-based gene therapy. No clear data exist to prove that organification is a crucial prerequisite for successful ^{131}I therapy. On the contrary, our results in the current study as well as in earlier studies in various non-organifying tumour entities, demonstrate that iodide organification is not required for accumulation of therapeutically effective radioiodide doses.

The differences in both *in vitro* and *in vivo* data between the two ATC cell lines used here are presumably due to differences in EGFR expression levels. Tumour heterogeneity is a typical problem seen in clinical practice – indeed, of the nine patient samples analysed for EGFR receptor expression in this study, one tumour showed slightly lower EGFR receptor expression, while one showed no expression at all. For this reason we are constantly broadening our arsenal of targeting strategies, so that different targeting ligands can be applied depending on receptor status. In this context, a further interesting candidate for ATC targeting is transferrin, as the transferrin receptor is highly expressed on ATC [237-239].

Due to the more promising results in SW1736, the subsequent evaluation of the therapeutic effectiveness of ^{131}I after LPEI-PEG-GE11-mediated systemic *NIS* gene delivery was performed in this model only. After three cycles of two applications of LPEI-PEG-GE11/NIS followed by a application of ^{131}I in SW1736 xenograft tumour carrying mice, we were able to demonstrate a significant delay in tumour growth in therapy animals compared to control groups, which was accompanied by a significant increase in survival time.

Taken together, our data clearly show the great potential of EGFR-targeted synthetic polymers to target NIS to ATC. Systemic application is of particular importance in ATC, as it rapidly metastasises to distant sites and, at the time of diagnosis, metastases, predominantly in the lung, liver, bone and brain are already present in 50 % of patients [209]. To our knowledge, this is the first study demonstrating successful reinstatement of NIS expression and therefore susceptibility to radioiodide uptake in ATC after systemic application of the therapeutic gene, an important prerequisite for clinical development.

6.6 Acknowledgements

We are grateful to Gerald Assmann (Institute of Pathology, LMU Munich, Munich, Germany) for assistance with staining and scoring of human ATC sections and Wolfgang Rödl (Department of Pharmacy, LMU Munich, Munich, Germany) for conjugate synthesis.

This work was supported by grants from the Deutsche Forschungsgemeinschaft within the Collaborative Research Centre SFB 824 (project C8) to C.S. and the Priority Programme SPP1629 to C.S. (SP 581/6-1, SP 581/6-2) and P.J.N. (NE 648/5-2), as well as a grant from the Wilhelm-Sander-Stiftung (2014.129.1) to C.S.

VII. CHAPTER 6

Imaging and targeted therapy of pancreatic ductal adenocarcinoma using the theranostic sodium iodide symporter (*NIS*) gene

Kathrin A Schmohl[1*], Aayush Gupta[2*], Geoffrey K Grünwald[1*], Marija Trajkovic-Arsic[3,4], Kathrin Klutz[1], Rickmer Braren[5], Markus Schwaiger[6], Peter J Nelson[7], Manfred Ogris[8], Ernst Wagner[9], Jens T Siveke[2,3,4] and Christine Spitzweg[1]

[1]Department of Internal Medicine II, University Hospital of Munich, LMU Munich, Munich Germany
[2]Department of Internal Medicine II, Klinikum rechts der Isar der Technischen Universität München, Munich, Germany
[3]West German Cancer Center, University Hospital Essen, Essen, Germany
[4]German Cancer Consortium (DKTK), partner site Essen and German Cancer Research Center (DKFZ), Heidelberg, Germany
[5]Department of Radiology, Klinikum rechts der Isar der Technischen Universität München, Munich, Germany
[6]Department of Nuclear Medicine, Klinikum rechts der Isar der Technischen Universität München, Munich, Germany
[7]Department of Internal Medicine IV, University Hospital of Munich, LMU Munich, Munich Germany
[8]Department of Pharmaceutical Chemistry, University of Vienna, Vienna, Austria
[9]Department of Pharmacy, LMU Munich, Munich, Germany
*KAS, AG and GKG contributed equally

This chapter is a pre-copy-edited version of a peer-reviewed article published in *Oncotarget* **2017**;8:33393-404.

Parts of this chapter are included in the doctoral thesis of Geoffrey K Grünwald. Geoffrey K Grünwald performed *in vitro* iodide uptake studies. Kathrin A Schmohl performed *ex vivo* tissue stainings. Geoffrey K Grünwald and Kathrin A Schmohl both performed *in vivo* scintigraphies, PET imaging, and the therapy study, and wrote the manuscript.

7.1 Abstract

The theranostic sodium iodide symporter (NIS) gene allows detailed molecular imaging of transgene expression and application of therapeutic radionuclides. As a crucial step towards clinical application, we investigated tumour specificity and transfection efficiency of epidermal growth factor receptor (EGFR)-targeted polyplexes as systemic *NIS* gene delivery vehicles in an advanced genetically engineered mouse model of pancreatic ductal adenocarcinoma (PDAC) that closely reflects human disease. PDAC was induced in mice by pancreas-specific activation of constitutively active $Kras^{G12D}$ and deletion of *Trp53*. We used tumour-targeted polyplexes (LPEI-PEG-GE11/NIS) based on linear polyethylenimine, shielded by polyethylene glycol and coupled with the EGFR-specific peptide ligand GE11, to target a *NIS*-expressing plasmid to high EGFR-expressing PDAC. *In vitro* iodide uptake studies in cell explants from murine EGFR-positive and EGFR-ablated PDAC lesions demonstrated high transfection efficiency and EGFR-specificity of LPEI-PEG-GE11/NIS. *In vivo* ^{123}I gamma camera imaging and three-dimensional high-resolution ^{124}I PET showed significant tumour-specific accumulation of radioiodide after systemic LPEI-PEG-GE11/NIS injection. Administration of ^{131}I in LPEI-PEG-GE11/NIS-treated mice resulted in significantly reduced tumour growth compared to controls as determined by magnetic resonance imaging, though survival was not significantly prolonged. This study opens the exciting prospect of NIS-mediated radionuclide imaging and therapy of PDAC after systemic non-viral *NIS* gene delivery.

7.2 Introduction

Pancreatic ductal adenocarcinoma (PDAC) is currently the fourth leading cause of cancer-related mortality in developed countries despite its comparably low incidence of less than 3 %, clearly demonstrating the lack of effective therapeutic strategies. The five-year survival rate is around 7 % for all stages of the disease and drops to below 2 % and a median survival of less than a year for patients with metastatic disease, mostly due to late diagnosis at the stage of inoperability and the unusually high resistance of PDAC to conventional radiation- and chemotherapy [240, 241]. Despite intensive scientific and industrial efforts, so far no significant extension of survival could be achieved by any of the numerous therapy approaches tested [242].

The genetic and morphological changes in the carcinogenesis of PDAC are well known and include the initiation and progression of premalignant lesions to invasive and metastatic pancreatic cancer [242-245]. The genetic hallmark of PDAC development is an activating mutation in the *KRAS* oncogene, followed by other genetic changes, commonly including inactivation of the tumour suppressors *TP53*, *CDKN2A* (*P16*^{INK4A}) and *SMAD4*, and activation of several growth factor receptors, such as the epidermal growth factor receptor (EGFR) [242, 246].

Against this background, several complex genetically modified mouse models of PDAC that mirror the typical changes found in human patients, have been generated in recent years [242, 243, 247-249]. One such model is the *Ptf1a*$^{+/Cre}$*;Kras*$^{+/LSL-G12D}$*;Trp53*$^{loxP/loxP}$ (*Kras;p53)* mouse. Here, PDAC is induced by pancreas-specific activation of constitutively active *Kras*^{G12D} in combination with conditional deletion of *Trp53* [247]. To restrict these genetic modifications to the pancreas, mice with the mutated alleles are interbred with animals that express the Cre recombinase driven by the pancreas-specific promoter for Ptf1a, a subunit of pancreas transcription factor 1 (Ptf1) that is required to commit cells to a pancreatic fate during embryonic development [243, 250]. Thus, the activation of the oncogenic *Kras*^{G12D} via excision of a transcriptionally inhibitory *LSL* (*loxP-STOP-loxP*) construct and deletion of the floxed tumour suppressor *Trp53* occur in the pancreas only, leading to ductal lesions with complete penetrance [243, 251]. The development of endogenous mouse models away from the usual transplant models represents a significant step in the evolution of preclinical models [252]. The morphological and molecular composition of endogenous tumours far better reflects human disease, making them highly suitable to predict the clinical effectiveness of a specific treatment strategy.

The sodium iodide symporter (NIS; *SLC5A5*) mediates the uptake of iodide into thyroid follicular cells allowing both diagnostic and therapeutic application of radioiodide in thyroid cancer patients [253, 254]. In our previous work, we have extensively investigated the dual reporter/therapy capacity of NIS in various non-thyroidal tumours and have proven the feasibility of extrathyroidal radioiodide therapy after tumour-selective *NIS* gene transfer [66, 70, 71, 77-79, 82, 83, 87, 99, 205]. Transfection of cancer cells with the *NIS* gene allows non-invasive monitoring of functional NIS expression and *in vivo*

biodistribution before the application of a therapeutic dose of radioiodide. One of the major hurdles of efficient and safe application of the *NIS* gene therapy concept in the clinical setting is optimal tumour-specific targeting in the presence of low toxicity and high transfection efficiency of gene delivery vectors, with the ultimate goal of systemic vector application.

In a previous study, we used synthetic polyplexes based on pseudodentritic oligoamines with high intrinsic tumour affinity for *NIS* gene therapy in a syngeneic neuroblastoma mouse model as well as a subcutaneous human hepatocellular carcinoma mouse model [82, 83]. After systemic *NIS* gene transfer, the tumour-selective accumulation of radioiodide was sufficient for a significant therapeutic effect. In addition to an intrinsic tumour affinity due to the so-called enhanced permeability and retention (EPR) effect based on 'leaky' tumour vasculature, the tumour targeting of polyplexes can be further optimised by the attachment of tumour-specific ligands. To this end, in a subsequent study, we used LPEI-PEG-GE11 polymers composed of linear polyethylenimine (LPEI), shielded by polyethylene glycol (PEG) and coupled to the synthetic peptide GE11 as an EGFR-specific ligand for *NIS* gene delivery [87]. After systemic application of these polymers condensed with *NIS* DNA, tumour-specific radioiodide accumulation demonstrated effective and EGFR-specific tumour targeting in a high EGFR-expressing xenograft mouse model of hepatocellular carcinoma. After the injection of a therapeutic dose of ^{131}I, tumoural iodide uptake was sufficiently high for a significant delay of tumour growth and prolongation of animal survival [87].

Based on our previous work and the well-known characteristic upregulation of EGFR in PDAC, we investigated the potential of EGFR-targeted polyplexes for systemic *NIS* gene therapy in an advanced endogenous mouse model of PDAC as a next step towards clinical application.

7.3 Materials and Methods

Establishment of genetically modified mice

Establishment of the *Kras;p53* (*Ptf1a*$^{+/Cre}$;*Kras*$^{+/LSL\text{-}G12D}$;*Trp53*$^{lox/loxP}$) and *Kras;p53;Egfr* (*Ptf1a*$^{+/Cre}$;*Kras*$^{+/LSL\text{-}G12D}$;*Trp53*$^{loxP/loxP}$;*Egfr*$^{fl/fl}$) strains has been described previously [243, 250, 251, 255, 256]. Mouse strains were maintained on a mixed C57BL/6;129/Sv background. Animals were kept under specific pathogen-free conditions with access to mouse chow and water *ad libitum*. Both male and female mice at 5-7.5 weeks of age were used for experiments. The experimental protocol was approved by the regional governmental commission for animals (Regierung von Oberbayern, Munich, Germany).

Preparation and culture of PDAC cell explants

Cell explants from primary PDAC of *Kras;p53* and *Kras;p53;Egfr* mice were isolated as described previously [257] and cultured in DMEM high glucose medium (Invitrogen, Karlsruhe, Germany) supplemented with 10% fetal bovine serum (v/v; PAA, Colbe, Germany), 100 U/mL penicillin/100 µg/mL streptomycin (Invitrogen) and 1% non-essential amino acids (v/v; Invitrogen). Cells were

maintained at 37°C and 5% CO_2 in an incubator with 95% humidity. Cell culture medium was replaced every second day and explants were passaged at 85% confluency.

Plasmid and polymer synthesis and polyplex formation

The human *NIS*-encoding plasmid and LPEI-based conjugates were cloned and synthesised, respectively, as described previously [87]. Plasmid DNA was condensed with polymers at indicated conjugate to plasmid (c/p) ratios (w/w) in HEPES-buffered glucose (HBG: 20 mmol/L HEPES, 5% glucose (w/v), pH 7.4) as described previously [216] and incubated at room temperature for 20 min before use. Final DNA concentrations were 2 µg/mL for *in vitro* studies and 200 µg/mL for *in vivo* studies.

Transient transfection

For *in vitro* transfection experiments, PDAC cell explants were grown to 60-80% confluency. Explants were incubated for 4 hours with polyplexes in the absence of serum and antibiotics followed by incubation with complete growth medium for 24 h. Either LPEI-PEG-GE11/NIS (EGFR-targeting of NIS due to the EGFR-specific ligand GE11), LPEI-PEG-Cys/NIS (no active targeting of NIS to EGFR, as the ligand GE11 is replaced by a cysteine residue), or LPEI-PEG-GE11 alone (polymer without NIS DNA) were added in c/p ratios as indicated. Transfection efficiency was evaluated by measurement of iodide uptake activity as described below. Transfections were done in triplicate for each separate explant.

In vitro ^{125}I uptake assay

Following transfections, iodide uptake of PDAC cell explants was determined at steady-state conditions as described previously [169, 258]. Results were normalised to cell viability that was measured using the commercially available MTS-assay (Promega, Mannheim, Germany) as described previously [170].

Radioiodide uptake after systemic NIS gene transfer *in vivo*

For the proof-of-principle of NIS-mediated tumour-specific radioiodide accumulation *in vivo*, polyplexes (LPEI-PEG-GE11/NIS, c/p 0.8) were applied via the tail vein (i.v.) at a DNA dose of 2.5 mg/kg (50 µg DNA in 250 µL HBG). Mice received 18.5 MBq ^{123}I (GE Healthcare, Braunschweig, Germany) intraperitoneally (i.p.) 24 h (n=9) or 48 h (n=7) after polyplex injection and radioiodide distribution was monitored by serial imaging on a gamma camera (Forte, ADAC Laboratories, Milpitas, CA, USA) equipped with a VXHR (ultra-high resolution) collimator as described previously [170]. Regions of interest were quantified and expressed as a fraction of the total amount of applied radionuclide per gram tumour tissue. The retention time within the tumour was determined by serial scanning after radioiodide injection. A subset of mice (n=2 for each time point) was pretreated i.p. with 2 mg of the competitive NIS inhibitor sodium perchlorate ($NaClO_4$; Sigma-Aldrich, Taufkirchen, Germany) 30 min before ^{123}I administration. Dosimetric calculations for ^{131}I were made using the

Medical Internal Radiation Dose (MIRD) technique and a RADAR dose factor (http://www.doseinfo-radar.com).In order to achieve better discrimination between uptake in the tumour and the adjacent stomach, 24 or 48 h after i.v. injection of polyplexes (LPEI-PEG-GE11/NIS, each time point n=5; LPEI-PEG-GE11/antisenseNIS, each time point n=1) mice received 10 MBq ^{124}I (Perkin Elmer, Waltham, MA, USA) i.p. and radioiodide biodistribution was monitored by static acquisition 3 h post injection using a micro PET system (Inveon, Siemens Preclinical Solutions, Erlangen, Germany). Mean tumoural radioiodide uptake was calculated in MBq/mL by manually placing 3D regions of interest in the tumour.

Analysis of NIS mRNA expression by quantitative real-time PCR (qPCR)

Total RNA was isolated from PDAC or non-target tissues (liver, lung) using the RNeasy Mini Kit (Qiagen, Hilden, Germany) according to the manufacturer's recommendations. Single-stranded oligo (dT)-primer cDNA was generated using Super Script III Reverse Transcriptase (Invitrogen). qPCR was performed with the cDNA from 1 µg RNA using SYBR Green PCR master mix (Qiagen) in a Rotor Gene 6000 (Corbett Research, Morthlake, New South Wales, Australia). The following primers were used: *NIS*, forward 5′-ACACCTTCTGGACCTTCGTG-3′, reverse 5′-GTCGCAGTCGGTGTAGAACA-3′ and *GAPDH*, forward 5′-GAGAAGGCTGGGGCTCATTT-3′, reverse 5′-CAGTGGGGACACGGAAGG-3′. Relative expression levels were calculated using the comparative $\Delta\Delta C_t$ method and internal *GAPDH* for normalization.

Analysis of tissue sections

Immunohistochemical and immunofluorescence staining of NIS was performed using a mouse monoclonal antibody directed against human NIS (kindly provided by John C Morris, Mayo Clinic, Rochester, MN, USA) as described previously [66, 215].

Radioiodide therapy

Starting when mice were around 30 d of age, tumour sizes were assessed weekly by high resolution magnetic resonance imaging (MRI) on a 3T clinical scanner (Philips Ingenia 3.0T; Royal Philips Electronics, Eindhoven, The Netherlands). Once tumours reached the inclusion size of 200-450 mm^3, therapy trials were started. To this end, 48 h after systemic administration of LPEI-PEG-GE11/NIS or, as control, LPEI-PEG-GE11/antisenseNIS, a therapeutic dose of 55.5 MBq ^{131}I (GE Healthcare) was administered i.p. (LPEI-PEG-GE11/NIS + ^{131}I n=6; LPEI-PEG-GE11/antisenseNIS + ^{131}I n=3). A second control group received saline only (n=4). The cycle consisting of systemic *NIS* gene transfer followed by radioiodide was repeated for a total of three times on days 0/2, 4/6 and 7/9. Mice from all groups were sacrificed when at least one endpoint criterion was reached. Endpoint criteria included a tumour volume >1000 mm^3, a body weight loss >15%, as well as a number of general physical, clinical and behavioural criteria. Body condition was monitored by independent animal care personnel blind to treatment and hypothesis.

Statistics

Results are reported as mean ± S.E.M., mean-fold change ± S.E.M. or, for survival plots, percent. Statistical significance was generally tested by two-tailed Student's t-test except for the therapy study. For tumour volumes, one-way ANOVA was performed, followed by Tukey's Honestly Significant Difference test. Statistical significance of Kaplan-Meier plots was analysed by log-rank test. *p*-values <0.05 were considered statistically significant (**p*<0.05; ***p*<0.01; ****p*<0.001; n/s not significant).

7.4 Results

Iodide uptake studies *in vitro*

In order to optimise transfection conditions for LPEI-PEG-GE11 polymers condensed with the *NIS* plasmid (LPEI-PEG-GE11/NIS) in high EGFR-expressing PDAC cell explants derived from *Kras;p53* mice (**Fig. 28A**), radioiodide uptake activity was evaluated 24 h after polyplex application (data not shown). A c/p ratio of 0.8 resulted in highest transfection efficiency at lowest cytotoxicity. Therefore, this c/p ratio was used in all subsequent experiments. Twenty-four hours after transfection with LPEI-PEG-GE11/NIS, cell explants from three different mice showed a 22-26-fold increase in ^{125}I accumulation as compared to cells incubated with the empty control vector LPEI-PEG-GE11 (**Fig. 28B**). Transfection with untargeted LPEI-PEG-Cys/NIS (targeting ligand GE11 replaced by a cysteine residue) resulted in significantly lower iodide uptake activity compared to EGFR-targeted LPEI-PEG-GE11/NIS (**Fig. 28B**). In both cases, iodide uptake was blocked upon additional treatment with the NIS-specific inhibitor perchlorate.

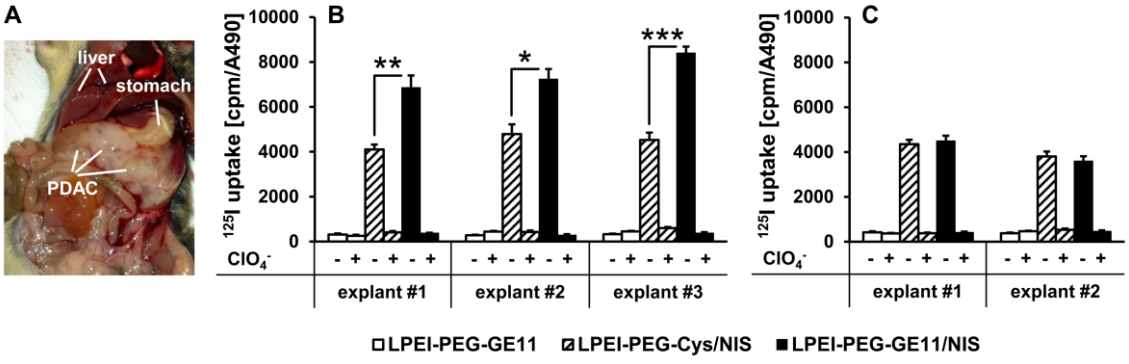

Figure 28. Iodide uptake in PDAC cell explants *in vitro*. *Kras;p53* mice develop PDAC that occupies a large portion of the abdominal cavity below the stomach (**A**). (**B**) PDAC cell explants from three separate mice (three technical replicates per mouse) transfected *in vitro* with LPEI-PEG-GE11/NIS showed a significant increase in perchlorate- (ClO_4^--) sensitive ^{125}I accumulation compared to transfection with LPEI-PEG-Cys/NIS (mean ± S.E.M.; **p*<0.05; ***p*<0.01; ****p*<0.001). No iodide uptake above background levels was observed in cells transfected with LPEI-PEG-GE11 alone. (**C**) Transfection of EGFR-ablated PDAC cell explants from two mice (three technical replicates per mouse) with LPEI-PEG-GE11/NIS and LPEI-PEG-Cys/NIS showed no significant differences between transfection with targeted or untargeted polyplexes, demonstrating EGFR-specificity of the targeting ligand GE11 (mean ± S.E.M.).

To further verify EGFR-specificity of the targeting ligand GE11, we performed additional iodide uptake studies in EGFR-ablated PDAC cell explants from *Kras;p53;Egfr* mice. No significant difference between transfection with targeted LPEI-PEG-GE11/NIS or untargeted LPEI-PEG-Cys/NIS polyplexes was observed (**Fig. 28C**). Polyplex-mediated *NIS* gene transfer did not affect cell viability for any of the treatment conditions compared to untreated cells as measured by MTS assay (data not shown).

^{123}I scintigraphy and ^{124}I PET imaging of EGFR-targeted NIS gene delivery

Functional NIS expression in mice with high EGFR-expressing PDAC was imaged by whole body ^{123}I gamma camera and ^{124}I PET imaging. Polyplexes were administered i.v. either 24 or 48 h before injection of the respective radionuclide for imaging.

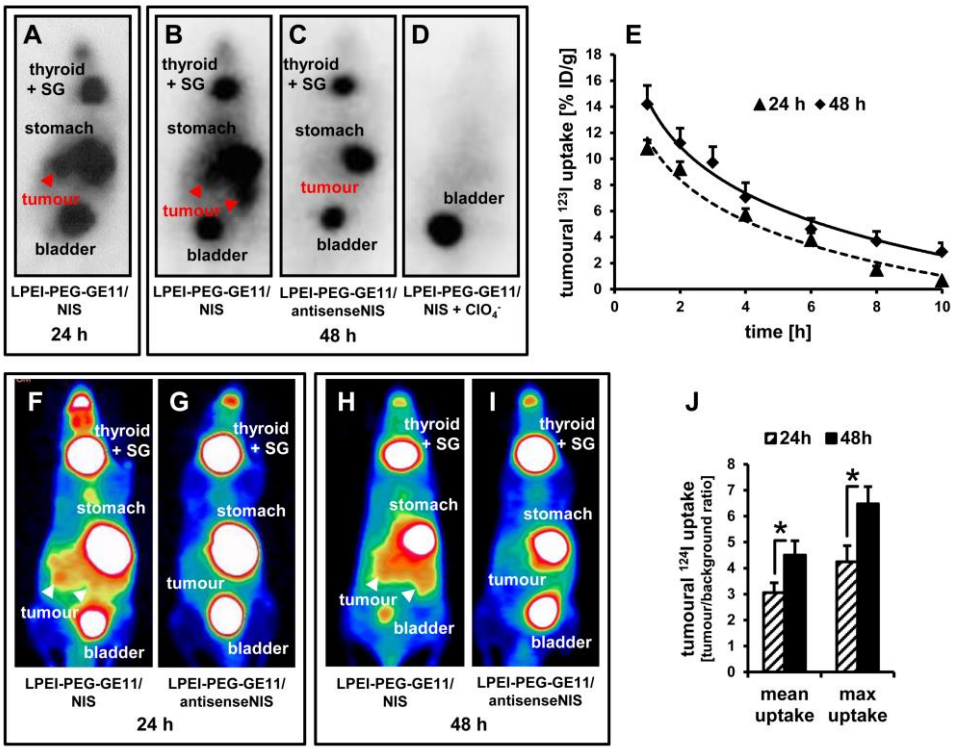

Figure 29. *In vivo* imaging of NIS-mediated iodide uptake. ^{123}I scintigraphy revealed pancreatic tumoural radioiodide uptake 24 h (**A**) and 48 h (**B**) after injection of mice with LPEI-PEG-GE11/NIS that was not seen after injection with non-coding LPEI-PEG-GE11/antisenseNIS (**C**). Iodide uptake was perchlorate-sensitive (**D**) and therefore indeed NIS-mediated. (**E**) Radionuclide retention time in tumours was determined by serial scanning over 10 h (mean ± S.E.M.; 24 h: n=9, 48 h: n=7). ^{124}I PET-imaging confirmed findings of scintigraphy and allowed better differentiation between tumoural and stomach radioiodide uptake (**F**, **H**). After injection of the control vector LPEI-PEG-GE11/antisenseNIS (**G**, **I**), no pancreatic iodide uptake activity above background levels could be detected. Significantly higher radioiodide accumulation 48 h after gene transfer as compared to 24 h was confirmed by PET (mean ± S.E.M.; n=5 each; *p<0.05) (**J**). SG: salivary glands.

In vivo ^{123}I gamma camera imaging revealed high levels of NIS-mediated radionuclide accumulation in pancreatic tumours both at 24 and 48 h after systemic injection of EGFR-targeted LPEI-PEG-GE11/NIS (**Fig. 29A, B**). Tumours accumulated 10.8 ± 0.7 % of the injected dose per gram (ID/g) with an average

biological half-life of 4 h at 24 h and 14.2 ± 1.4 % ID/g with an average biological half-life of 4.5 h at 48 h (**Fig. 29E**). For ^{131}I, a tumour-absorbed dose of 74.7 mGy/MBq/g tumour with an effective half-life of 3.2 h (24 h after polyplex administration) and 96.5 mGy/MBq/g tumour, effective half-life 4.5 h (48 h after polyplex administration), was calculated. In contrast, injection of non-coding control polyplexes LPEI-PEG-GE11/antisenseNIS (*NIS* sequence back to front) resulted in no significant tumoural radioiodide accumulation (**Fig. 29C**). In addition to ^{123}I uptake in the tumour, radioiodide accumulation was also observed in the stomach, the thyroid and the salivary glands, as they physiologically express NIS, as well as in the urinary bladder due to renal radionuclide elimination (**Fig. 29A-C**). To further confirm that tumoural iodide uptake was indeed NIS-mediated, LPEI-PEG-GE11/NIS-injected mice were additionally treated with the competitive NIS-inhibitor perchlorate 30 min before ^{123}I administration, which completely blocked polyplex-mediated tumoural iodide accumulation in addition to physiological uptake in the stomach, the thyroid gland and the salivary glands (**Fig. 29D**).

To better distinguish tumoural uptake from iodide accumulation in the stomach, we additionally employed three-dimensional high-resolution ^{124}I PET to image radioiodide biodistribution. Again, systemic injection of LPEI-PEG-GE11/NIS resulted in strong transfection of tumour tissue at both time points (**Fig. 29F, H**), an effect that was not seen in mice treated with LPEI-PEG-GE11/antisenseNIS (**Fig. 29G, I**). Quantification of tumoural ^{124}I uptake again revealed significantly higher radioiodide accumulation 48 h after i.v. injection of LPEI-PEG-GE11/NIS as compared to 24 h after NIS gene transfer (**Fig. 29J**).

Ex vivo analysis of NIS expression in PDAC

48 h after polyplex administration, mice were sacrificed and dissected. Tumours and non-target organs (liver, lung) were analysed for *NIS* mRNA expression by qPCR. A 20-fold increase in *NIS* mRNA expression was detected in PDAC lesions from mice injected with LPEI-PEG-GE11/NIS as compared to untreated tumours (**Fig. 30A**). In contrast, no significant *NIS* mRNA expression above background levels was observed in non-target organs and tumours of mice treated with the control vector LPEI-PEG-GE11/antisenseNIS (**Fig. 30A**). In tumours from LPEI-PEG-GE11/NIS-treated mice, areas of NIS-specific immunoreactivity were observed surrounding ductal lesions by immunohistochemical and immunofluorescence staining using a human NIS-specific antibody (**Fig. 30B**). NIS staining was found to be both cell membrane-associated and cytoplasmic. In contrast, tumours from mice treated with the control vector LPEI-PEG-GE11/antisenseNIS showed no NIS-specific immunoreactivity (**Fig. 30B**).

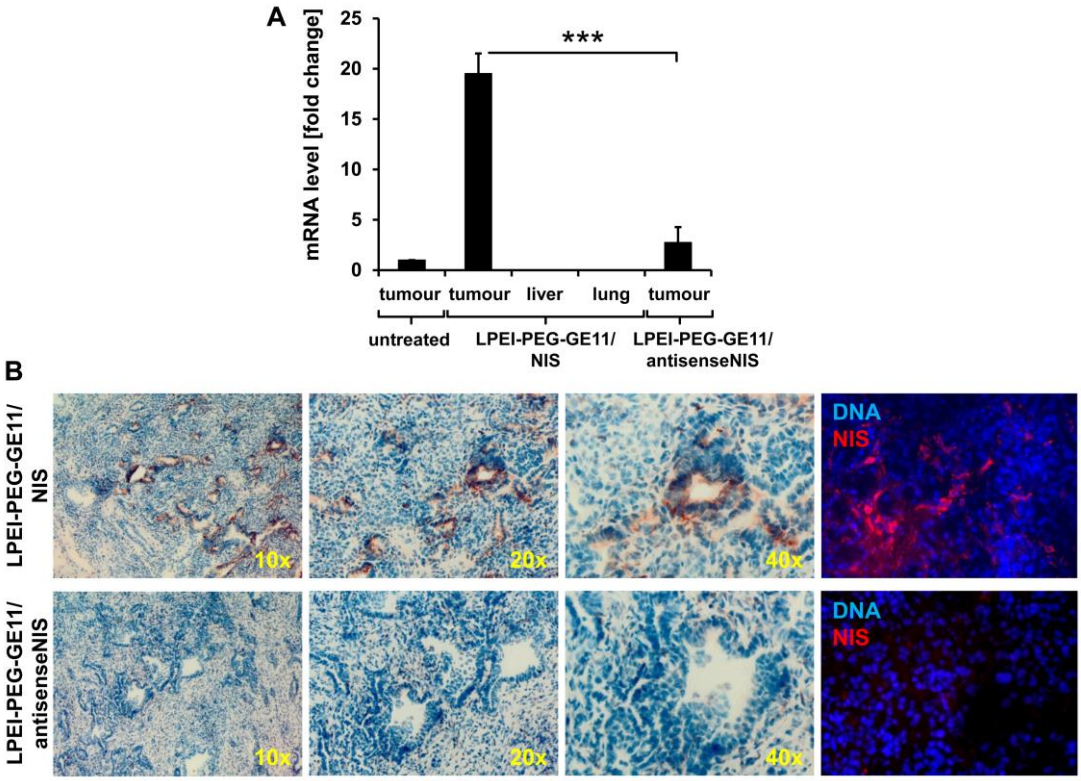

Figure 30. Analysis of NIS mRNA and protein distribution *ex vivo*. NIS-specific qPCR analysis revealed a 20-fold increase of *NIS* mRNA expression in pancreatic tumours of mice injected with LPEI-PEG-GE11/NIS as compared to tumours of untreated mice. In contrast, *NIS* mRNA was not increased in non-target organs and in tumours of mice injected with the control vector LPEI-PEG-GE11/antisenseNIS (mean-fold change ± S.E.M.; ***p<0.001) (**A**). Both immunohistochemical (**B**, upper three panels; magnification: 10×, 20× and 40×) and immunofluorescence staining (**B**, bottom panel; magnification: 200×) of sections of pancreatic tumours revealed areas of NIS-specific immunoreactivity after systemic application of LPEI-PEG-GE11/NIS. In contrast, tumours treated with the control vector LPEI-PEG-GE11/antisenseNIS showed no NIS-specific immunoreactivity.

NIS-mediated ^{131}I therapy of PDAC

PDAC-bearing mice were treated with three cycles of LPEI-PEG-GE11/NIS followed by ^{131}I 48 h later – the optimal time point for radionuclide injection based on the imaging studies. Controls were injected with non-coding LPEI-PEG-GE11/antisenseNIS and ^{131}I or saline only. Tumour progression was monitored by MRI. Mice in the therapy group showed a significant stabilization of tumour growth and, in two cases, even a reduction in tumour volume (**Fig. 31A, D**), while aggressive tumour growth was observed in both control groups (**Fig. 31B-D**). This led to an enhanced survival in the therapy group that lived up to 28 days post therapy start with a median survival of 25 days, as compared to the antisenseNIS group that survived up to 13 days with a median survival of 11 days and saline controls that lived up to 21 days, median survival 21 days (**Fig. 31E**). The effect on mouse survival was, however, not significant.

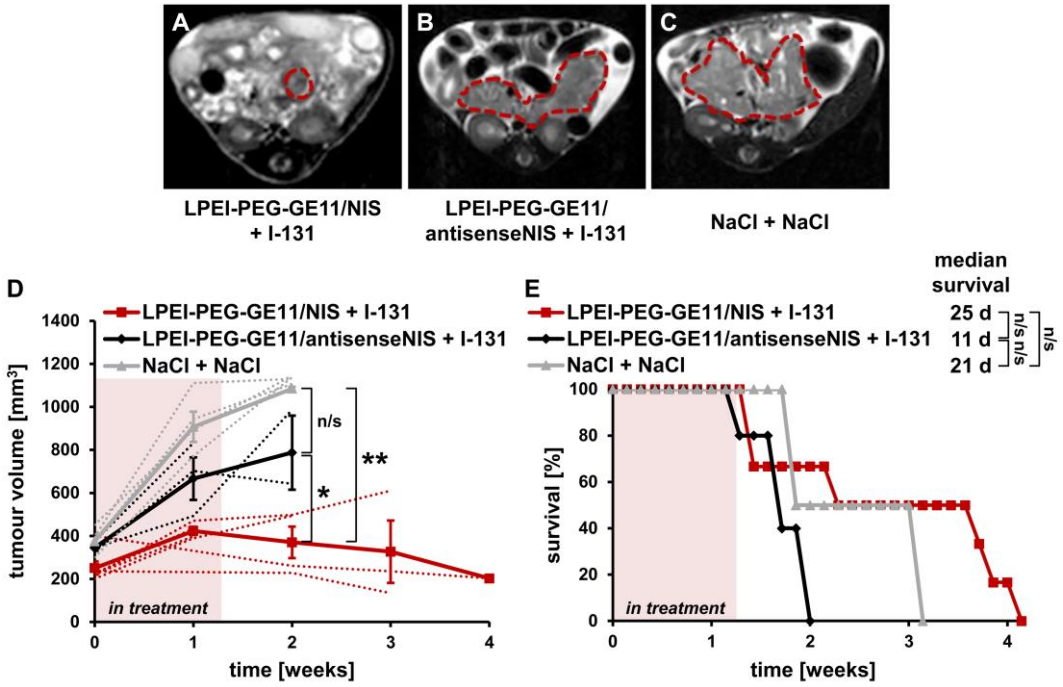

Figure 31. Therapeutic application of ^{131}I after NIS gene transfer *in vivo*. *Kras;p53* mice were treated with three cycles of i.v. injection of polyplexes on days 0/4/7 followed by i.p. injection of 55.5 MBq ^{131}I 48 h later, on days 2/6/9. Tumour sizes were monitored weekly by MRI. Exemplary MRI images of endpoint tumour sizes from an LPEI-PEG-GE11/NIS + ^{131}I- (**A**), an LPEI-PEG-GE11/antisenseNIS + ^{131}I- (**B**) and a NaCl + NaCl-treated *Kras;p53* mouse are shown (**C**). Tumours are highlighted by red dotted lines. (**D**) Mice treated with LPEI-PEG-GE11/NIS + ^{131}I (n=6) showed a stabilization in tumour volume compared to control groups LPEI-PEG-GE11/antisenseNIS + ^{131}I (n=3; mean ± S.E.M.; **p*<0.05) and NaCl + NaCl (n=4; ***p*<0.01). Mean tumour volumes (solid lines) and volumes for individual mice (dotted lines) are shown. (**E**) Injection of LPEI-PEG-GE11/NIS + ^{131}I led to an increased overall and median survival in the therapy group (n=6) compared to control groups injected with LPEI-PEG-GE11/antisenseNIS + ^{131}I (n=3; n/s) or NaCl + NaCl (n=4; n/s).

7.5 Discussion

While the incidence of PDAC is gradually increasing, the prognosis of patients with pancreatic cancer has not significantly changed over the last 20 years – despite numerous advances in diagnostic imaging, surgical techniques and chemotherapeutic strategies [242, 259]. Intensified chemotherapy protocols in patients with advanced pancreatic cancer show a significant, yet still unsatisfactory survival benefit [260]. So far, no targeted agent or approach has changed this fatal course of the disease, even though preclinical trials in *in vitro* cell culture systems and *in vivo* xenograft models had shown promising results [242, 260]. These set-backs can mainly be attributed to the complexity of the disease. The homogeneous molecular equipment, simple stromal architecture and immune deficiency of xenograft models limits their transferability to the clinical setting. Endogenously grown tumours, in contrast, are genetically and morphologically heterogeneous, less vascularised and harbour a far more complex microenvironment with high immunosuppression and extensive desmoplasia [261, 262]. Genetically engineered mouse models that closely reflect the key aspects of pancreatic carcinogenesis have been

shown to correlate well with data from clinical trials and provide an exciting new platform to predict human tumour responses to treatment [252].

After the proof-of-principle of our polyplex-mediated *NIS* gene therapy concept in different subcutaneous xenograft tumour models [82, 83, 87], the genetically engineered mouse model of PDAC used in this study provides an important step towards further development towards clinical application. Based on the known activity of EGFR in PDAC and this model, we chose EGFR-targeted LPEI-PEG-GE11 polymers as delivery vehicles for the *NIS* gene [87, 263, 264].

Transfection of PDAC explant cell cultures with LPEI-PEG-GE11/NIS led to significant perchlorate-sensitive and therefore NIS-mediated radioiodide accumulation. The empty vector LPEI-PEG-GE11 did not result in iodide accumulation above background levels, further confirming NIS-dependency of radioiodide accumulation. Iodide uptake was significantly reduced after transfection with non-targeted LPEI-PEG-Cys/NIS, demonstrating improved transfection efficiency using the targeting ligand GE11. EGFR-specificity of targeting was further substantiated by the observation that in EGFR-negative cultures derived from *Kras;p53;Egfr* mice, no significant difference between transfection with EGFR-targeted or non-targeted vectors was observed. Translating these promising *in vitro* results to systemic vector application *in vivo*, intravenous administration of LPEI-PEG-GE11/NIS resulted in a significant perchlorate-sensitive tumour-specific iodide uptake in mice harbouring endogenous PDAC tumours, as demonstrated by ^{123}I gamma camera imaging. Three-dimensional ^{124}I PET imaging with increased sensitivity and resolution was employed for more accurate quantification of tumoural radioiodide uptake, as radionuclide signals from pancreatic lesions partially overlap with stomach signals based on physiological gastric NIS expression. Results from PET imaging confirmed gamma camera imaging results with strong radioiodide signals in pancreatic tumours. Control experiments with LPEI-PEG-GE11/antisenseNIS showed no significant tumoural radioiodide accumulation above background levels, confirming NIS-specificity of tumoural tracer uptake. These molecular imaging data were further corroborated by NIS-specific immunohistochemistry and immunofluorescence as well as qPCR analysis.

Both the abundance and the permeability of the tumour's vasculature are crucial for sufficient transgene delivery into the tumour [265, 266]. One of the main factors thought to hamper efficient drug delivery to PDAC, is its highly desmoplastic stroma alongside its high interstitial pressure and poor vascularization [267]. Thus, the enhanced permeability and retention effect that is caused by the irregular, 'leaky' tumour vasculature and is usually exploited for passive targeting of therapeutic agents to tumour sites, is limited in PDAC [266, 268]. For this reason, an additional tumour-targeting strategy is particularly important. Our imaging data convincingly demonstrate that targeting our polyplexes to EGFR allows strong transfection of pancreatic tumours with *NIS*. In a previous study, using the same vector construct in a subcutaneous hepatocellular carcinoma xenograft model, a tumour-absorbed dose of 47 mGy/MBq/g was calculated for ^{131}I 24 h after polyplex administration [87], while in the current study, a dose of 74.7 mGy/MBq/g tumour 24 h post polyplex injection was achieved. We mainly

attribute this significantly enhanced tumoural radioiodide uptake to the very high EGFR expression in PDAC. NIS staining was restricted to areas of high EGFR expression surrounding ductal lesions [246]. This focal pattern of transgene expression further underlines the advantage of NIS as therapy gene in this setting, as the high radionuclide bystander effect allows destruction of tumour cells beyond transfected cells.

Building on these promising results, the next logical step was to evaluate the therapeutic effectiveness of ^{131}I in the PDAC mouse model after LPEI-PEG-GE11-mediated systemic *NIS* gene delivery. We were able to demonstrate stabilization, and, in two cases, even a pronounced reduction, of tumour growth after application of three cycles of LPEI-PEG-GE11/NIS followed by ^{131}I. Mouse survival was prolonged in the therapy group, especially compared to the non-coding LPEI-PEG-GE11/antisenseNIS-treated control group, although without reaching statistical significance, despite the strong effects on tumour growth. Interestingly, while animals in the saline group had to be sacrificed due to compromised well-being owing to excessive tumour growth, the non-coding control group showed signs of ill health at much lower tumour volumes and had to be sacrificed. Similarly, effects on animal health were observed in the therapy group, though to a lower extent. We attribute this observation to toxicity of the LPEI-based conjugates, possibly combined with effects from ^{131}I. Due to the stabilization of tumour growth in therapy animals, they fared better than the non-coding control group that was potentially affected by side effects from polyplex and radioiodide injection in addition to rapid tumour growth. To date, the use of LPEI-based polymers did not affect animal health in any of our previous studies, nor was viability of PDAC cell explants affected in the current study. LPEI has been shown to exhibit certain cytotoxic effects both *in vitro* and *in vivo* [269-273], though LPEI-based polyplexes have already been tested in a clinical trial for bladder cancer therapy and no adverse effects were reported [274]. Similarly, we have so far only encountered side effects from ^{131}I in one previous study with the objective to radioablate mouse thyroids under intentional stimulation of thyroidal radioiodide uptake [143]. Symptoms developed with a delay of seven days after radioiodide application, while in the current study, animal health deteriorated from the beginning of treatment [143]. However, our earlier work was done in subcutaneous xenograft models, where tumour growth *per se* has no impact on animal health. In contrast, *Kras;p53* mice with their extremely aggressive pancreatic tumour growth and subsequent rapid health deterioration, seem to react more unfavourably to the polyplexes and/or radioiodide treatment. LPEI is seen as the ‘gold standard’ for non-viral DNA delivery, as it shows such high transfection efficiency and flexibility at relatively low toxicity, compared to other viral and non-viral gene delivery approaches. To further refine our approach and solve the toxicity issue, we are currently developing sequence-defined polymers with higher biocompatibility for targeted *NIS* gene delivery [205].

In conclusion, our data clearly show the high potential of EGFR-targeted nanoparticle vectors to target the *NIS* gene to PDAC. After systemic application of LPEI-PEG-GE11/NIS, we were able to reach sufficient iodide concentrations at the tumour site to (1) produce a strong enough signal to image pancreatic tumours *in situ* and (2) provoke a therapeutic effect. Based on its role as potent and well

characterised reporter gene, *NIS* allows non-invasive imaging and detailed characterization of *in vivo* biodistribution of functional NIS expression as an essential prerequisite for exact planning and monitoring of clinical gene therapy trials with the aim of individualization of the *NIS* gene therapy concept in the clinical setting.

7.6 Acknowledgements

We are grateful to Sissy M Jhiang (Ohio State University, Columbus, OH, USA) for supplying the full-length human *NIS* complementary DNA and to John C Morris (Mayo Clinic, Rochester, MN, USA) for providing the NIS mouse monoclonal antibody. We also thank Nathalie Schwenk (LMU Munich, Munich, Germany) for her help with *in vitro* and *ex vivo* studies, Sybille Reder, Stefan Ambros, Klemens Scheidhauer and Jakob Allmann (Klinikum rechts der Isar der Technischen Universität München, Munich, Germany) for assistance with PET and MRI studies, Wolfgang Rödl (LMU Munich, Munich, Germany) for conjugate synthesis as well as Doris Mayr (LMU Munich, Munich, Germany) for preparation of paraffin-embedded slides.

This work was supported by grants from the Deutsche Forschungsgemeinschaft within the Collaborative Research Center SFB 824 to C.S. (project C8) and J.T.S. (project C4) and within the Priority Programme SPP1629 to C.S. and P.J.N. (SP 581/6-1, SP 581/6-2, NE 648/5-2), as well as a grant from the Wilhelm-Sander-Stiftung to C.S. (2014.129.1), a grant within the European Commission Seventh Framework Program (FP7/CAM-PaC under grant agreement n°602783) and a grant from the German Cancer Consortium (DKTK) to J.T.S., a grant from the excellence cluster Nanosystems Initiative Munich to E.W. as well as a grant from the Center for Nanoscience (CeNS) to M.O.

VIII. SUMMARY

While a great amount of attention is being given to the fight against cancer and considerable advances have been made, many cancers remain deadly diseases. Understanding tumour biology is fundamental to disease management and the development of effective therapeutic strategies. The work presented in this thesis touches on both tumour biology, specifically on thyroid hormone effects on tumours and tumour-associated mesenchymal stem cells (MSCs), and on the development of treatment strategies, specifically on the evaluation of non-viral tumour-targeted gene delivery vehicles for systemic sodium iodide symporter (*NIS*) gene therapy.

Initially, an effective protocol for radioiodide ablation of the mouse thyroid gland was established, thus generating a hypothyroid *in vivo* model that is tailored to the use of *NIS* as reporter gene, in which interference from both endogenous thyroid hormones and thyroidal NIS are avoided.

Subsequently, thyroid hormone effects on MSCs in the tumour milieu were investigated. Non-classical thyroid hormone signalling via cell surface receptor integrin αvβ3 has been shown to drive tumour cell proliferation and survival, as well as angiogenesis and inflammation. This phenomenon is of course undesirable in cancer patients and, indeed, over the past century, several clinical and experimental studies have implicated thyroid hormones in cancer progression. Integrin αvβ3 is abundantly expressed on most cancer cells and the growing endothelium associated with tumours, but also on MSCs. These multipotent progenitor cells actively home to growing tumours where they differentiate into carcinoma-associated fibroblast (CAF)-like cells and blood vessel-stabilising pericytes, and thus support the tumour's fibrovascular network. Integrin αvβ3 expression on MSCs makes them susceptible to thyroid hormone stimulation. Indeed, the work presented here demonstrates that thyroid hormones stimulate the differentiation of MSCs towards a CAF-/pericyte-like and hypoxia-responsive, pro-angiogenic phenotype, characterised by the secretion of numerous paracrine pro-angiogenic factors, in addition to driving their migration, invasion, and recruitment to the tumour microenvironment in an experimental hepatocellular carcinoma model *in vitro* and *in vivo*. The deaminated thyroid hormone metabolite tetrac, a specific inhibitor of thyroid hormone action at the integrin site, reverses these effects. The modulation of MSC signalling and recruitment by thyroid hormones via integrin αvβ3 adds a further layer to the multifaceted effects of thyroid hormones on tumour progression, and suggests a novel mechanism for the anti-tumour activity of tetrac. In addition, modulation of MSC recruitment is of clinical interest in tissue regeneration and in the field of cancer gene therapy, where MSCs are being used as Trojan horses to deliver therapeutic payloads, including the *NIS* gene, into tumours.

To assess the relevance of integrin αvβ3 expression on the cancer cells themselves as opposed to effects on angiogenesis and the tumour stroma in general, we compared the effects of thyroid hormones versus tetrac in two murine xenograft tumour models with and without integrin αvβ3 expression. Tumour growth was significantly increased in hyperthyroid mice and significantly decreased in hypothyroid and

tetrac-treated euthyroid mice, resulting in either a reduced or prolonged survival, respectively, compared to euthyroid mice in αvβ3-positive human anaplastic thyroid cancer xenografts. Both proliferation and vascularisation were significantly increased in tumours from hyperthyroid mice as compared to hypothyroid and tetrac-treated mice. No differences in tumour growth, survival, or proliferation were observed between the different thyroid hormone states in mice bearing αvβ3-negative hepatocellular carcinoma xenografts. The blood vessel density, however, was significantly decreased in hypothyroid and tetrac-treated mice compared to both euthyroid and hyperthyroid mice in this model.

The modulation of MSC recruitment, differentiation, and angiogenic signalling, in addition to the regulation of tumour growth in αvβ3-positive tumours by thyroid hormones via integrin αvβ3 have important implications for the management of cancer patients, especially for those with thyroid dysfunction and thyroid cancer patients treated with thyroid-stimulating hormone-suppressive L-thyroxine doses.

Addressing the second topic of the thesis, selective transfer of the theranostic *NIS* gene into tumour cells allows systemic application of radionuclides for non-invasive imaging as well as therapy. For clinical development of the *NIS* gene therapy approach, tumour targeting needs to be highly specific and efficient at low toxicity, and requires systemic application for the treatment of metastatic disease. To investigate the potential of targeting the epidermal growth factor receptor (EGFR), which is highly expressed on many cancer cells, for systemic non-viral *NIS* gene transfer, the well-established cationic polymer linear polyethylenimine (LPEI) was shielded with polyethylene glycol (PEG) and coupled to the EGFR-specific peptide ligand GE11. Two different tumour models were used, specifically anaplastic thyroid carcinoma xenografts that have lost the ability to express NIS in the process of dedifferentiation, and, as a further step towards clinical application, an advanced genetically engineered mouse model of pancreatic ductal adenocarcinoma (PDAC) that closely mirrors human disease. In both models, high NIS- and EGFR-specific iodide uptake was achieved *in vitro* and *in vivo*. This resulted in a significant delay in tumour growth in both models in subsequent ^{131}I therapy studies that was accompanied by a significantly prolonged survival in the anaplastic thyroid carcinoma model. The work reported here was the first study to demonstrate successful re-instatement of NIS-mediated radioiodide uptake in anaplastic thyroid carcinoma after systemic application of *NIS* as a theranostic gene. Further, the successful targeting and tumour growth reduction in PDAC proves the applicability of this approach in a highly complex model that closely emulates human PDAC. Taken together, these data in two highly aggressive tumour entities clearly demonstrate the great potential of EGFR-targeted nanoparticle vectors to selectively deliver NIS to EGFR-expressing tumours after systemic application, an important prerequisite for the treatment of metastatic disease by *NIS* gene therapy.

IX. PUBLICATIONS

9.1 Original Papers

2019

1. **Schmohl KA**, Han Y, Tutter M, Schwenk N, Ziegler SI, Bartenstein P, Nelson PJ, Spitzweg C. Thyroid status affects tumour growth in integrin αvβ3-positive tumours only. [Manuscript in preparation].

2. **Schmohl KA**, Müller AM, Dohmann M, Spellerberg R, Urnauer S, Schwenk N, Ziegler SI, Bartenstein P, Nelson PJ, Spitzweg C. Integrin αvβ3-mediated effects of thyroid hormones on mesenchymal stem cells in tumour angiogenesis. *Thyroid* [In print].

3. Schug C, Kitzberger C, Sievert W, Spellerberg R, Tutter M, **Schmohl KA**, Eberlein B, Biedermann T, Steiger K, Zach C, Schwaiger M, Multhoff G, Wagner E, Nelson PJ, Spitzweg C. Radiation-induced amplification of TGFB1-induced mesenchymal stem cell-mediated sodium iodide symporter (*NIS*) gene ^{131}I therapy. *Clin Cancer Res* **2019**;25:5997-6008.

4. Urnauer S, **Schmohl KA**, Tutter M, Schug C, Schwenk N, Morys S, Ziegler S, Bartenstein P, Clevert DA, Wagner E, Spitzweg C. Dual-targeted NIS polyplexes – a theranostic strategy toward tumors with heterogeneous receptor expression. *Gene Ther* **2019**;26:93-108.

5. Schug C, Gupta A, Urnauer S, Steiger K, Cheung PF, Neander C, Savvatakis K, **Schmohl KA**, Trajkovic-Arsic M, Schwenk N, Schwaiger M, Nelson PJ, Siveke JT, Spitzweg C. A novel approach for image-guided ^{131}I therapy of pancreatic ductal adenocarcinoma using mesenchymal stem cell-mediated NIS gene delivery. *Mol Cancer Res* **2019**;17:310-20.

6. Schug C, Urnauer S, Jäckel C, **Schmohl KA**, Tutter M, Steiger K, Schwenk N, Schwaiger M, Wagner E, Nelson PJ, Spitzweg C. TGFB1-driven mesenchymal stem cell-mediated *NIS* gene transfer. *Endocr Relat Cancer* **2019**;26:89-101.

2018

7. Schug C, Sievert W, Urnauer S, Müller AM, **Schmohl KA**, Wechselberger A, Schwenk N, Lauber K, Schwaiger M, Multhoff G, Wagner E, Nelson PJ, Spitzweg C. External beam radiation therapy enhances mesenchymal stem cell-mediated sodium iodide symporter gene delivery. *Hum Gene Ther* **2018**;29:1287-300.

2017

8. Urnauer S, Müller AM, Schug C, **Schmohl KA**, Tutter M, Schwenk N, Rödl W, Morys S, Ingrisch M, Bertram J, Bartenstein P, Clevert DA, Wagner E, Spitzweg C. EGFR-targeted nonviral NIS gene transfer for bioimaging and therapy of disseminated colon cancer metastases. *Oncotarget* **2017**;8:92195-208.

9. **Schmohl KA**, Dolp P, Schug C, Knoop K, Klutz K, Schwenk N, Bartenstein P, Nelson PJ, Ogris M, Wagner E, Spitzweg C. Reintroducing the sodium iodide symporter (NIS) to anaplastic thyroid carcinoma. *Thyroid* **2017**;27:1534-43.

10. **Schmohl KA**, Gupta A, Grünwald GK, Trajkovic-Arsic M, Klutz K, Braren R, Schwaiger M, Nelson PJ, Ogris M, Wagner E, Siveke JT, Spitzweg C. Imaging and targeted therapy of pancreatic ductal adenocarcinoma using the theranostic sodium iodide symporter (NIS) gene. *Oncotarget* **2017**;8:33393-404.

2016

11. Müller AM, **Schmohl KA**, Knoop K, Schug C, Urnauer S, Hagenhoff A, Clevert D-A, Ingrisch M, Niess H, Carlsen J, Zach C, Wagner E, Bartenstein P, Nelson PJ, Spitzweg C. Hypoxia-targeted ^{131}I therapy of hepatocellular cancer after systemic mesenchymal stem cell-mediated sodium iodide symporter gene delivery. *Oncotarget* **2016**;7:54795-810.

12. Urnauer S, Morys S, Krhac Levacic A, Müller AM, Schug C, **Schmohl KA**, Schwenk N, Zach C, Carlsen J, Bartenstein P, Wagner E, Spitzweg C. Sequence-defined cMET/HGFR-targeted polymers as gene delivery vehicles for the theranostic sodium iodide symporter (NIS) gene. *Mol Ther* **2016**;24:1395-404.

2015

13. **Schmohl KA**, Müller AM, Wechselberger A, Rühland S, Salb N, Schwenk N, Heuer H, Carlsen J, Göke B, Nelson PJ, Spitzweg C. Thyroid hormones and tetrac: new regulators of tumour stroma formation via integrin αvβ3. *Endocr Relat Cancer* **2015**;22:941-52.

14. **Schmohl KA**, Müller AM, Schwenk N, Knoop K, Rijntjes E, Köhrle J, Heuer H, Bartenstein P, Göke B, Nelson PJ, Spitzweg C. Establishment of an Effective Radioiodide Thyroid Ablation Protocol in Mice. *Eur Thyroid J* **2015**;4:74-80.

15. Knoop K, Schwenk N, **Schmohl K**, Müller A, Zach C, Cyran C, Carlsen J, Böning G, Bartenstein P, Göke B, Wagner E, Nelson PJ, Spitzweg C. Mesenchymal stem cell-mediated, tumor stroma-targeted radioiodine therapy of metastatic colon cancer using the sodium iodide symporter as theranostic gene. *J Nucl Med* **2015**;56:600-6.

9.2 Reviews

2019

16. **Schmohl KA**, Müller AM, Nelson PJ, Spitzweg C. Thyroid hormone effects on mesenchymal stem cell biology in the tumour microenvironment. *Exp Clin Endocrinol Diabetes* **2019** [Epub ahead of print].

17. **Schmohl KA**, Nelson PJ, Spitzweg C. Tetrac as an anti-angiogenic agent in cancer. *Endocr Relat Cancer* **2019**;26:R287-304.

9.3 Oral Presentations

2019

03/2019 62. Deutscher Kongress für Endokrinologie, Göttingen, Germany
Schmohl KA, Schwenk N, Bartenstein P, Nelson PJ, Spitzweg C. Non-genomic effects of thyroid hormones on mesenchymal stem cells in tumour angiogenesis

02/2019 18th Retreat of the Dept. of Medicine IV, LMU Munich, Frauenchiemsee, Germany
Schmohl KA, Müller AM, Dohmann M, Spellerberg R, Urnauer S, Schwenk N, Ziegler SI, Nelson PJ, Spitzweg C. Non-genomic effects of thyroid hormones on mesenchymal stem cells in tumour angiogenesis

2018

10/2018 88th Annual Meeting of the American Thyroid Association, Washington DC, USA
Schmohl KA, Urnauer S, Schwenk N, Bartenstein P, Nelson PJ, Spitzweg C. Non-genomic effects of thyroid hormones on mesenchymal stem cells in tumour angiogenesis (highlighted oral presentation)

09/2018 41st Annual Meeting of the European Thyroid Association, Newcastle, UK
Schmohl KA, Urnauer S, Schwenk N, Bartenstein P, Nelson PJ, Spitzweg C. Non-genomic effects of thyroid hormones on mesenchymal stem cells in tumour angiogenesis

06/2018 6th Annual Meeting of the Priority Programme Thyroid Trans Act, Berlin, Germany
Schmohl KA, Nelson PJ, Spitzweg C. Plasma membrane-mediated non-genomic effects of T4, T3 and thyroid hormone metabolite tetrac on different aspects of mesenchymal stem cell biology and their signalling pathways

05/2018 20th European Congress of Endocrinology, Barcelona, Spain

Schmohl KA (invited speaker). Tetrac as an antiangiogenic agent in cancer

2017

10/2017 87th Annual Meeting of the American Thyroid Association, Victoria, BC, Canada
Schmohl KA, Dohmann M, Wechselberger A, Nelson PJ, Spitzweg C. Non-genomic effects of thyroid hormones on mesenchymal stem cells and angiogenesis

09/2017 40th Annual Meeting of the European Thyroid Association, Belgrade, Serbia
Schmohl KA, Dohmann M, Wechselberger A, Nelson PJ, Spitzweg C. Non-genomic effects of thyroid hormones on mesenchymal stem cells and angiogenesis

06/2017 5th Annual Meeting of the Priority Programme Thyroid Trans Act, Bremen, Germany
Schmohl KA, Nelson PJ, Spitzweg C. Plasma membrane-mediated non-genomic effects of T4, T3 and thyroid hormone metabolite tetrac on different aspects of mesenchymal stem cell biology and their signalling pathways

05/2017 Aktuelles zum Thema Schilddrüse – Update 2017, Munich, Germany
Schmohl KA. Beeinflussen Schilddrüsenhormone das Tumorwachstum? – from Bench to Bedside (*Do thyroid hormones influence tumour growth? – from bench to bedside*)

03/2017 60. Deutscher Kongress für Endokrinologie, Würzburg, Germany
Schmohl KA, Dohmann M, Wechselberger A, Nelson PJ, Spitzweg C. Non-genomic effects of thyroid hormones on mesenchymal stem cells and angiogenesis

02/2017 17th Retreat of the Dept. of Medicine IV, LMU Munich, Frauenchiemsee, Germany
Schmohl KA, Müller AM, Wechselberger A, Rühland S, Dohmann M, Schwenk N, Nelson PJ, Spitzweg C. Thyroid hormones and tetrac – new regulators of tumour stroma formation via integrin αvβ3

2016

06/2016 4th Annual Meeting of the Priority Programme Thyroid Trans Act, Essen, Germany
Schmohl KA, Müller AM, Wechselberger A, Nelson PJ, Spitzweg C. Plasma membrane-mediated non-genomic effects of T4, T3 and thyroid hormone metabolite tetrac on different aspects of mesenchymal stem cell biology and their signalling pathways

05/2016 18th European Congress of Endocrinology, Munich, Germany
Schmohl KA, Dohmann M, Wechselberger A, Nelson PJ, Spitzweg C. Non-genomic effects of thyroid hormones on endothelial cell tube formation

2015

11/2015 Retreat of the Dept. of Medicine II, LMU Munich, Munich, Germany
Schmohl KA, Müller AM, Wechselberger A, Rühland S, Salb N, Dohmann M, Schwenk N, Nelson PJ, Spitzweg C. Thyroid hormones and tetrac – new regulators of tumour stroma formation via integrin αvβ3

04/2015 3rd Annual Meeting of the Priority Programme Thyroid Trans Act, Berlin, Germany
Schmohl KA, Müller AM, Wechselberger A, Nelson PJ, Spitzweg C. Plasma membrane-mediated non-genomic effects of T4, T3 and thyroid hormone metabolite tetrac on the tumour microenvironment

2014

12/2014 30. Arbeitstagung Experimentelle Schilddrüsenforschung (AESF), Bremen, Germany
Schmohl KA, Müller AM, Salb N, Rühland S, Wechselberger A, Schwenk N, Nelson PJ, Spitzweg C. Analysis of the effects of T3, T4 and tetrac on mesenchymal stem cell biology

06/2014 96th Annual Meeting of the Endocrine Society, Chicago, IL, USA
Schmohl KA, Müller AM, Salb N, Knoop K, Wechselberger A, Schwenk N, Nelson PJ, Spitzweg C. Effects of thyroid hormones T3 and T4 on mesenchymal stem cell biology

04/2014 2nd Annual Meeting of the Priority Programme Thyroid Trans Act, Essen, Germany
Schmohl KA & Müller AM. Regulation of the tumour microenvironment by thyroid hormones

9.4 Poster Presentations

2019

10/2019 89th Annual Meeting of the American Thyroid Association, Chicago, IL, USA
Schmohl KA, Han Y, Tutter M, Schwenk N, Nelson PJ, Spitzweg C. Stimulation of tumour growth by thyroid hormone depends on integrin αvβ3 expression

2018

10/2018 88th Annual Meeting of the American Thyroid Association, Washington DC, USA
Schmohl KA, Kitzberger C, Kälin RE, Glaß R, Nelson PJ, Spitzweg C. Mesenchymal stem cell-mediated sodium iodide symporter (NIS) reporter gene delivery in an orthotopic glioblastoma mouse model

2018 Annual Trainee Poster Contest winner, best basic research poster

05/2018 20th European Congress of Endocrinology, Barcelona, Spain
Schmohl KA, Dohmann M, Schwenk N, Bartenstein P, Nelson PJ, Spitzweg C. Non-genomic effects of thyroid hormones on mesenchymal stem cells in tumour angiogenesis

03/2018 100th Annual Meeting of the Endocrine Society, Chicago, IL, USA
Schmohl KA, Urnauer S, Schwenk N, Bartenstein P, Nelson PJ, Spitzweg C. Non-genomic effects of thyroid hormones on mesenchymal stem cells in tumour angiogenesis

2017

04/2017 99th Annual Meeting of the Endocrine Society, Orlando, FL, USA
Schmohl KA, Dohmann M, Wechselberger A, Nelson PJ, Spitzweg C. Non-genomic effects of thyroid hormones on endothelial cell tube formation

2016

09/2016 86th Annual Meeting of the American Thyroid Association, Denver, CO, USA
Schmohl KA, Grünwald GK, Gupta A, Trajkovic-Arsic M, Klutz K, Schwenk N, Braren R, Senekowitsch-Schmidtke R, Schwaiger M, Wagner E, Ogris M, Siveke J, Spitzweg C. Systemic epidermal growth factor receptor-targeted sodium iodide symporter (NIS) gene delivery in a genetically engineered mouse model of pancreatic ductal adenocarcinoma

09/2016 86th Annual Meeting of the American Thyroid Association, Denver, CO, USA
Schmohl KA, Dohmann M, Wechselberger A, Nelson PJ, Spitzweg C. Non-genomic effects of thyroid hormones on endothelial cell tube formation

05/2016 DACH-Tagung der Deutschen, Österreichischen und Schweizerischen Gesellschaften für Endokrinologie 2016, Munich, Germany
Schmohl KA, Dohmann M, Wechselberger A, Nelson PJ, Spitzweg C. Non-genomic effects of thyroid hormones on endothelial cell tube formation

04/2016 98th Annual Meeting of the Endocrine Society, Boston, MA, USA
Schmohl KA, Dohmann M, Wechselberger A, Nelson PJ, Spitzweg C. Non-genomic effects of thyroid hormones on endothelial cell tube formation

2015

10/2015 15th International Thyroid Congress (ITC), Orlando, FL, USA
Schmohl KA, Dohmann M, Wechselberger A, Nelson PJ, Spitzweg C. Non-genomic effects of thyroid hormones on endothelial cell tube formation

03/2015 58. Symposium der Deutschen Gesellschaft für Endokrinologie, Lübeck, Germany
Schmohl KA, Müller AM, Salb N, Rühland S, Wechselberger A, Schwenk N, Nelson PJ, Spitzweg C. Analysis of the effects of T3, T4 and tetrac on mesenchymal stem cell biology

2014

12/2014 1st International Conference of Thyroid Trans Act (TTA IC), Bremen, Germany
Schmohl KA, Müller AM, Salb N, Rühland S, Wechselberger A, Schwenk N, Nelson PJ, Spitzweg C. Analysis of the effects of T3, T4 and tetrac on mesenchymal stem cell biology

10/2014 84th Annual Meeting of the American Thyroid Association, Coronado, CA, USA
Schmohl KA, Müller AM, Salb N, Knoop K, Wechselberger A, Schwenk N, Nelson PJ, Spitzweg C. Influence of thyroid hormones T3 and T4 on the hypoxia response network

09/2014 38th Annual Meeting of the European Thyroid Association, Santiago de Compostela, Spain
Schmohl KA, Müller AM, Salb N, Wechselberger A, Knoop K, Schwenk N, Nelson PJ, Spitzweg C. Effects of thyroid hormones T3 and T4 on mesenchymal stem cell differentiation and migration

03/2014 57. Symposium der Deutschen Gesellschaft für Endokrinologie, Dresden, Germany
Schmohl KA, Müller AM, Knoop K, Schwenk N, Wechselberger A, Nelson PJ, Spitzweg C. Effects of thyroid hormones T3 and T4 on mesenchymal stem cell differentiation

2013

10/2013 83th Annual Meeting of the American Thyroid Association, San Juan, Puerto Rico
Müller AM*, **Schmohl KA***, Knoop K, Schwenk N, Wechselberger A, Nelson PJ, Spitzweg C. Effects of thyroid hormones T3 and T4 on mesenchymal stem cell differentiation. *equal contribution

9.5 Grants and Awards

2019

10/2019 E. Chester Ridgway Trainee Grant, American Thyroid Association for the 89th Annual Meeting of the American Thyroid Association, Chicago, IL, USA

Travel grant, Deutsche Gesellschaft für Endokrinologie for the 89th Annual Meeting of the American Thyroid Association, Chicago, IL, USA

2018

10/2018 2018 Annual Trainee Poster Contest winner, best basic research poster at the 88th Annual Meeting of the American Thyroid Association, Washington DC, USA

10/2018 E. Chester Ridgway Trainee Grant, American Thyroid Association for the 88th Annual Meeting of the American Thyroid Association, Washington DC, USA

Travel grant, Deutsche Gesellschaft für Endokrinologie for the 88th Annual Meeting of the American Thyroid Association, Washington DC, USA

09/2018 Travel grant, European Thyroid Association for the 41st Annual Meeting of the European Thyroid Association, Newcastle, UK

05/2018 Invited speaker, European Society of Endocrinology at the 20th European Congress of Endocrinology, Barcelona, Spain

2017

10/2017 E. Chester Ridgway Trainee Grant, American Thyroid Association for the 87th Annual Meeting of the American Thyroid Association, Victoria, BC, Canada

09/2017 Travel grant, European Thyroid Association for the 40th Annual Meeting of the European Thyroid Association, Belgrade, Serbia

03/2017 Travel grant, Deutsche Gesellschaft für Endokrinologie for the 60. Deutscher Kongress für Endokrinologie, Würzburg, Germany

2016

09/2016 Travel grant, GlaxoSmithKline Stiftung for the 86th Annual Meeting of the American Thyroid Association, Denver, CO, USA

E. Chester Ridgway Trainee Grant, American Thyroid Association for the 86th Annual Meeting of the American Thyroid Association, Denver, CO, USA

Travel grant, Deutsche Gesellschaft für Endokrinologie for the 86th Annual Meeting of the American Thyroid Association, Denver, CO, USA

2015

10/2015 E. Chester Ridgway Trainee Grant, American Thyroid Association for the 15th International Thyroid Congress (ITC), Orlando, FL, USA

Travel grant, Deutsche Gesellschaft für Endokrinologie for the 15th International Thyroid Congress (ITC), Orlando, FL, USA

Travel grant, European Thyroid Association for the 15th International Thyroid Congress (ITC), Orlando, FL, USA

03/2015 Travel grant, Deutsche Gesellschaft für Endokrinologie for the 58. Symposium der Deutschen Gesellschaft für Endokrinologie, Lübeck, Germany

2014

03/2014 Travel grant, Deutsche Gesellschaft für Endokrinologie for the 57. Symposium der Deutschen Gesellschaft für Endokrinologie, Dresden, Germany

X. REFERENCES

1. Bray F, Ferlay J, Soerjomataram I, Siegel RL, Torre LA, Jemal A. Global cancer statistics 2018: GLOBOCAN estimates of incidence and mortality worldwide for 36 cancers in 185 countries. *CA Cancer J Clin* **2018**;68:394-424.

2. Rous P. The challenge to man of the neoplastic cell. *Cancer Res* **1967**;27:1919-24.

3. Hanahan D, Weinberg RA. The hallmarks of cancer. *Cell* **2000**;100:57-70.

4. Hanahan D, Weinberg RA. Hallmarks of cancer: the next generation. *Cell* **2011**;144:646-74.

5. Cammarota F, Laukkanen MO. Mesenchymal Stem/Stromal Cells in Stromal Evolution and Cancer Progression. *Stem Cells Int* **2016**;2016:4824573.

6. Wels J, Kaplan RN, Rafii S, Lyden D. Migratory neighbors and distant invaders: tumor-associated niche cells. *Genes Dev* **2008**;22:559-74.

7. Dvorak HF. Tumors: wounds that do not heal-redux. *Cancer Immunol Res* **2015**;3:1-11.

8. Hagenhoff A, Bruns CJ, Zhao Y, von Luttichau I, Niess H, Spitzweg C, *et al.* Harnessing mesenchymal stem cell homing as an anticancer therapy. *Expert Opin Biol Ther* **2016**;16:1079-92.

9. Dvorak HF. Tumors: wounds that do not heal. Similarities between tumor stroma generation and wound healing. *N Engl J Med* **1986**;315:1650-9.

10. Vitale I, Manic G, Galassi C, Galluzzi L. Stress responses in stromal cells and tumor homeostasis. *Pharmacol Ther* **2019**;200:55-68.

11. Chandler C, Liu T, Buckanovich R, Coffman LG. The double edge sword of fibrosis in cancer. *Transl Res* **2019**;209:55-67.

12. Bussard KM, Mutkus L, Stumpf K, Gomez-Manzano C, Marini FC. Tumor-associated stromal cells as key contributors to the tumor microenvironment. *Breast Cancer Res* **2016**;18:84.

13. Pinto M, Soares P, Ribatti D. Thyroid hormone as a regulator of tumor induced angiogenesis. *Cancer Lett* **2011**;301:119-26.

14. Bronckaers A, Hilkens P, Martens W, Gervois P, Ratajczak J, Struys T, *et al.* Mesenchymal stem/stromal cells as a pharmacological and therapeutic approach to accelerate angiogenesis. *Pharmacol Ther* **2014**;143:181-96.

15. Ellis LM. Epidermal growth factor receptor in tumor angiogenesis. *Hematol Oncol Clin North Am* **2004**;18:1007-21.

16. Avraamides CJ, Garmy-Susini B, Varner JA. Integrins in angiogenesis and lymphangiogenesis. *Nat Rev Cancer* **2008**;8:604-17.

17. Turley SJ, Cremasco V, Astarita JL. Immunological hallmarks of stromal cells in the tumour microenvironment. *Nat Rev Immunol* **2015**;15:669-82.

18. Dwyer RM, Kerin MJ. Mesenchymal stem cells and cancer: tumor-specific delivery vehicles or therapeutic targets? *Hum Gene Ther* **2010**;21:1506-12.

19. Spaeth EL, Dembinski JL, Sasser AK, Watson K, Klopp A, Hall B, *et al.* Mesenchymal stem cell transition to tumor-associated fibroblasts contributes to fibrovascular network expansion and tumor progression. *PLoS One* **2009**;4:e4992.

20. Schmohl KA, Müller AM, Wechselberger A, Rühland S, Salb N, Schwenk N, *et al.* Thyroid hormones and tetrac: new regulators of tumour stroma formation via integrin αvβ3. *Endocr Relat Cancer* **2015**;22:941-52.

21. Gieniec KA, Butler LM, Worthley DL, Woods SL. Cancer-associated fibroblasts-heroes or villains? *Br J Cancer* **2019**;121:293-302.

22. Bergers G, Song S. The role of pericytes in blood-vessel formation and maintenance. *Neuro Oncol* **2005**;7:452-64.

23. Armulik A, Genove G, Betsholtz C. Pericytes: developmental, physiological, and pathological perspectives, problems, and promises. *Dev Cell* **2011**;21:193-215.

24. Barcellos-de-Souza P, Gori V, Bambi F, Chiarugi P. Tumor microenvironment: bone marrow-mesenchymal stem cells as key players. *Biochim Biophys Acta* **2013**;1836:321-35.

25. Taylor E, Heyland A. Evolution of thyroid hormone signaling in animals: Non-genomic and genomic modes of action. *Mol Cell Endocrinol* **2017**;459:14-20.

26. Wu SY, Green WL, Huang WS, Hays MT, Chopra IJ. Alternate pathways of thyroid hormone metabolism. *Thyroid* **2005**;15:943-58.

27. Kohrle J. Thyroid Hormones and Derivatives: Endogenous Thyroid Hormones and Their Targets. *Methods Mol Biol* **2018**;1801:85-104.

28. Kelly GS. Peripheral metabolism of thyroid hormones: a review. *Altern Med Rev* **2000**;5:306-33.

29. Davis PJ, Leonard JL, Lin HY, Leinung M, Mousa SA. Molecular Basis of Nongenomic Actions of Thyroid Hormone. *Vitam Horm* **2018**;106:67-96.

30. Cheng SY, Leonard JL, Davis PJ. Molecular aspects of thyroid hormone actions. *Endocr Rev* **2010**;31:139-70.

31. Moeller LC, Führer D. Thyroid hormone, thyroid hormone receptors, and cancer: a clinical perspective. *Endocr Relat Cancer* **2013**;20:R19-29.

32. Brent GA. Mechanisms of thyroid hormone action. *J Clin Invest* **2012**;122:3035-43.

33. Bergh JJ, Lin HY, Lansing L, Mohamed SN, Davis FB, Mousa S, *et al.* Integrin alphaVbeta3 contains a cell surface receptor site for thyroid hormone that is linked to activation of mitogen-activated protein kinase and induction of angiogenesis. *Endocrinology* **2005**;146:2864-71.

34. Desgrosellier JS, Cheresh DA. Integrins in cancer: biological implications and therapeutic opportunities. *Nat Rev Cancer* **2010**;10:9-22.

35. Xiong JP, Stehle T, Diefenbach B, Zhang R, Dunker R, Scott DL, *et al.* Crystal structure of the extracellular segment of integrin alpha Vbeta3. *Science* **2001**;294:339-45.

36. Dijkgraaf I, Beer AJ, Wester HJ. Application of RGD-containing peptides as imaging probes for alphavbeta3 expression. *Front Biosci (Landmark Ed)* **2009**;14:887-99.

37. Ruoslahti E, Pierschbacher MD. New perspectives in cell adhesion: RGD and integrins. *Science* **1987**;238:491-7.

38. Cody V, Davis PJ, Davis FB. Molecular modeling of the thyroid hormone interactions with alpha v beta 3 integrin. *Steroids* **2007**;72:165-70.

39. Lin HY, Sun M, Tang HY, Lin C, Luidens MK, Mousa SA, *et al.* L-Thyroxine vs. 3,5,3'-triiodo-L-thyronine and cell proliferation: activation of mitogen-activated protein kinase and phosphatidylinositol 3-kinase. *Am J Physiol Cell Physiol* **2009**;296:C980-91.

40. Lin HY, Chin YT, Yang YC, Lai HY, Wang-Peng J, Liu LF, *et al.* Thyroid Hormone, Cancer, and Apoptosis. *Compr Physiol* **2016**;6:1221-37.

41. Davis PJ, Lin HY, Tang HY, Davis FB, Mousa SA. Adjunctive input to the nuclear thyroid hormone receptor from the cell surface receptor for the hormone. *Thyroid* **2013**;23:1503-9.

42. Mousa SA, Davis FB, Mohamed S, Davis PJ, Feng X. Pro-angiogenesis action of thyroid hormone and analogs in a three-dimensional in vitro microvascular endothelial sprouting model. *Int Angiol* **2006**;25:407-13.

43. Burger AG, Engler D, Sakoloff C, Staeheli V. The effects of tetraiodothyroacetic and triiodothyroacetic acids on thyroid function in euthyroid and hyperthyroid subjects. *Acta Endocrinol (Copenh)* **1979**;92:455-67.

44. Moreno M, de Lange P, Lombardi A, Silvestri E, Lanni A, Goglia F. Metabolic effects of thyroid hormone derivatives. *Thyroid* **2008**;18:239-53.

45. Davis PJ, Glinsky GV, Lin HY, Leith JT, Hercbergs A, Tang HY, *et al*. Cancer Cell Gene Expression Modulated from Plasma Membrane Integrin αvβ3 by Thyroid Hormone and Nanoparticulate Tetrac. *Front Endocrinol* **2015**;5:240.

46. Davis PJ, Lin HY, Hercbergs AA, Keating KA, Mousa SA. How thyroid hormone works depends upon cell type, receptor type, and hormone analogue: implications in cancer growth. *Discov Med* **2019**;27:111-7.

47. Schmohl KA, Nelson PJ, Spitzweg C. Tetrac as an anti-angiogenic agent in cancer. *Endocr Relat Cancer* **2019**;26:R287-r304.

48. Krashin E, Piekielko-Witkowska A, Ellis M, Ashur-Fabian O. Thyroid Hormones and Cancer: A Comprehensive Review of Preclinical and Clinical Studies. *Front Endocrinol (Lausanne)* **2019**;10:59.

49. Shoemaker JP, Bradley RL, Hoffman RV. Increased Survival and Inhibition of Mammary Tumors in Hypothyroid Mice. *J Surg Res* **1976**;21:151-4.

50. Kumar MS, Chiang T, Deodhar SD. Enhancing effect of thyroxine on tumor growth and metastases in syngeneic mouse tumor systems. *Cancer Res* **1979**;39:3515-8.

51. Mishkin SY, Pollack R, Yalovsky MA, Morris HP, Mishkin S. Inhibition of local and metastatic hepatoma growth and prolongation of survival after induction of hypothyroidism. *Cancer Res* **1981**;41:3040-5.

52. Theodossiou C, Skrepnik N, Robert EG, Prasad C, Axelrad TW, Schapira DV, *et al*. Propylthiouracil-induced hypothyroidism reduces xenograft tumor growth in athymic nude mice. *Cancer* **1999**;86:1596-601.

53. Theodossiou C, Schwarzenberger P. Propylthiouracil reduces xenograft tumor growth in an athymic nude mouse prostate cancer model. *Am J Med Sci* **2000**;319:96-9.

54. Martinez-Iglesias O, Garcia-Silva S, Regadera J, Aranda A. Hypothyroidism enhances tumor invasiveness and metastasis development. *PLoS One* **2009**;4:e6428.

55. Hercbergs A, Goyal LK, Suh JH, Lee S, Reddy CA, Cohen BH, *et al.* Propylthiouracil-induced chemical hypothyroidism with high-dose tamoxifen prolongs survival in recurrent high grade glioma: a phase I/II study. *Anticancer Res* **2003**;23:617-26.

56. Hercbergs A, Ashur-Fabian O, Garfield D. Thyroid hormones and cancer: clinical studies of hypothyroidism in oncology. *Curr Opin Endocrinol Diabetes Obes* **2010**;17:432-6.

57. Ashur-Fabian O, Blumenthal DT, Bakon M, Nass D, Davis PJ, Hercbergs A. Long-term response in high-grade optic glioma treated with medically induced hypothyroidism and carboplatin: a case report and review of the literature. *Anti-Cancer Drugs* **2013**;24:315-23.

58. Hercbergs A, Johnson RE, Ashur-Fabian O, Garfield DH, Davis PJ. Medically induced euthyroid hypothyroxinemia may extend survival in compassionate need cancer patients: an observational study. *Oncologist* **2015**;20:72-6.

59. Mulligan RC. The basic science of gene therapy. *Science* **1993**;260:926-32.

60. Brenner MK, Gottschalk S, Leen AM, Vera JF. Is cancer gene therapy an empty suit? *Lancet Oncol* **2013**;14:e447-e56.

61. Spitzweg C, Harrington KJ, Pinke LA, Vile RG, Morris JC. Clinical review 132: The sodium iodide symporter and its potential role in cancer therapy. *J Clin Endocrinol Metab* **2001**;86:3327-35.

62. Seidlin SM, Marinelli LD, Oshry E. Radioactive iodine therapy; effect on functioning metastases of adenocarcinoma of the thyroid. *J Am Med Assoc* **1946**;132:838-47.

63. Dai G, Levy O, Carrasco N. Cloning and characterization of the thyroid iodide transporter. *Nature* **1996**;379:458-60.

64. Smanik PA, Liu Q, Furminger TL, Ryu K, Xing S, Mazzaferri EL, *et al.* Cloning of the human sodium lodide symporter. *Biochem Biophys Res Commun* **1996**;226:339-45.

65. Ravera S, Reyna-Neyra A, Ferrandino G, Amzel LM, Carrasco N. The Sodium/Iodide Symporter (NIS): Molecular Physiology and Preclinical and Clinical Applications. *Annu Rev Physiol* **2017**;79:261-89.

66. Knoop K, Kolokythas M, Klutz K, Willhauck MJ, Wunderlich N, Draganovici D, *et al.* Image-guided, tumor stroma-targeted 131I therapy of hepatocellular cancer after systemic mesenchymal stem cell-mediated NIS gene delivery. *Mol Ther* **2011**;19:1704-13.

67. Hingorani M, Spitzweg C, Vassaux G, Newbold K, Melcher A, Pandha H, *et al.* The biology of the sodium iodide symporter and its potential for targeted gene delivery. *Curr Cancer Drug Targets* **2010**;10:242-67.

68. Spitzweg C. Gene therapy in thyroid cancer. *Horm Metab Res* **2009**;41:500-9.

69. Meyer M, Wagner E. Recent developments in the application of plasmid DNA-based vectors and small interfering RNA therapeutics for cancer. *Hum Gene Ther* **2006**;17:1062-76.

70. Knoop K, Schwenk N, Dolp P, Willhauck MJ, Zischek C, Zach C, *et al.* Stromal targeting of sodium iodide symporter using mesenchymal stem cells allows enhanced imaging and therapy of hepatocellular carcinoma. *Hum Gene Ther* **2013**;24:306-16.

71. Knoop K, Schwenk N, Schmohl K, Müller A, Zach C, Cyran C, *et al.* Mesenchymal stem cell-mediated, tumor stroma-targeted radioiodine therapy of metastatic colon cancer using the sodium iodide symporter as theranostic gene. *J Nucl Med* **2015**;56:600-6.

72. Müller AM, Schmohl KA, Knoop K, Schug C, Urnauer S, Hagenhoff A, *et al.* Hypoxia-targeted 131I therapy of hepatocellular cancer after systemic mesenchymal stem cell-mediated sodium iodide symporter gene delivery. *Oncotarget* **2016**;7:54795-810.

73. Schug C, Urnauer S, Jaeckel C, Schmohl KA, Tutter M, Steiger K, *et al.* TGFB1-driven mesenchymal stem cell-mediated NIS gene transfer. *Endocr Relat Cancer* **2019**;26:89-101.

74. Schug C, Kitzberger C, Sievert W, Spellerberg R, Tutter M, Schmohl KA, *et al.* Radiation-Induced Amplification of TGFB1-Induced Mesenchymal Stem Cell-Mediated Sodium Iodide Symporter (NIS) Gene (131)I Therapy. *Clin Cancer Res* **2019**;25:5997-6008.

75. Schug C, Sievert W, Urnauer S, Muller AM, Schmohl KA, Wechselberger A, *et al.* External Beam Radiation Therapy Enhances Mesenchymal Stem Cell-Mediated Sodium-Iodide Symporter Gene Delivery. *Hum Gene Ther* **2018**;29:1287-300.

76. Schug C, Gupta A, Urnauer S, Steiger K, Cheung PF, Neander C, *et al.* A Novel Approach for Image-Guided ^{131}I Therapy of Pancreatic Ductal Adenocarcinoma Using Mesenchymal Stem Cell-Mediated NIS Gene Delivery. *Mol Cancer Res* **2019**;17:310-20.

77. Grunwald GK, Klutz K, Willhauck MJ, Schwenk N, Senekowitsch-Schmidtke R, Schwaiger M, *et al.* Sodium iodide symporter (NIS)-mediated radiovirotherapy of hepatocellular cancer using a conditionally replicating adenovirus. *Gene Ther* **2013**;20:625-33.

78. Grunwald GK, Vetter A, Klutz K, Willhauck MJ, Schwenk N, Senekowitsch-Schmidtke R, *et al.* Systemic image-guided liver cancer radiovirotherapy using dendrimer-coated adenovirus encoding the sodium iodide symporter as theranostic gene. *J Nucl Med* **2013**;54:1450-7.

79. Grunwald GK, Vetter A, Klutz K, Willhauck MJ, Schwenk N, Senekowitsch-Schmidtke R, *et al.* EGFR-Targeted Adenovirus Dendrimer Coating for Improved Systemic Delivery of the Theranostic NIS Gene. *Mol Ther Nucleic Acids* **2013**;2:e131.

80. Ediriwickrema A, Saltzman WM. Nanotherapy for Cancer: Targeting and Multifunctionality in the Future of Cancer Therapies. *ACS Biomater Sci Eng* **2015**;1:64-78.

81. Hall A, Lachelt U, Bartek J, Wagner E, Moghimi SM. Polyplex Evolution: Understanding Biology, Optimizing Performance. *Mol Ther* **2017**;25:1476-90.

82. Klutz K, Willhauck MJ, Dohmen C, Wunderlich N, Knoop K, Zach C, *et al.* Image-guided tumor-selective radioiodine therapy of liver cancer after systemic nonviral delivery of the sodium iodide symporter gene. *Hum Gene Ther* **2011**;22:1563-74.

83. Klutz K, Russ V, Willhauck MJ, Wunderlich N, Zach C, Gildehaus FJ, *et al.* Targeted radioiodine therapy of neuroblastoma tumors following systemic nonviral delivery of the sodium iodide symporter gene. *Clin Cancer Res* **2009**;15:6079-86.

84. Iyer AK, Khaled G, Fang J, Maeda H. Exploiting the enhanced permeability and retention effect for tumor targeting. *Drug Discov Today* **2006**;11:812-8.

85. Greish K. Enhanced permeability and retention (EPR) effect for anticancer nanomedicine drug targeting. *Methods Mol Biol* **2010**;624:25-37.

86. Schafer A, Pahnke A, Schaffert D, van Weerden WM, de Ridder CM, Rodl W, *et al.* Disconnecting the yin and yang relation of epidermal growth factor receptor (EGFR)-mediated delivery: a fully synthetic, EGFR-targeted gene transfer system avoiding receptor activation. *Hum Gene Ther* **2011**;22:1463-73.

87. Klutz K, Schaffert D, Willhauck MJ, Grunwald GK, Haase R, Wunderlich N, *et al.* Epidermal growth factor receptor-targeted (131)I-therapy of liver cancer following systemic delivery of the sodium iodide symporter gene. *Mol Ther* **2011**;19:676-85.

88. Spitzweg C, Morris JC. The sodium iodide symporter: its pathophysiological and therapeutic implications. *Clin Endocrinol (Oxf)* **2002**;57:559-74.

89. Hamilton JG. The use of radioactive tracers in biology and medicine. *Radiology* **1942**;39:541-72.

90. Gorbman A. Effects of radiotoxic dosages of I131 upon thyroid and contiguous tissues in mice. *Proc Soc Exp Biol Med* **1947**;66:212.

91. Gorbman A. Functional and structural changes consequent to high dosages of radioactive iodine. *J Clin Endocrinol Metab* **1950**;10:1177-91.

92. Sloviter HA. The effect of complete ablation of thyroid tissue by radioactive iodine on the survival of tumor-bearing mice. *Cancer Res* **1951**;11:447-9.

93. Silberberg R, Silberberg M. Skeletal effects of radio-iodine induced thyroid deficiency in mice as influenced by sex, age and strain. *Am J Anat* **1954**;95:263-89.

94. Ross DS, Downing MF, Chin WW, Kieffer JD, Ridgway EC. Divergent changes in murine pituitary concentration of free alpha- and thyrotropin beta-subunits in hypothyroidism and after thyroxine administration. *Endocrinology* **1983**;112:187-93.

95. Shupnik MA, Chin WW, Ross DS, Downing MF, Habener JF, Ridgway EC. Regulation by thyroxine of the mRNA encoding the alpha subunit of mouse thyrotropin. *J Biol Chem* **1983**;258:15120-4.

96. Kasuga Y, Matsubayashi S, Sakatsume Y, Akasu F, Jamieson C, Volpe R. The effect of xenotransplantation of human thyroid tissue following radioactive iodine-induced thyroid ablation on thyroid function in the nude mouse. *Clin Invest Med* **1991**;14:277-81.

97. Abel ED, Boers ME, Pazos-Moura C, Moura E, Kaulbach H, Zakaria M, *et al.* Divergent roles for thyroid hormone receptor beta isoforms in the endocrine axis and auditory system. *J Clin Invest* **1999**;104:291-300.

98. Barca-Mayo O, Liao XH, DiCosmo C, Dumitrescu A, Moreno-Vinasco L, Wade MS, *et al.* Role of type 2 deiodinase in response to acute lung injury (ALI) in mice. *Proc Natl Acad Sci U S A* **2011**;108:E1321-9.

99. Klutz K, Willhauck MJ, Wunderlich N, Zach C, Anton M, Senekowitsch-Schmidtke R, *et al.* Sodium iodide symporter (NIS)-mediated radionuclide ((131)I, (188)Re) therapy of liver cancer after transcriptionally targeted intratumoral in vivo NIS gene delivery. *Hum Gene Ther* **2011**;22:1403-12.

100. Trujillo MA, Oneal MJ, McDonough S, Qin R, Morris JC. A probasin promoter, conditionally replicating adenovirus that expresses the sodium iodide symporter (NIS) for radiovirotherapy of prostate cancer. *Gene Ther* **2010**;17:1325-32.

101. Baril P, Martin-Duque P, Vassaux G. Visualization of gene expression in the live subject using the Na/I symporter as a reporter gene: applications in biotherapy. *Br J Pharmacol* **2010**;159:761-71.

102. Penheiter AR, Russell SJ, Carlson SK. The sodium iodide symporter (NIS) as an imaging reporter for gene, viral, and cell-based therapies. *Curr Gene Ther* **2012**;12:33-47.

103. Spitzweg C, Joba W, Schriever K, Goellner JR, Morris JC, Heufelder AE. Analysis of human sodium iodide symporter immunoreactivity in human exocrine glands. *J Clin Endocrinol Metab* **1999**;84:4178-84.

104. Bandyopadhyay U, Biswas K, Banerjee RK. Extrathyroidal actions of antithyroid thionamides. *Toxicol Lett* **2002**;128:117-27.

105. Cano-Europa E, Blas-Valdivia V, Franco-Colin M, Gallardo-Casas CA, Ortiz-Butron R. Methimazole-induced hypothyroidism causes cellular damage in the spleen, heart, liver, lung and kidney. *Acta Histochem* **2011**;113:1-5.

106. Spitzweg C, Joba W, Morris JC, Heufelder AE. Regulation of sodium iodide symporter gene expression in FRTL-5 rat thyroid cells. *Thyroid* **1999**;9:821-30.

107. Bianco AC, Anderson G, Forrest D, Galton VA, Gereben B, Kim BW, *et al.* American Thyroid Association Guide to investigating thyroid hormone economy and action in rodent and cell models. *Thyroid* **2014**;24:88-168.

108. Dingli D, Diaz RM, Bergert ER, O'Connor MK, Morris JC, Russell SJ. Genetically targeted radiotherapy for multiple myeloma. *Blood* **2003**;102:489-96.

109. Hervas F, Morreale de Escobar G, Escobar Del Rey F. Rapid effects of single small doses of L-thyroxine and triiodo-L-thyronine on growth hormone, as studied in the rat by radioimmunoassy. *Endocrinology* **1975**;97:91-101.

110. Zavacki AM, Ying H, Christoffolete MA, Aerts G, So E, Harney JW, *et al.* Type 1 iodothyronine deiodinase is a sensitive marker of peripheral thyroid status in the mouse. *Endocrinology* **2005**;146:1568-75.

111. Antonica F, Kasprzyk DF, Opitz R, Iacovino M, Liao XH, Dumitrescu AM, *et al.* Generation of functional thyroid from embryonic stem cells. *Nature* **2012**;491:66-71.

112. Boschi F, Pagliazzi M, Rossi B, Cecchini MP, Gorgoni G, Salgarello M, *et al.* Small-animal radionuclide luminescence imaging of thyroid and salivary glands with Tc99m-pertechnetate. *J Biomed Opt* **2013**;18:76005.

113. Choi JS, Park IS, Kim SK, Lim JY, Kim YM. Morphometric and functional changes of salivary gland dysfunction after radioactive iodine ablation in a murine model. *Thyroid* **2013**;23:1445-51.

114. Dwyer RM, Khan S, Barry FP, O'Brien T, Kerin MJ. Advances in mesenchymal stem cell-mediated gene therapy for cancer. *Stem Cell Res Ther* **2010**;1:25.

115. Spaeth E, Klopp A, Dembinski J, Andreeff M, Marini F. Inflammation and tumor microenvironments: defining the migratory itinerary of mesenchymal stem cells. *Gene Ther* **2008**;15:730-8.

116. Klopp AH, Spaeth EL, Dembinski JL, Woodward WA, Munshi A, Meyn RE, *et al.* Tumor irradiation increases the recruitment of circulating mesenchymal stem cells into the tumor microenvironment. *Cancer Res* **2007**;67:11687-95.

117. Conrad C, Gupta R, Mohan H, Niess H, Bruns CJ, Kopp R, *et al.* Genetically engineered stem cells for therapeutic gene delivery. *Curr Gene Ther* **2007**;7:249-60.

118. Zischek C, Niess H, Ischenko I, Conrad C, Huss R, Jauch KW, *et al.* Targeting tumor stroma using engineered mesenchymal stem cells reduces the growth of pancreatic carcinoma. *Ann Surg* **2009**;250:747-53.

119. Conrad C, Husemann Y, Niess H, von Luettichau I, Huss R, Bauer C, *et al.* Linking transgene expression of engineered mesenchymal stem cells and angiopoietin-1-induced differentiation to target cancer angiogenesis. *Ann Surg* **2011**;253:566-71.

120. Niess H, Bao Q, Conrad C, Zischek C, Notohamiprodjo M, Schwab F, *et al.* Selective targeting of genetically engineered mesenchymal stem cells to tumor stroma microenvironments using tissue-specific suicide gene expression suppresses growth of hepatocellular carcinoma. *Ann Surg* **2011**;254:767-75.

121. Ponte AL, Marais E, Gallay N, Langonne A, Delorme B, Herault O, *et al.* The in vitro migration capacity of human bone marrow mesenchymal stem cells: comparison of chemokine and growth factor chemotactic activities. *Stem Cells* **2007**;25:1737-45.

122. Kholodenko IV, Konieva AA, Kholodenko RV, Yarygin KN. Molecular mechanisms of migration and homing of intravenously transplanted mesenchymal stem cells. *J Tissue Eng Regen Med* **2013**;2:2.

123. Dwyer RM, Ryan J, Havelin RJ, Morris JC, Miller BW, Liu Z, *et al.* Mesenchymal Stem Cell-mediated delivery of the sodium iodide symporter supports radionuclide imaging and treatment of breast cancer. *Stem Cells* **2011**;29:1149-57.

124. Dembinski JL, Wilson SM, Spaeth EL, Studeny M, Zompetta C, Samudio I, *et al.* Tumor stroma engraftment of gene-modified mesenchymal stem cells as anti-tumor therapy against ovarian cancer. *Cytotherapy* **2013**;15:20-32.

125. Zhu Y, Cheng M, Yang Z, Zeng CY, Chen J, Xie Y, *et al.* Mesenchymal stem cell-based NK4 gene therapy in nude mice bearing gastric cancer xenografts. *Drug Des Devel Ther* **2014**;8:2449-62.

126. Zhang X, Yao S, Liu C, Jiang Y. Tumor tropic delivery of doxorubicin-polymer conjugates using mesenchymal stem cells for glioma therapy. *Biomaterials* **2015**;39:269-81.

127. Mishra PJ, Mishra PJ, Humeniuk R, Medina DJ, Alexe G, Mesirov JP, *et al.* Carcinoma-associated fibroblast-like differentiation of human mesenchymal stem cells. *Cancer Res* **2008**;68:4331-9.

128. Kidd S, Spaeth E, Watson K, Burks J, Lu H, Klopp A, *et al.* Origins of the tumor microenvironment: quantitative assessment of adipose-derived and bone marrow-derived stroma. *PLoS One* **2012**;7:e30563.

129. Luidens MK, Mousa SA, Davis FB, Lin HY, Davis PJ. Thyroid hormone and angiogenesis. *Vascul Pharmacol* **2010**;52:142-5.

130. Davis PJ, Davis FB, Mousa SA, Luidens MK, Lin HY. Membrane receptor for thyroid hormone: physiologic and pharmacologic implications. *Annu Rev Pharmacol Toxicol* **2011**;51:99-115.

131. Davis PJ, Davis FB, Lin HY, Mousa SA, Zhou M, Luidens MK. Translational implications of nongenomic actions of thyroid hormone initiated at its integrin receptor. *Am J Physiol Endocrinol Metab* **2009**;297:E1238-46.

132. Yalcin M, Lin HY, Sudha T, Bharali DJ, Meng R, Tang HY, *et al.* Response of human pancreatic cancer cell xenografts to tetraiodothyroacetic acid nanoparticles. *Horm Cancer* **2013**;4:176-85.

133. Davis PJ, Lin HY, Sudha T, Yalcin M, Tang HY, Hercbergs A, *et al.* Nanotetrac targets integrin αvβ3 on tumor cells to disorder cell defense pathways and block angiogenesis. *Onco Targets Ther* **2014**;7:1619-24.

134. Dominici M, Le Blanc K, Mueller I, Slaper-Cortenbach I, Marini F, Krause D, *et al.* Minimal criteria for defining multipotent mesenchymal stromal cells. The International Society for Cellular Therapy position statement. *Cytotherapy* **2006**;8:315-7.

135. Edelstein A, Amodaj N, Hoover K, Vale R, Stuurman N. Computer control of microscopes using microManager. *Curr Protoc Mol Biol* **2010**;Chapter 14:Unit14.20.

136. Huisken J, Swoger J, Del Bene F, Wittbrodt J, Stelzer EH. Optical sectioning deep inside live embryos by selective plane illumination microscopy. *Science* **2004**;305:1007-9.

137. Pitrone PG, Schindelin J, Stuyvenberg L, Preibisch S, Weber M, Eliceiri KW, *et al.* OpenSPIM: an open-access light-sheet microscopy platform. *Nat Methods* **2013**;10:598-9.

138. Gualda E, Moreno N, Tomancak P, Martins GG. Going "open" with mesoscopy: a new dimension on multi-view imaging. *Protoplasma* **2014**;251:363-72.

139. Rühland S, Wechselberger A, Spitzweg C, Huss R, Nelson PJ, Harz H. Quantification of in vitro mesenchymal stem cell invasion into tumor spheroids using selective plane illumination microscopy. *J Biomed Opt* **2015**;20:040501.

140. Preibisch S, Saalfeld S, Schindelin J, Tomancak P. Software for bead-based registration of selective plane illumination microscopy data. *Nat Methods* **2010**;7:418-9.

141. Bolte S, Cordelieres FP. A guided tour into subcellular colocalization analysis in light microscopy. *J Microsc* **2006**;224:213-32.

142. Ollion J, Cochennec J, Loll F, Escude C, Boudier T. TANGO: a generic tool for high-throughput 3D image analysis for studying nuclear organization. *Bioinformatics* **2013**;29:1840-1.

143. Schmohl KA, Müller AM, Schwenk N, Knoop K, Rijntjes E, Köhrle J, *et al.* Establishment of an effective radioiodide thyroid ablation protocol in mice. *Eur Thyroid J* **2015**;4:74-80.

144. Groba C, Mayerl S, van Mullem AA, Visser TJ, Darras VM, Habenicht AJ, *et al.* Hypothyroidism compromises hypothalamic leptin signaling in mice. *Mol Endocrinol* **2013**;27:586-97.

145. Jin ZH, Furukawa T, Claron M, Boturyn D, Coll JL, Fukumura T, *et al.* Positron emission tomography imaging of tumor angiogenesis and monitoring of antiangiogenic efficacy using the novel tetrameric peptide probe 64Cu-cyclam-RAFT-c(-RGDfK-)4. *Angiogenesis* **2012**;15:569-80.

146. Cayrol F, Diaz Flaque MC, Fernando T, Yang SN, Sterle HA, Bolontrade M, *et al.* Integrin alphavbeta3 acting as membrane receptor for thyroid hormones mediates angiogenesis in malignant T cells. *Blood* **2015**;125:841-51.

147. Hercbergs A, Davis FB, Lin HY, Luidens MK, Meng R, Ashur-Fabian O, *et al.* Integrin-Mediated Actions of Thyroid Hormone Analogues on Tumor Cell Chemosensitivity, Integrin-Growth Factor Receptor Crosstalk and Inflammatory Gene Expression. *Cancer Clin Oncol* **2012**;1:32-40.

148. Balzan S, Del Carratore R, Nardulli C, Sabatino L, Lubrano V, Iervasi G. The Stimulative Effect of T3 and T4 on Human Myocardial Endothelial Cell Proliferation, Migration and Angiogenesis. *J Clin Exp Cardiolog* **2013**;4:280-6.

149. Cohen K, Flint N, Shalev S, Erez D, Baharal T, Davis PJ, *et al.* Thyroid hormone regulates adhesion, migration and matrix metalloproteinase 9 activity via αvβ3 integrin in myeloma cells. *Oncotarget* **2014**;5:6312-22.

150. De Vito P, Balducci V, Leone S, Percario Z, Mangino G, Davis PJ, *et al.* Nongenomic effects of thyroid hormones on the immune system cells: New targets, old players. *Steroids* **2012**;77:988-95.

151. Uchibori R, Tsukahara T, Ohmine K, Ozawa K. Cancer gene therapy using mesenchymal stem cells. *Int J Hematol* **2014**;99:377-82.

152. Chen J, Crawford R, Chen C, Xiao Y. The key regulatory roles of the PI3K/Akt signaling pathway in the functionalities of mesenchymal stem cells and applications in tissue regeneration. *Tissue Eng Part B Rev* **2013**;19:516-28.

153. Franco OE, Shaw AK, Strand DW, Hayward SW. Cancer associated fibroblasts in cancer pathogenesis. *Semin Cell Dev Biol* **2010**;21:33-9.

154. Yalcin M, Bharali DJ, Lansing L, Dyskin E, Mousa SS, Hercbergs A, *et al.* Tetraidothyroacetic acid (tetrac) and tetrac nanoparticles inhibit growth of human renal cell carcinoma xenografts. *Anticancer Res* **2009**;29:3825-31.

155. Carmeliet P. Angiogenesis in life, disease and medicine. *Nature* **2005**;438:932-6.

156. Helfrich I, Schadendorf D. Blood vessel maturation, vascular phenotype and angiogenic potential in malignant melanoma: one step forward for overcoming anti-angiogenic drug resistance? *Mol Oncol* **2011**;5:137-49.

157. Friedenstein AJ, Piatetzky S, II, Petrakova KV. Osteogenesis in transplants of bone marrow cells. *J Embryol Exp Morphol* **1966**;16:381-90.

158. Friedenstein AJ, Chailakhjan RK, Lalykina KS. The development of fibroblast colonies in monolayer cultures of guinea-pig bone marrow and spleen cells. *Cell Tissue Kinet* **1970**;3:393-403.

159. Mafi P, Hindocha S, Mafi R, Griffin M, Khan WS. Adult mesenchymal stem cells and cell surface characterization - a systematic review of the literature. *Open Orthop J* **2011**;5:253-60.

160. Varner JA, Cheresh DA. Integrins and cancer. *Curr Opin Cell Biol* **1996**;8:724-30.

161. Davis PJ, Sudha T, Lin HY, Mousa SA. Thyroid Hormone, Hormone Analogs, and Angiogenesis. *Compr Physiol* **2015**;6:353-62.

162. Mousa SA, Lin HY, Tang HY, Hercbergs A, Luidens MK, Davis PJ. Modulation of angiogenesis by thyroid hormone and hormone analogues: implications for cancer management. *Angiogenesis* **2014**;17:463-9.

163. Liu X, Zheng N, Shi YN, Yuan J, Li L. Thyroid hormone induced angiogenesis through the integrin αvβ3/protein kinase D/histone deacetylase 5 signaling pathway. *J Mol Endocrinol* **2014**;52:245-54.

164. Davis PJ, Davis FB, Cody V. Membrane receptors mediating thyroid hormone action. *Trends Endocrinol Metab* **2005**;16:429-35.

165. Thalmeier K, Meissner P, Reisbach G, Falk M, Brechtel A, Dormer P. Establishment of two permanent human bone marrow stromal cell lines with long-term post irradiation feeder capacity. *Blood* **1994**;83:1799-807.

166. Von Luttichau I, Notohamiprodjo M, Wechselberger A, Peters C, Henger A, Seliger C, *et al.* Human adult CD34- progenitor cells functionally express the chemokine receptors CCR1, CCR4, CCR7, CXCR5, and CCR10 but not CXCR4. *Stem Cells Dev* **2005**;14:329-36.

167. Jackel C, Nogueira MS, Ehni N, Kraus C, Ranke J, Dohmann M, *et al.* A vector platform for the rapid and efficient engineering of stable complex transgenes. *Sci Rep* **2016**;6:34365.

168. Larsen PR, Kronenberg HM, Melmed S, Polonsky KS (eds). Williams Textbook of Endocrinology, 10th ed. **2003** Philadelphia, PA: WB Saunders.

169. Spitzweg C, Zhang S, Bergert ER, Castro MR, McIver B, Heufelder AE, *et al.* Prostate-specific antigen (PSA) promoter-driven androgen-inducible expression of sodium iodide symporter in prostate cancer cell lines. *Cancer Res* **1999**;59:2136-41.

170. Willhauck MJ, Sharif Samani BR, Gildehaus FJ, Wolf I, Senekowitsch-Schmidtke R, Stark HJ, *et al.* Application of 188rhenium as an alternative radionuclide for treatment of prostate cancer after tumor-specific sodium iodide symporter gene expression. *J Clin Endocrinol Metab* **2007**;92:4451-8.

171. Carpentier G, Martinelli M, Courty J, Cascone I. Angiogenesis Analyzer for ImageJ. *Abstract presented at the 4th ImageJ User and Developer Conference, Mondorf-les-Bains, Luxembourg, October 24-26* **2012**;Abstract no. 2-919941-18-6:198-201.

172. Semenza GL. Targeting HIF-1 for cancer therapy. *Nat Rev Cancer* **2003**;3:721-32.

173. Moeller LC, Dumitrescu AM, Refetoff S. Cytosolic action of thyroid hormone leads to induction of hypoxia-inducible factor-1alpha and glycolytic genes. *Mol Endocrinol* **2005**;19:2955-63.

174. Moeller LC, Cao X, Dumitrescu AM, Seo H, Refetoff S. Thyroid hormone mediated changes in gene expression can be initiated by cytosolic action of the thyroid hormone receptor beta through the phosphatidylinositol 3-kinase pathway. *Nucl Recept Signal* **2006**;4:e020.

175. Lin HY, Su YF, Hsieh MT, Lin S, Meng R, London D, *et al.* Nuclear monomeric integrin αv in cancer cells is a coactivator regulated by thyroid hormone. *FASEB Journal* **2013**;27:3209-16.

176. Lin HY, Cody V, Davis FB, Hercbergs A, Luidens MK, Mousa SA, *et al.* Identification and functions of the plasma membrane receptor for thyroid hormone analogues. *Discov Med* **2011**;11:337-47.

177. Leith JT, Hercbergs A, Kenney S, Mousa SA, Davis PJ. Activation of tumor cell integrin alphavbeta3 by radiation and reversal of activation by chemically modified tetraiodothyroacetic acid (tetrac). *Endocr Res* **2018**:1-5.

178. Welf ES, Naik UP, Ogunnaike BA. A spatial model for integrin clustering as a result of feedback between integrin activation and integrin binding. *Biophys J* **2012**;103:1379-89.

179. Farwell AP, Tranter MP, Leonard JL. Thyroxine-dependent regulation of integrin-laminin interactions in astrocytes. *Endocrinology* **1995**;136:3909-15.

180. Davis PJ, Mousa SA, Cody V, Tang HY, Lin HY. Small molecule hormone or hormone-like ligands of integrin αVβ3: implications for cancer cell behavior. *Horm Cancer* **2013**;4:335-42.

181. Somanath PR, Ciocea A, Byzova TV. Integrin and growth factor receptor alliance in angiogenesis. *Cell Biochem Biophys* **2009**;53:53-64.

182. Lin HY, Glinsky GV, Mousa SA, Davis PJ. Thyroid hormone and anti-apoptosis in tumor cells. *Oncotarget* **2015**;6:14735-43.

183. Mousa SA, Glinsky GV, Lin HY, Ashur-Fabian O, Hercbergs A, Keating KA, *et al.* Contributions of Thyroid Hormone to Cancer Metastasis. *Biomedicines* **2018**;6.

184. Hercbergs A, Davis PJ, Lin HY, Mousa SA. Possible contributions of thyroid hormone replacement to specific behaviors of cancer. *Biomed Pharmacother* **2016**;84:655-9.

185. Schmohl KA, Mueller AM, Dohmann M, Spellerberg R, Urnauer S, Schwenk N, *et al.* Integrin αvβ3-mediated effects of thyroid hormones on mesenchymal stem cells in tumour angiogenesis. *Thyroid* **2019**; [In print].

186. Davis PJ, Glinsky GV, Lin HY, Incerpi S, Davis FB, Mousa SA, *et al.* Molecular mechanisms of actions of formulations of the thyroid hormone analogue, tetrac, on the inflammatory response. *Endocr Res* **2013**;38:112-8.

187. Campbell ID, Humphries MJ. Integrin Structure, Activation, and Interactions. *Cold Spring Harb Perspect Biol* **2011**;3:a004994.

188. Nieberler M, Reuning U, Reichart F, Notni J, Wester HJ, Schwaiger M, *et al.* Exploring the Role of RGD-Recognizing Integrins in Cancer. *Cancers* **2017**;9:116.

189. Tang HY, Lin HY, Zhang S, Davis FB, Davis PJ. Thyroid hormone causes mitogen-activated protein kinase-dependent phosphorylation of the nuclear estrogen receptor. *Endocrinology* **2004**;145:3265-72.

190. Bharali DJ, Yalcin M, Davis PJ, Mousa SA. Tetraiodothyroacetic acid-conjugated PLGA nanoparticles: a nanomedicine approach to treat drug-resistant breast cancer. *Nanomedicine (Lond)* **2013**;8:1943-54.

191. Davis FB, Tang HY, Shih A, Keating T, Lansing L, Hercbergs A, *et al.* Acting via a cell surface receptor, thyroid hormone is a growth factor for glioma cells. *Cancer Res* **2006**;66:7270-5.

192. Lin HY, Tang HY, Keating T, Wu YH, Shih A, Hammond D, *et al.* Resveratrol is pro-apoptotic and thyroid hormone is anti-apoptotic in glioma cells: both actions are integrin and ERK mediated. *Carcinogenesis* **2008**;29:62-9.

193. Lin HY, Tang HY, Shih A, Keating T, Cao G, Davis PJ, *et al.* Thyroid hormone is a MAPK-dependent growth factor for thyroid cancer cells and is anti-apoptotic. *Steroids* **2007**;72:180-7.

194. Barreiro Arcos ML, Gorelik G, Klecha A, Genaro AM, Cremaschi GA. Thyroid hormones increase inducible nitric oxide synthase gene expression downstream from PKC-zeta in murine tumor T lymphocytes. *Am J Physiol Cell Physiol* **2006**;291:C327-36.

195. Meng R, Tang HY, Westfall J, London D, Cao JH, Mousa SA, *et al.* Crosstalk between integrin alphavbeta3 and estrogen receptor-alpha is involved in thyroid hormone-induced proliferation in human lung carcinoma cells. *PLoS One* **2011**;6:e27547.

196. Mousa SA, Yalcin M, Bharali DJ, Meng R, Tang HY, Lin HY, *et al.* Tetraiodothyroacetic acid and its nanoformulation inhibit thyroid hormone stimulation of non-small cell lung cancer cells in vitro and its growth in xenografts. *Lung Cancer* **2012**;76:39-45.

197. Cohen K, Ellis M, Khoury S, Davis PJ, Hercbergs A, Ashur-Fabian O. Thyroid hormone is a MAPK-dependent growth factor for human myeloma cells acting via alphavbeta3 integrin. *Mol Cancer Res* **2011**;9:1385-94.

198. Cohen K, Ellis M, Shinderman E, Khoury S, Davis PJ, Hercbergs A, *et al.* Relevance of the thyroid hormones-alphavbeta3 pathway in primary myeloma bone marrow cells and to bortezomib action. *Leuk Lymphoma* **2015**;56:1107-14.

199. Shinderman-Maman E, Cohen K, Weingarten C, Nabriski D, Twito O, Baraf L, *et al.* The thyroid hormone-alphavbeta3 integrin axis in ovarian cancer: regulation of gene transcription and MAPK-dependent proliferation. *Oncogene* **2016**;35:1977-87.

200. Latteyer S, Christoph S, Theurer S, Hones GS, Schmid KW, Fuehrer D, *et al.* Thyroxine promotes lung cancer growth in an orthotopic mouse model. *Endocr Relat Cancer* **2019**; [Epub ahead of print].

201. Rebbaa A, Chu F, Davis FB, Davis PJ, Mousa SA. Novel function of the thyroid hormone analog tetraiodothyroacetic acid: a cancer chemosensitizing and anti-cancer agent. *Angiogenesis* **2008**;11:269-76.

202. Yalcin M, Bharali DJ, Dyskin E, Dier E, Lansing L, Mousa SS, *et al.* Tetraiodothyroacetic acid and tetraiodothyroacetic acid nanoparticle effectively inhibit the growth of human follicular thyroid cell carcinoma. *Thyroid* **2010**;20:281-6.

203. Yalcin M, Dyskin E, Lansing L, Bharali DJ, Mousa SS, Bridoux A, *et al.* Tetraiodothyroacetic acid (tetrac) and nanoparticulate tetrac arrest growth of medullary carcinoma of the thyroid. *J Clin Endocrinol Metab* **2010**;95:1972-80.

204. Urnauer S, Schmohl KA, Tutter M, Schug C, Schwenk N, Morys S, *et al.* Dual-targeted NIS polyplexes-a theranostic strategy toward tumors with heterogeneous receptor expression. *Gene Ther* **2019**;26:93-108.

205. Urnauer S, Morys S, Krhac Levacic A, Muller AM, Schug C, Schmohl KA, *et al.* Sequence-defined cMET/HGFR-targeted Polymers as Gene Delivery Vehicles for the Theranostic Sodium Iodide Symporter (NIS) Gene. *Mol Ther* **2016**;24:1395-404.

206. Langhans SA. Three-Dimensional in Vitro Cell Culture Models in Drug Discovery and Drug Repositioning. *Front Pharmacol* **2018**;9:6.

207. Smith N, Nucera C. Personalized therapy in patients with anaplastic thyroid cancer: targeting genetic and epigenetic alterations. *J Clin Endocrinol Metab* **2015**;100:35-42.

208. Siironen P, Hagstrom J, Maenpaa HO, Louhimo J, Heikkila A, Heiskanen I, *et al.* Anaplastic and poorly differentiated thyroid carcinoma: therapeutic strategies and treatment outcome of 52 consecutive patients. *Oncology* **2010**;79:400-8.

209. Bisof V, Rakusic Z, Despot M. Treatment of patients with anaplastic thyroid cancer during the last 20 years: whether any progress has been made? *Eur Arch Otorhinolaryngol* **2015**;272:1553-67.

210. Schmohl KA, Gupta A, Grunwald GK, Trajkovic-Arsic M, Klutz K, Braren R, *et al.* Imaging and targeted therapy of pancreatic ductal adenocarcinoma using the theranostic sodium iodide symporter (NIS) gene. *Oncotarget* **2017**;8:33393-404.

211. Prabhakar U, Maeda H, Jain RK, Sevick-Muraca EM, Zamboni W, Farokhzad OC, *et al.* Challenges and key considerations of the enhanced permeability and retention effect for nanomedicine drug delivery in oncology. *Cancer Res* **2013**;73:2412-7.

212. Mickler FM, Mockl L, Ruthardt N, Ogris M, Wagner E, Brauchle C. Tuning nanoparticle uptake: live-cell imaging reveals two distinct endocytosis mechanisms mediated by natural and artificial EGFR targeting ligand. *Nano Lett* **2012**;12:3417-23.

213. Schiff BA, McMurphy AB, Jasser SA, Younes MN, Doan D, Yigitbasi OG, *et al.* Epidermal growth factor receptor (EGFR) is overexpressed in anaplastic thyroid cancer, and the EGFR inhibitor gefitinib inhibits the growth of anaplastic thyroid cancer. *Clin Cancer Res* **2004**;10:8594-602.

214. Schuell B, Gruenberger T, Scheithauer W, Zielinski C, Wrba F. HER 2/neu protein expression in colorectal cancer. *BMC Cancer* **2006**;6:123.

215. Spitzweg C, Baker CH, Bergert ER, O'Connor MK, Morris JC. Image-guided radioiodide therapy of medullary thyroid cancer after carcinoembryonic antigen promoter-targeted sodium iodide symporter gene expression. *Hum Gene Ther* **2007**;18:916-24.

216. Russ V, Gunther M, Halama A, Ogris M, Wagner E. Oligoethylenimine-grafted polypropylenimine dendrimers as degradable and biocompatible synthetic vectors for gene delivery. *J Control Release* **2008**;132:131-40.

217. Smallridge RC, Marlow LA, Copland JA. Anaplastic thyroid cancer: molecular pathogenesis and emerging therapies. *Endocr Relat Cancer* **2009**;16:17-44.

218. Schmutzler C, Winzer R, Meissner-Weigl J, Kohrle J. Retinoic acid increases sodium/iodide symporter mRNA levels in human thyroid cancer cell lines and suppresses expression of functional symporter in nontransformed FRTL-5 rat thyroid cells. *Biochem Biophys Res Commun* **1997**;240:832-8.

219. Haugen BR. Redifferentiation therapy in advanced thyroid cancer. *Curr Drug Targets Immune Endocr Metabol Disord* **2004**;4:175-80.

220. Jeong H, Kim YR, Kim KN, Choe JG, Chung JK, Kim MK. Effect of all-trans retinoic acid on sodium/iodide symporter expression, radioiodine uptake and gene expression profiles in a human anaplastic thyroid carcinoma cell line. *Nucl Med Biol* **2006**;33:875-82.

221. Pugliese M, Fortunati N, Germano A, Asioli S, Marano F, Palestini N, *et al.* Histone deacetylase inhibition affects sodium iodide symporter expression and induces 131I cytotoxicity in anaplastic thyroid cancer cells. *Thyroid* **2013**;23:838-46.

222. Frohlich E, Wahl R. The current role of targeted therapies to induce radioiodine uptake in thyroid cancer. *Cancer Treat Rev* **2014**;40:665-74.

223. Schwertheim S, Wein F, Lennartz K, Worm K, Schmid KW, Sheu-Grabellus SY. Curcumin induces G2/M arrest, apoptosis, NF-kappaB inhibition, and expression of differentiation genes in thyroid carcinoma cells. *J Cancer Res Clin Oncol* **2017**;143:1143-54.

224. Gruning T, Tiepolt C, Zophel K, Bredow J, Kropp J, Franke WG. Retinoic acid for redifferentiation of thyroid cancer--does it hold its promise? *Eur J Endocrinol* **2003**;148:395-402.

225. Rothenberg SM, McFadden DG, Palmer EL, Daniels GH, Wirth LJ. Redifferentiation of iodine-refractory BRAF V600E-mutant metastatic papillary thyroid cancer with dabrafenib. *Clin Cancer Res* **2015**;21:1028-35.

226. Ho AL, Grewal RK, Leboeuf R, Sherman EJ, Pfister DG, Deandreis D, *et al.* Selumetinib-enhanced radioiodine uptake in advanced thyroid cancer. *N Engl J Med* **2013**;368:623-32.

227. Shimura H, Haraguchi K, Miyazaki A, Endo T, Onaya T. Iodide uptake and experimental 131I therapy in transplanted undifferentiated thyroid cancer cells expressing the Na+/I- symporter gene. *Endocrinology* **1997**;138:4493-6.

228. Lee YJ, Chung JK, Shin JH, Kang JH, Jeong JM, Lee DS, *et al.* In vitro and in vivo properties of a human anaplastic thyroid carcinoma cell line transfected with the sodium iodide symporter gene. *Thyroid* **2004**;14:889-95.

229. Lee YJ, Chung JK, Kang JH, Jeong JM, Lee DS, Lee MC. Wild-type p53 enhances the cytotoxic effect of radionuclide gene therapy using sodium iodide symporter in a murine anaplastic thyroid cancer model. *Eur J Nucl Med Mol Imaging* **2010**;37:235-41.

230. Ke CC, Hsieh YJ, Hwu L, Wang FH, Chen FD, Chu LS, *et al.* Evaluation of lentiviral-mediated expression of sodium iodide symporter in anaplastic thyroid cancer and the efficacy of in vivo imaging and therapy. *J Oncol* **2011**;2011:178967.

231. Reddi HV, Madde P, McDonough SJ, Trujillo MA, Morris JC, 3rd, Myers RM, *et al.* Preclinical efficacy of the oncolytic measles virus expressing the sodium iodide symporter in iodine non-avid anaplastic thyroid cancer: a novel therapeutic agent allowing noninvasive imaging and radioiodine therapy. *Cancer Gene Ther* **2012**;19:659-65.

232. Kryeziu K, Jungwirth U, Hoda MA, Ferk F, Knasmuller S, Karnthaler-Benbakka C, *et al.* Synergistic anticancer activity of arsenic trioxide with erlotinib is based on inhibition of EGFR-mediated DNA double-strand break repair. *Mol Cancer Ther* **2013**;12:1073-84.

233. Meireles AM, Preto A, Rocha AS, Rebocho AP, Maximo V, Pereira-Castro I, *et al.* Molecular and genotypic characterization of human thyroid follicular cell carcinoma-derived cell lines. *Thyroid* **2007**;17:707-15.

234. Spitzweg C, Morris JC. Gene therapy for thyroid cancer: current status and future prospects. *Thyroid* **2004**;14:424-34.

235. Huang M, Batra RK, Kogai T, Lin YQ, Hershman JM, Lichtenstein A, *et al.* Ectopic expression of the thyroperoxidase gene augments radioiodide uptake and retention mediated by the sodium iodide symporter in non-small cell lung cancer. *Cancer Gene Ther* **2001**;8:612-8.

236. Boland A, Magnon C, Filetti S, Bidart JM, Schlumberger M, Yeh P, *et al.* Transposition of the thyroid iodide uptake and organification system in nonthyroid tumor cells by adenoviral vector-mediated gene transfers. *Thyroid* **2002**;12:19-26.

237. Urnauer S, Klutz K, Grunwald GK, Morys S, Schwenk N, Zach C, *et al.* Systemic tumor-targeted sodium iodide symporter (NIS) gene therapy of hepatocellular carcinoma mediated by B6 peptide polyplexes. *J Gene Med* **2017**;19.

238. Parenti R, Salvatorelli L, Magro G. Anaplastic Thyroid Carcinoma: Current Treatments and Potential New Therapeutic Options with Emphasis on TfR1/CD71. *Int J Endocrinol* **2014**;2014:685396.

239. Zhang W, Rodl W, He D, Doblinger M, Lachelt U, Wagner E. Combination of sequence-defined oligoaminoamides with transferrin-polycation conjugates for receptor-targeted gene delivery. *J Gene Med* **2015**;17:161-72.

240. Siegel RL, Miller KD, Jemal A. Cancer statistics, 2015. *CA Cancer J Clin* **2015**;65:5-29.

241. Narayanan V, Weekes CD. Molecular therapeutics in pancreas cancer. *World J Gastrointest Oncol* **2016**;8:366-79.

242. Mazur PK, Siveke JT. Genetically engineered mouse models of pancreatic cancer: unravelling tumour biology and progressing translational oncology. *Gut* **2012**;61:1488-500.

243. Hingorani SR, Petricoin EF, Maitra A, Rajapakse V, King C, Jacobetz MA, *et al.* Preinvasive and invasive ductal pancreatic cancer and its early detection in the mouse. *Cancer Cell* **2003**;4:437-50.

244. Izeradjene K, Combs C, Best M, Gopinathan A, Wagner A, Grady WM, *et al.* Kras(G12D) and Smad4/Dpc4 haploinsufficiency cooperate to induce mucinous cystic neoplasms and invasive adenocarcinoma of the pancreas. *Cancer Cell* **2007**;11:229-43.

245. Siveke JT, Schmid RM. Chromosomal instability in mouse metastatic pancreatic cancer--it's Kras and Tp53 after all. *Cancer Cell* **2005**;7:405-7.

246. Ardito CM, Gruner BM, Takeuchi KK, Lubeseder-Martellato C, Teichmann N, Mazur PK, *et al.* EGF receptor is required for KRAS-induced pancreatic tumorigenesis. *Cancer Cell* **2012**;22:304-17.

247. Bardeesy N, Aguirre AJ, Chu GC, Cheng KH, Lopez LV, Hezel AF, *et al.* Both p16(Ink4a) and the p19(Arf)-p53 pathway constrain progression of pancreatic adenocarcinoma in the mouse. *Proc Natl Acad Sci U S A* **2006**;103:5947-52.

248. Schneider G, Siveke JT, Eckel F, Schmid RM. Pancreatic cancer: basic and clinical aspects. *Gastroenterology* **2005**;128:1606-25.

249. Siveke JT, Einwachter H, Sipos B, Lubeseder-Martellato C, Kloppel G, Schmid RM. Concomitant pancreatic activation of Kras(G12D) and Tgfa results in cystic papillary neoplasms reminiscent of human IPMN. *Cancer Cell* **2007**;12:266-79.

250. Kawaguchi Y, Cooper B, Gannon M, Ray M, MacDonald RJ, Wright CV. The role of the transcriptional regulator Ptf1a in converting intestinal to pancreatic progenitors. *Nat Genet* **2002**;32:128-34.

251. Marino S, Vooijs M, van Der Gulden H, Jonkers J, Berns A. Induction of medulloblastomas in p53-null mutant mice by somatic inactivation of Rb in the external granular layer cells of the cerebellum. *Genes Dev* **2000**;14:994-1004.

252. Singh M, Lima A, Molina R, Hamilton P, Clermont AC, Devasthali V, *et al.* Assessing therapeutic responses in Kras mutant cancers using genetically engineered mouse models. *Nat Biotechnol* **2010**;28:585-93.

253. Carrasco N. Iodide transport in the thyroid gland. *Biochim Biophys Acta* **1993**;1154:65-82.

254. Jhiang SM, Cho JY, Ryu KY, DeYoung BR, Smanik PA, McGaughy VR, *et al.* An immunohistochemical study of Na+/I- symporter in human thyroid tissues and salivary gland tissues. *Endocrinology* **1998**;139:4416-9.

255. Lee TC, Threadgill DW. Generation and validation of mice carrying a conditional allele of the epidermal growth factor receptor. *Genesis* **2009**;47:85-92.

256. Natarajan A, Wagner B, Sibilia M. The EGF receptor is required for efficient liver regeneration. *Proc Natl Acad Sci U S A* **2007**;104:17081-6.

257. Heid I, Lubeseder-Martellato C, Sipos B, Mazur PK, Lesina M, Schmid RM, *et al.* Early requirement of Rac1 in a mouse model of pancreatic cancer. *Gastroenterology* **2011**;141:719-30, 30.e1-7.

258. Weiss SJ, Philp NJ, Grollman EF. Iodide transport in a continuous line of cultured cells from rat thyroid. *Endocrinology* **1984**;114:1090-8.

259. Rahib L, Smith BD, Aizenberg R, Rosenzweig AB, Fleshman JM, Matrisian LM. Projecting cancer incidence and deaths to 2030: the unexpected burden of thyroid, liver, and pancreas cancers in the United States. *Cancer Res* **2014**;74:2913-21.

260. Schober M, Javed MA, Beyer G, Le N, Vinci A, Sund M, *et al.* New Advances in the Treatment of Metastatic Pancreatic Cancer. *Digestion* **2015**;92:175-84.

261. Olive KP, Jacobetz MA, Davidson CJ, Gopinathan A, McIntyre D, Honess D, *et al.* Inhibition of Hedgehog signaling enhances delivery of chemotherapy in a mouse model of pancreatic cancer. *Science* **2009**;324:1457-61.

262. Mahajan UM, Teller S, Sendler M, Palankar R, van den Brandt C, Schwaiger T, *et al.* Tumour-specific delivery of siRNA-coupled superparamagnetic iron oxide nanoparticles, targeted against PLK1, stops progression of pancreatic cancer. *Gut* **2016**;65:1838-49.

263. Li Z, Zhao R, Wu X, Sun Y, Yao M, Li J, *et al.* Identification and characterization of a novel peptide ligand of epidermal growth factor receptor for targeted delivery of therapeutics. *FASEB J* **2005**;19:1978-85.

264. Schaffert D, Kiss M, Rodl W, Shir A, Levitzki A, Ogris M, *et al.* Poly(I:C)-mediated tumor growth suppression in EGF-receptor overexpressing tumors using EGF-polyethylene glycol-linear polyethylenimine as carrier. *Pharm Res* **2011**;28:731-41.

265. Smrekar B, Wightman L, Wolschek MF, Lichtenberger C, Ruzicka R, Ogris M, *et al.* Tissue-dependent factors affect gene delivery to tumors in vivo. *Gene Ther* **2003**;10:1079-88.

266. Cabral H, Matsumoto Y, Mizuno K, Chen Q, Murakami M, Kimura M, *et al.* Accumulation of sub-100 nm polymeric micelles in poorly permeable tumours depends on size. *Nat Nanotechnol* **2011**;6:815-23.

267. Miller BW, Morton JP, Pinese M, Saturno G, Jamieson NB, McGhee E, *et al.* Targeting the LOX/hypoxia axis reverses many of the features that make pancreatic cancer deadly: inhibition of LOX abrogates metastasis and enhances drug efficacy. *EMBO Mol Med* **2015**;7:1063-76.

268. Li J, Liu F, Gupta S, Li C. Interventional Nanotheranostics of Pancreatic Ductal Adenocarcinoma. *Theranostics* **2016**;6:1393-402.

269. Grandinetti G, Smith AE, Reineke TM. Membrane and nuclear permeabilization by polymeric pDNA vehicles: efficient method for gene delivery or mechanism of cytotoxicity? *Mol Pharm* **2012**;9:523-38.

270. Moghimi SM, Symonds P, Murray JC, Hunter AC, Debska G, Szewczyk A. A two-stage poly(ethylenimine)-mediated cytotoxicity: implications for gene transfer/therapy. *Mol Ther* **2005**;11:990-5.

271. Hall A, Larsen AK, Parhamifar L, Meyle KD, Wu LP, Moghimi SM. High resolution respirometry analysis of polyethylenimine-mediated mitochondrial energy crisis and cellular stress: Mitochondrial proton leak and inhibition of the electron transport system. *Biochim Biophys Acta* **2013**;1827:1213-25.

272. Chollet P, Favrot MC, Hurbin A, Coll JL. Side-effects of a systemic injection of linear polyethylenimine-DNA complexes. *J Gene Med* **2002**;4:84-91.

273. Wiseman JW, Goddard CA, McLelland D, Colledge WH. A comparison of linear and branched polyethylenimine (PEI) with DCChol/DOPE liposomes for gene delivery to epithelial cells in vitro and in vivo. *Gene Ther* **2003**;10:1654-62.

274. Sidi AA, Ohana P, Benjamin S, Shalev M, Ransom JH, Lamm D, *et al.* Phase I/II marker lesion study of intravesical BC-819 DNA plasmid in H19 over expressing superficial bladder cancer refractory to bacillus Calmette-Guerin. *J Urol* **2008**;180:2379-83.

XI. ACKNOWLEDGEMENTS

I would like to take the opportunity to thank the many people without whom this thesis could never have been.

Foremost, I would like to express my gratitude to Prof. Dr. Christine Spitzweg for the opportunity to do my research in her lab. Thank you Christine for the continuous support, the freedom to explore new projects and develop my own ideas, and your maddening sense for applying pressure when I needed it. I would particularly like to acknowledge the generous and amazingly frequent opportunities to present my work at international conferences, including multiple trips to North America. Thank you for all the memorable moments in the man-eating lab – the elk-antler sing-along Christmas parties all around Munich, the Mickey Mouse ears in Orlando, the impressive architecture boat ride in Chicago, the ETA dinner in Belgrade, and the countless Coke light retrieval expeditions around the world, to name just a few.

I would like to thank Prof. Dr. Ernst Wagner for taking me under his wings as an external doctoral student. Thank you Ernst for your scientific input and support. You truly are the fastest email answerer with a professor title I have ever met.

Thank you Prof. Dr. Peter Nelson for your enthusiasm, immense knowledge, and kindness. Quite a few of the weird many-legged creature's legs started life as "wouldn't it be cool if…" in one of our joint lab meetings. *Schnick-schnack*, *Doktorarbeit* – it really was that easy.

Thank you to my fellow lab mates, past and present, for keeping days and nights in the lab entertaining, or, when they were not, bearable. Nathalie, fellow half-Brit, for putting up with sitting next to me for so long, my superman antics (sorry for that), and the singing (did someone say warthog?). Kerstin for being, at times, the only one more interested in all things outdoorsy than in handbags and nail varnish. Andrea of the perfect female hormone levels and royal undergarments, for not getting me arrested smuggling all your handbag-bargains over diverse borders – who would have thought there is a life after thyroid hormone stimulations? *Einhornpower*! Sarah for all the fiddly surgeries we did together and the fun time in Denver. Christina for never giving up and checking out the holy halls of the ROB for us – including the lair of the chief herself. Sorry for all the nicknames! Speaking of nicknames, Mariella, thank you for putting up with more talks than sightseeing at conferences and sorry for overly public displays of enthusiasm for uncomfortable time courses and too many control groups (I couldn't have you finishing before me). Yang, for being my deputy smelly mouse tamer when I was away at a conference again. It cannot be easy being the only guy and the only non-German – I bet Mike Tuttle is impressed! Carolin for entertaining stories of mice and men when the hour was late. Rebekka and her *Bollerbuchse* for bringing a bit of Northern flair to the lab ("THAT is NOT windy"). And thank you to everyone else I

have spent more or less lab time with over the years: Aayush, Alex, Elke, Geoff, Karoline, Katja, Maike, Matthias, Nicole, Svenja, Viktoria – it was a blast!

Thank you to all the nice and helpful people in the Nelson and Wagner labs, our friendly lab neighbours all around, especially our new neighbours with all the fancy lab equipment (SO jealous). Ralf for saving everyone when everything is broken. Everyone from the Nuclear Medicine in Großhadern, especially Rosel, Karin, and Barbara, and former 'Nukies' Janette and Roswitha for all your assistance. Thank you to all our collaboration partners, especially within the SFB 824 and the SPP 1629, and the DGE and the ETA for the generous financial support of all my travels. Special thanks go out to the ATA for accepting me as a trainee year after year after year, for just being all-around really nice people, and for the most memorable dinner this side of the Atlantic.

On the domestic front, thank you to all my lovely friends near and far, foremost Julia and Bernd, and everyone else who kept me sane by schlepping me to the mountains or, if all else failed, the climbing gym. You know who you are (and yes, I am scared of forgetting someone). My family, especially my parents and my siblings Sarah, Nicky, and Sebastian, who have always supported me and shown interest in what I do – I know I am really bad at explaining it all in normal words. Mike, for your love, support, and encouragement. And for being the bigger nerd (no discussion).

Last but definitely not least, I would like to say thank you and sorry to all my murine lab mates – even those who bit me or peed on me, I am sure I deserved it.